Low Temperature Photoconductivity of Hydrogenated Amorphous Silicon(a-Si:H) Thin Films

By

Gökhan ERDOĞAN

A Dissertation Submitted to the
Graduate School in Partial Fulfillment of the
Requirements for the Degree of

MASTER OF SCIENCE

Department: Materials Science and Engineering
Major: Materials Science

İzmir Institute of Technology
İzmir, Turkey

September, 2001

We approve the thesis of **Gökhan ERDOĞAN**

Date of Signature

28.09.2001

Assoc. Prof. Dr. Mehmet GÜNEŞ
Supervisor
Department of Physics

28.09.2001

Assoc. Prof. Dr. Orhan ÖZTÜRK
Co-Supervisor
Department of Physics

28.09.2001

Prof. Dr. Muhsin ÇİFTÇİOĞLU
Department of Chemical Engineering

28.09.2001

Asst. Prof. Dr. Sami SÖZÜER
Department of Physics

28.09.2001

Asst. Prof. Dr. Salih OKUR
Department of Physics

28.09.2001

Prof. Dr. Muhsin ÇİFTÇİOĞLU
Head of Interdisciplinary Materials Science and Engineering Program

ACKNOWLEDGEMENTS

I would like to thank to Assoc. Prof. Dr. Mehmet Güneş and Assoc. Prof. Dr. Orhan Öztürk for their supervision, help, support and encouragement they provided during this thesis.

I also would like to thank to other members of the thesis committee, Prof. Dr. Muhsin Ciftçioğlu, Asst. Prof. Dr. Sami Sözüer and Asst. Prof. Dr. Salih Okur for their valuable comments and suggestions.

I am very greatful to Prof. C.R. Wronski of Pennsylvania State University, Dr. M. Bennette of Solarex, Prof. J. Abelson of University of Illinois-Urbana Champagne, Dr. Q. Wang of National Renewable Energy Laboratory, Colorado and Dr. J. Yang of United Solar Systems Corporation of Michigan for providing undoped hydrogenated amorphous silicon thin films prepared under various deposition conditions and Prof. S. Kasap of University of Saskatchewan for donating red LED array light source, ENH, ELH light bulbs and heater for annealing box, without those this study was almost impossible.

I would like to thank to my Institution, İzmir Institute of Technology, for providing full time Research Assistanship during my graduate study.

Special thanks go to all research assistants for their friendship and their helps during this thesis.

Finally, I would like to thank to my family, especially to my lovely mother for her delicious meals during long nights in research laboratory, for their help, support and patience.

ABSTRACT

In this study low temperature photoconductivity of undoped hydrogenated amorphous silicon(a-Si:H) thin films have been studied to investigate the effect of native and Staebler-Wronski defects. The study covers undoped a-Si:H films prepared by various deposition techniques such as DC glow discharge, RF-PECVD with and without H-dilution, RF magnetron sputtering and hot-wire(HW) CVD.

In the annealed state, the samples were characterized using temperature dependence of dark conductivity, steady-state photoconductivity, σ_{ph}, versus light intensity at room temperature and steady-state photoconductivity versus temperature down to 90 ^{0}K at three different intensities. Activation energy ,E_F, of the samples changes from 0.60 eV to 1.0 eV. σ_{ph} shows a few orders of magnitude higher values from the dark conductivity and its magnitude is sample dependent due to differences in deposition conditions. The intensity dependence of σ_{ph} ,γ, ($\sigma_{ph} \alpha F^{\gamma}$) is close to unity and varies between 0.70 to 0.90, indicating recombination kinetics through the midgap defect states in the bandgap of a-Si:H. Low temperature photoconductivity versus 1000/T spectrum shows three distinctly different regions. In Region I, σ_{ph} decreases with temperature until a transition temperature. Then Region II begins, where σ_{ph} begins to increase resulting a peak in spectrum or remains to be unchanged until a second transition temperature to Region III, where σ_{ph} continuously decreases with T. Transition temperatures and the degree of increase in σ_{ph} in Region II is sample dependent. These results indicate the presence of at least two different types of midgap defect states in the bandgap and exponential tail state present in the annealed state.

In the light soaked state, Staebler-Wronski effect (SWE) was investigated after exposing the samples to white light illumination of a few suns intensity. The characterization involves dark conductivity and steady-state photoconductivity at room temperature and σ_{ph} versus temperature down to 90 ^{0}K for different intensities. Dark conductivity values decreased a certain factor indicating a slight shift in E_F through midgap. σ_{ph} values decreased substantially from its annealed values due to creation of Steabler-Wronski defects in the bandgap. The intensity dependence of σ_{ph} become almost equal and close to unity for all the films even it shows slight variation in the annealed state. The shape of low temperature photoconductivity spectra becomes almost the same for all samples even drastic differences were observed in the annealed state. The spectrum is mainly dominated by only two regions. Region I dominates from room temperature down to 170 ^{0}K, where σ_{ph} decreases with a

constant slope as T decreases. After that temperature, Region II sets in. σ_{ph} remains to be constant until temperature used in this study. Region III can only be detected at higher intensity and temperatures lower than 90 ^{0}K. Results indicate that more defects around the midgap are created by light, which decrease σ_{ph} and relatively less defects are created away from midgap and closer to band edge, which improve σ_{ph} instead of decreasing it as temperature decreases. The defect states in Region I responsible for decreasing σ_{ph} are more likely that they are neutral silicon dangling bond defects ,D^0, and those in Region II responsible for increasing σ_{ph} are non-D^0 defect states. They act as photosensitising defects with a very low capture cross-sections for electrons. They could be charged silicon dangling bonds ,D^+ and D^-, or floating bonds results in defect models proposed for a-Si:H.

ÖZ

Bu çalışmada Staebler-Wronski ve doğal elektronik yerelleşmiş kusurları araştırmak için katkılanmamış hidrojenlendirilmiş amorf silisyum (a-Si:H) ince filmlerin düşük sıcaklıklardaki fotoiletkenlikleri incelenmiştir. Çalışma değişik tekniklerle hazırlanmış katkılanmamış hidrojenli amorf silisyum ince filmleri kapsamaktadır. Bu teknikler; doğru akım "glow discharge" (SiH_4 gazının doğru akım altında ayrıştırılması), radyo dalgası plazma yardımlı kimyasal buharlaşma (seyreltilmiş hidrojenli ve seyreltilmemiş hidrojenli), radyo frekanslı manyetik alandaki argon gazı püskürtmesi ve sıcak-katot kimyasal buharlaşması ile büyütme teknikleridir.

Örnekler tavlanmış durumda sıcaklığa bağlı karanlık iletkenlik, oda sıcaklığında ışık şiddetine bağlı fotoiletkenlik ve üç farklı ışık şiddetinde $90K^0$'ya kadar sıcaklığa bağlı fotoiletkenlik yöntemleriyle karakterize edilmiştir. Filmlerin aktivasyon enerjileri 0.60eV-1.0eV arasında değişmektedir. Fotoiletkenlik değerleri karanlık iletkenlik değerlerinden birkaç mertebe yüksektir. Bu farklar farklı büyütme tekniklerinden dolayı örneklere bağımlıdır. Fotoiletkenliğin ışık şiddetine bağımlılığı ,γ, ($\sigma_{ph} \propto F^{\gamma}$), tavlanmış durum için 0.70 ile 0.90 arasında değişmektedir. Bu değerler rekombinasyon kinetiğinin bant ortası elektronik kusurlardan geçtiğini gösterir. Düşük sıcaklık fotoiletkenliğinde iletkenliğin 1000/T'ye bağlı spektrumu üç farklı bölge gösterir. 1.Bölge'de fotoiletkenlik bir geçiş sıcaklığına kadar azalır ve sonra 2.Bölge başlar. 2.Bölge'de fotoiletkenlik spektrumu ya bir tepe gösterir yada ikinci bir geçiş sıcaklığına kadar sabit kalır. Fotoiletkenliğin sıcaklıkla azalmaya başladığı 2. geçiş sıcaklığından sonra 3.Bölge başlar. 2.Bölge'deki geçiş sıcaklığı ve fotoiletkenliğin azalma miktarı örneklere bağımlıdır. Bu sonuçlar tavlanmış durumda bant ortası düzeyde en az iki tip kusur ve eksponansiyel olarak artan kuyruk (tail) düzeyi olduğunu gösterir.

Staebler-Wronski(SW) etkisi ışık altında bozunuma uğratılmış durumda, örneklerin birkaç güneş ışığı şiddetinde aydınlatılmasıyla araştırılmıştır. Örnekler ışık altında bozunuma uğratılmış durumda, sıcaklığa bağlı karanlık iletkenlik, oda sıcaklığında ışık şiddetine bağlı fotoiletkenlik ve üç farklı ışık şiddetinde $90K^0$ ' ya kadar sıcaklığa bağlı fotoiletkenlik yöntemleriyle karakterize edilmiştir. Karanlık iletkenlik değerleri Fermi düzeyindeki hafif kaymanın göstergesi olarak belirli oranlarda azalmıştır. Fotoiletkenlik değerleri SW elektronik kusurlarının oluşmasından dolayı tavlanmış durumdaki değerlerinin çok altındadır. Fotoiletkenliğin ışık şiddetine bağımlılığı tüm filmler için, tavlanmış durumda küçük değişmeler göstermesine karşın,

1’e oldukça yakınlaşmıştır. Düşük sıcaklık spektrumu tüm filmler için tavlanmış durumda büyük farklılıklar göstermesine karşın, ışık altında bozunuma uğratılmış durumda hemen hemen aynıdır. Fotoiletkenlik spektrumunda $90K^0$ ’ya kadar yalnız 2 bölge baskın olmuştur. 1. bölge $170K^0$ ’ya kadar baskındır ve fotoiletkenlik sabit bir eğimde sıcaklıkla azalır. $170K^0$ geçiş sıcaklığından sonra 2. Bölge başlar ve fotoiletkenlik $90K^0$ ’ya kadar sabit kalır. 3. Bölge ancak yüksek ışık şiddetinde ve daha düşük sıcaklıklarda gözlenebilir. Sonuçlar, bant boşluğunun ortalarında fotoiletkenliği azaltan kusurların baskın olduğunu gösterir. Bant ortası elektronik düzeylerden uzaklarda ve bant ucuna yakın yerlerde, fotoiletkenliği sıcaklıkla azaltmak yerine arttıran kusurlar nispeten daha az oluşturulur. 1.Bölge’deki fotoiletkenliği azaltan kusurlar nötür-silisyum sallanan bağlardır (D^0). 2.Bölge’deki fotoiletkenliği arttıran kusur düzeyleri D^0 olmayan (non-D^0) kusurlardır. Bu kusurlar elektronlar için yakalama kesitleri küçük olan foto-duyarlı kusurlardır. Bunlar a-Si:H için önerilen modellerin sonucuna göre, yüklü silikon sallanan bağlar (D^+ ve D^-) ya da yüzen bağlar olabilirler.

TABLE OF CONTENTS

LIST OF FIGURES

LIST OF TABLES

CHAPTER 1

INTRODUCTION

Amorphous semiconductors are a class of semiconducting materials that do not show the long range order typical of crystalline materials with a periodic potential. Most of the properties of semiconductors arise from the crystalline nature of the material. This includes the concept of bandgap and band edges. The atoms in crystalline materials are arranged in a perfect lattice. For example, silicon is an ideal semiconductor in crystalline form, in which silicon atoms are covalently bonded with four nearest neighbors in tetrahedral directions. As a result of this configuration, the bonding states, valance band, are completely occupied with electrons and the antibonding states, conduction band, are empty. There is a sharp distinction between valance band and conduction band which is seen in Figure 1.1. This sharp structure that is evident in density of states g (E) at many different energies arises directly from long range periodicity and these energies are called van Hove singularities [1].

As a semiconducting material, silicon is the second most abundant material on Earth. It is reasonably cheap, chemically and electronically well suited to device applications whereas it is quite expensive to fabricate single crystal devices. In contrast amorphous semiconductors do not have perfect long range order, in which the atoms are randomly oriented but on a local scale the short range order of atoms is maintained where atoms still have the same number of nearest neighbor atom configuration as in perfect crystals. This results in similar energy band structure at higher energies like in crystalline semiconductors. In the absence of long range order, van Hove singularity is expected to disappear and be replaced by more gradually decreasing density of states. These regions of gradually decreasing density of states, g (E), are called band tails. The valance band tail states are covalent bonds that are weaker than normal. This can happen when the covalent angle is bent from its equilibrium value. When the band is stretched due to internal strains, or when some antibonding orbital is mixed in, these produce potential fluctuations, which push states up and down and prevent any sharp feature in g (E) as seen in Figure 1.1. All these effects are expected to produce also a tail of states extending down in energy from the conduction band [2]. These localized tail states are weakened or modified band states. They do not conduct, which means a charged carrier trapped in such a state has zero mobility.

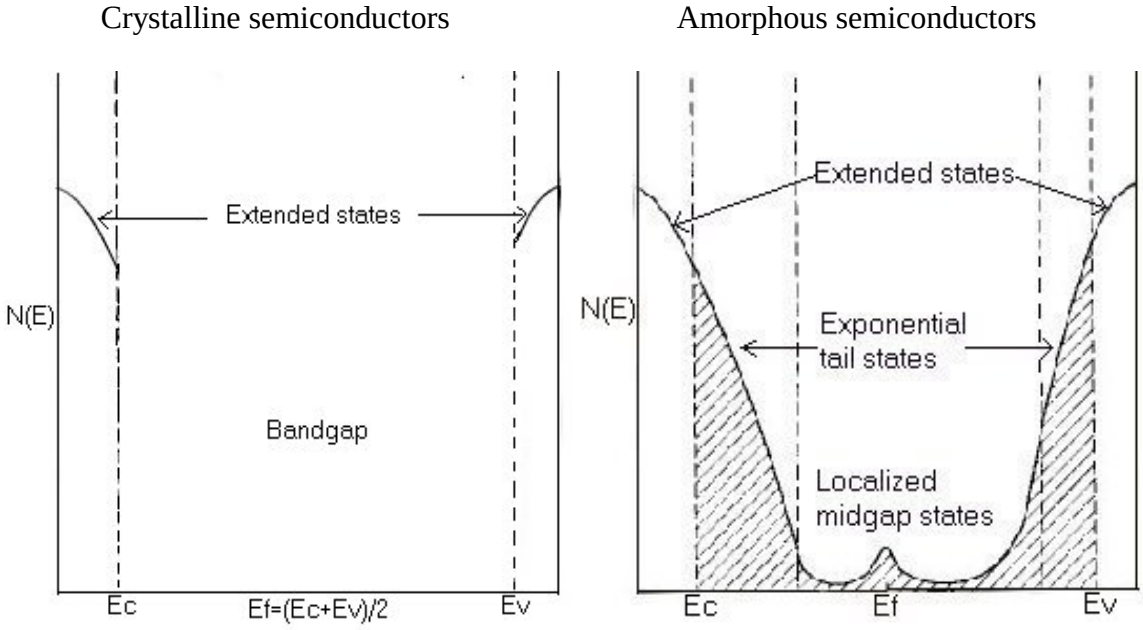

Figure 1.1. Band structure for crystalline and amorphous semiconductors.

In addition to the localized tail states, there are also localized deep gap states around the midgap. These localized midgap defects are due to loss of the long range order. They originate from the unsatisfied bonds, dangling bonds [DBs], and weak bonds. The amount of localized midgap defect states are in the order of 10^{19}-10^{20} cm^{-3} in amorphous silicon (a-Si). Therefore, they do not allow this material to be useful for electronic device applications. It is impossible to increase the conductivity by the incorporation of impurities as expected to act as donors and acceptors like in crystalline semiconductors. There were two possible reason for this: First; due to lack of long range order, the impurity can be incorporated into the random network lattice of the amorphous material in such a way as to satisfy its bond requirements without leading to an extra electron (donor) or a missing electron (acceptor). Second; because of random disorder, there is a high density of localized states throughout the bandgap [3]. Their density is so high that they effectively pin the Fermi level, all of the extra electrons or holes that would be contributed by impurities are captured in the high density of localized states at the Fermi level and preventing its motion. As a result, amorphous silicon (a-Si) is not a suitable material for electronic device applications.

However, Chittick et al. discovered in 1969 that the incorporation of hydrogen by decomposition of silane (SiH_4) in plasma drastically reduced the density of gap states by saturating DBs in the amorphous silicon network. Then, this new material is named

as hydrogenated amorphous silicon (a-Si:H)[4]. The density of localized midgap states decreased down to 10^{15}-10^{16} cm^{-3} in range. This discovery attracted much attention on hydrogenated amorphous silicon based materials in worldwide. A few years later, in 1975, Spear and Le Comber showed that hydrogenated amorphous silicon could be doped as n-type or p-type by phosphorus and boron atoms respectively [5]. Because of the fact that a-Si:H materials can be doped as n-type or p-type, this material have the chances to be used as p-n junction device and for other electronic device applications. Right after that, in 1976, Carlson and Wronski made the first a-Si: H solar cell [6]. Those discoveries and outstanding optoelectronic properties of hydrogenated amorphous silicon over the crystalline counterpart such as a continuously adjustable bandgap through alloying with germanium, hydrogen and carbon, large optical absorption coefficient over the visible wavelength range, low densities of midgap states and capability of depositing large area thin films on various substrate materials triggered worldwide interest on hydrogenated amorphous silicon based films and their device applications. Those are thin film transistors for flat panel displays, solar cells for power generation, xerography, image sensors, radiation detectors, photovoltaic cells for calculators, watches, photoreceptors, electro photography, led printers and also base for many other electronic device applications.

The most popular techniques to deposit a-Si: H thin films are direct current (DC) glow discharge, radio frequency (RF) plasma enhanced chemical vapor deposition (PECVD), RF magnetron sputtering and Hot-Wire chemical vapor deposition (HWCVD). In DC Glow discharge deposition process, the plasma is initiated by applying a direct current (DC) to triode system [7], where the discharge is maintained between a solid electrode and a grid and the substrate is mounted on a third electrode. The substrate is grounded, so that energetic ions from the discharge are decelerated as they move from the cathode to the growing film. On the other hand, in RF-PECVD deposition process the plasma is initiated by applying an RF signal to diode system, where the discharge is maintained between two electrodes, one of which serves as the holder for the substrate. Electrons collide with silane to dissociate the silane molecules into a mixture of reactive species of ions and free radicals and these species are diffused to the surface of the substrate [7]. In RF Magnetron sputtering, a gas, usually argon, is ionized by RF electric field [8]. The positive ions are then accelerated in the electric field towards a target of the material to be deposited, atoms of the target are kicked out, and evaporate into the vacuum chamber. By holding a substrate opposite of the target,

the evaporated material condenses on a substrate and a thin film is formed. The Hot-Wire Chemical Vapor Deposition (HWCVD), also known as Catalytic Chemical Vapor Deposition (cat-CVD), is a deposition technique that consists of the thermal decomposition of SiH_4 and H_2 mixtures at a resistively heated filament (usually tungsten or tantalum) at thousands of Kelvin (K^0) to produce atomic silicon and hydrogen, then low H-content device quality a-Si: H films are produced. The HWCVD has been proven to grow silicon thin films (amorphous and microcrystalline) at relatively high deposition rates (up to some nm/s) and low substrate temperatures (lower than 200^0C). This makes this technique very feasible to obtain large area thin film silicon devices onto low cost substrates [9].

As mentioned above in the deposition methods, due to non-equilibrium deposition process, there exist localized states in the band gap of material. These are called midgap states originating from impurities or from atoms which have either fewer or more covalent bonds than desired by their normal valency[2]. These defect states are believed to be three-fold coordinated silicon DBs[10]. The defect states present as grown (or in the annealed state) are called native defect states. They control many transport properties such as photoconductivity and sub-bandgap absorption in films. Even though hydrogenation of a-Si network decreased the large density of localized defect states for an acceptable level, after a short period of time, in 1977 Staebler and Wronski [11] discovered that dark and photoconductivity measured in a-Si:H thin films degrade under extended light illumination. This degradation is completely reversible after annealing the films at temperatures above 150^0C in dark. Then the characteristic of sample is restored to its original values. This effect is intrinsic to a-Si:H films and known as the Staebler-Wronski effect (SWE). In this effect, new defects are created by light illumination in the band gap of a-Si:H. Because of this effect, electrical characteristics of films (dark and steady-state photoconductivity) and conversion efficiency of solar cells made using a-Si:H absorber layer decrease enormously from its initial values. Later works showed reversible light induced changes in many other properties of the material such as photolumiscence[12], density of states measured by electron spin resonance(ESR)[13], sub-band gap absorption[14], diffusion length of carriers[15] and solar cell performance[16]. In adition, field effect measurements[17] also show that new states are created both in the upper and the lower half of the band gap, which is also evidenced by photoconductivity measurements using above-band gap

and sub-bandgap light[18]. Due to light induced changes, the SWE in a-Si:H is the most diffucult challenge that this material faces before its larger scale applications.

The degradation experiments carried out under 1 sun illumination (1 sun light intensity is called AM 1.5 with total power of 100mW/cm^2) was then later performed under high intensity (~10-50suns) light soaking to determine the final value of the localized midgap defect states and thus the stabilized solar cell efficiencies. Both experiments on either thin films and solar cells indicated that the densities of localized midgap defect states increases up to 5-7x10^{17} cm^{-3}. This greatly reduces the solar cell performances and limited the predicted lifetime for solar cells. Then the new goals were set by the Standard Material Adisory Research Team (SMART)[19] to reduce the final density of saturated defect density by changing the deposition conditions. This new approach was to produce more stable a-Si:H films for solar cells. There are two new approaches for this goal: First one is to use hydrogen dilution technique in RF-PECVD and DC Glow discharge systems and second one is development of HWCVD technique. Hydrogen dilution technique is the introduction of H_2 gas through the silane(SiH_4) in the plasma at some definite ratios, R=(H_2)/(SiH_4+H_2). The dilution ratio may change from 0 to 10 or to even higher values. It was shown that increasing H_2 dilution ratios(0-10) improves both thin film and solar cell performance after long-term degradation studies [20-23]. However, increasing the dilution ratio more(R>25), does not result in more stable a-Si:H films. But microcrystalline phases start forming in the matrix of a-Si:H. Then most of the electrical and optical parameters such as band gap and defect densities change. This new material is not hydrogenated amorphous silicon anymore but hydrogenated microcrystalline silicon(μc-Si:H). The second new approach to make more stable a-Si:H films was hot-wire CVD deposition process developed at NREL[9,24]. In this technique higher substrate temperatures allows the growth of more stable materials with greater deposition rates and lower hydrogen content. Simple system design eliminates use of very high frequencies in deposition[25,26].

Since the localized midgap states are modified enormously by the deposition conditions and they determine the electrical and optical properties of films and solar cells, their characterization have great importance. Commonly used techniques to characterize the properties of thin films are summarized below. Optical absorption using Transmission&Reflection data [27], spectroscopic ellipsometry [28] and photoelectron spectroscopy [29] techniques are used to probe the extended states at higher energies. Transient photoconductivity and drift mobility measurement techniques are used to

probe exponential CB and VB tail states [30]. In addition Subgap absorption spectroscopy is also used to characterize the VB tail states [31-33]. In a-Si:H thin films, extended states and exponential valance band tail states are well characterized and almost the same for good quality films prepared by different deposition techniques. For example, the slope of the VB tails is around 50meV and that of the CB tails is between 25-30meV for device quality a-Si: H [2]. However the defects localized in the band gap other than tail states differ enormously in any sample due to deposition conditions. Therefore, there is no unique a-Si: H thin films as reported by SMART group [19]. Electron spin resonance, (ESR), is one of the fundamental techniques used to probe the midgap states, which are occupied by single electron, called D^0 states [34]. Whereas this technique is very sensitive to large density of surface states for films of a micron thick. Space charge limited currents (SCLC) was used to probe defect states over a limited energy range, around the Fermi level [35]. Capacitance techniques [36] cannot be applied to the undoped intrinsic a-Si: H films due to its high resistivity. Both SCLC and capacitance techniques cannot be used on films because these techniques require the use of thin doped layers as contacts. Steady-state photoconductivity is sensitive to both density and nature of all defect states acting as the recombination centers between the quasi-Fermi levels in the bandgap [37]. Sub-bandgap absorption measurements are sensitive to the densities, nature and energy location of defect states below and above the midgap [31]. The techniques used to measure sub-bandgap absorption are Photothermal Deflection Spectroscopy (PDS)[38], Constant Photocurrent Method (CPM)[39] and Dual Beam Photoconductivity (DBP)[40]. Among these techniques, PDS is sensitive to transitions from and into the defect states near midgap and is also sensitive to surface and interface states [41] just like ESR. In contrast, CPM detects signals from the bulk of the film and is sensitive to defect states only below the Fermi level. These states are also detected by DBP, which also has the advantage that using different bias light intensities allows the densities, nature and energy location of midgap states below as well as above the Fermi level to be investigated. Furthermore, temperature and intensity dependence of photoconductivity can also be used to probe the effects of nature and densities of midgap states over a wide energy range in the bandgap[42-53].

Vanier et al. [43] have reported the behavior of Arrhenius plots of low temperature σ_{ph} for different light intensities in 1981. The main feature of those plots is the existence of thermal quenching which is the increasing of σ_{ph} with decreasing

temperature in particular temperature ranges. Moreover, the σ_{ph} maxima and the minima for different light intensities seem to be thermally activated. Among the models proposed, some only attempted to explain the general behavior of σ_{ph} [43,48,54-57] while the others deal with the physical parameters of the material studied [37,58].

Finally, McMahon and Xi [49], Okamoto et al. [58], Vaillant et al. [59] and Yoon et al. [51] have used, in their σ_{ph} simulation, the well known scheme for the localized gap states in a-Si: H including an exponential energy dependence of the band tails [60,61] and the [DB] defect with a positive correlation energy [62,63]. However, these numerical simulations are unable to explain all the experimental features of σ_{ph} against 1000/T curves nor do they allow information to be obtained directly on the physical parameters of a-Si: H.

According to summary above it can be said that the interpretation of the general behavior of photoconductivity at different temperatures is subject to controversy. In particular the different features (maximum, minimum, activation energies, variation in these energies at low temperatures, etc.) on photoconductivity versus 1000/T curves for different light intensities have not been related directly to the localized states in the mobility gap[52]. The data published by different groups show that a wide range of properties can be observed in samples produced under variety of deposition conditions. Such properties may be correlated with alloy composition and structure, including hydrogen concentration, silicon-hydrogen bonding configurations, impurity content, film morphology etc. [43]

Even though there are several diffuculties to characterize the localized defect states in detail, there are no well established theoretical model for these defect states yet. Cohen-Fritzsche-Ovshinski (CFO) proposed the first defect model, which consists of conduction and valence band tail states only. This model can only explain the experimental time-of-flight measurement of electrons and holes, which is governed by the exponential tail states only in the energy range of 0.1 to 0.3 eV from the mobility edges [64]. Then Stutzmann proposed that weak Si-Si bonds are broken during the light soaking and they are converted to the neutral silicon DB defects with an increase of ESR signal and decrease of photoconductivity [65]. Thus, in this model significant charged defect states, $D^-$and D^+, are not present and only a negligible amount of charges occur from the overlapping of donor-like and acceptor-like defect states around the Fermi level. In this model, $D^-$and D^0 defect states have positive correlation energy [34].

In contrast, Adler [10] proposed a model where pairs of oppositely charged DBs (D^+ and D^-) get converted into neutral DBs (D^0) by trapping electrons and holes. The model assumes a negative correlation energy for the D defect. This model was supported by the work of Bar-Yam and Joannopoulos[66] who showed that a distribution of thermodynamic transition energy levels of the three-fold coordinated Si DB defects could lead to large concentrations of charged defects, $D^-$and D^+, in inhomogeneous a-Si:H. Alternatively, Pantelides proposed a model that the defect states in a-Si:H are the combination of three-fold and five-fold coordinated Si DB defects in contrast to the defect models based on three-fold coordination. These five-fold coordinated defects are called floating bonds [67]. According to this model, $D^-$and D^+ defect states have negative correlation energy like in Adler's model and large density of charged defect states, $D^-$and D^+, are present in a-Si: H materials.

In 1990, Branz and Silver used the approach of Bar-Yam and Joanopoulos and considered the thermodynamic equilibrium of the three-fold coordinated Si DB defects in a-Si: H and showed that potential fluctuations due to material inhomogeneity can result in large concentrations of charged DB defects [68]. Further support of charged defects in a-Si: H was proposed by Schumm and Bauer [69] and Powell and Dean [70] with their "defect pool model", which also predicted the presence of neutral, negatively and positively charged silicon DB states with a negative correlation energy. There have been many results which include light induced ESR (LESR)[71], IR-LESR [72], electron spin-echo-envelope modulation (ESEEM) study [73], temperature dependence of photoconductivity [58], sub-bandgap absorption model [31-33], support the idea that charged defect states with negative correlation energy exist in undoped a-Si: H films. However, those models cannot explain all the observed experimental results in films and solar cells consistently.

Recently, Branz[74-76] and Biswas et al.[77,78] proposed new defect models for the light induced metastability in a-Si:H. The model proposed by M. Branz[54] about light-induced metastability is called *H-collision model*. The model suggests that recombination of excess carriers creates mobile H atoms and DBs. Normally, mobile H retraps to DBs and there is no net creation of DBs. Whereas, rare H collisions can account for the SW effect. Two metastable DBs are created when two mobile H meet and associate into a metastable complex containing two Si-H bonds, $M(Si\text{-}H)_2$. The created DBs are remote from the $M(Si\text{-}H)_2$ center. The model is consistent with spectroscopic constraints on microscopic SW models and with the kinetic experiments,

including light-induced annealing and pulsed illumination[75], continuous illumination below room temperature [76], and excitation with energetic electron beams [79].

The model proposed by Biswas at al. for the generation of metastable DBs is called *silicon network rebonding model*. It involves breaking of weak silicon bonds and formation of isolated DBs, through rebonding of the silicon network. Hydrogen motion is not involved in metastable defect formation. Defect formation proceeds by breaking weak silicon bonds and formation of DB-floating bond (FB) pairs. The FBs migrate through the network and annihilate, producing isolated DBs. This is similar to Pantallide's Floating bond model. There are three steps for the metastability mechanism[78]. In the first step, weak silicon bonds are broken from non-radiative recombination of photoexcited carriers. The bond breaking generates a pair consisting of a dangling bond and a nearby floating bond. In the second step, the FB diffuses away from the location of the DB, and migrates through the silicon network since the FB is a mobile species. In the third step, two migrating FBs in the network come in close proximity and recombine generating a new weak bond in the lattice. The net result is to produce DBs that are spatially separated from each other, consistent with spin resonance data [73].

There is a strong analogy between *the H-collision model* proposed by Branz and the *silicon network rebonding model* by Biswas at al. The FBs of the silicon network-rebonding model are the analog of the H in the H-collision model. The mathematics of defect formation for the silicon network-rebonding model is very similar to the collision model. There are however major differences in the physics of defect creation. Most notably, hydrogen is not directly involved in the degradation; instead defect creation involves rearrangements of the silicon network. Atomic diffusion is not present in silicon network rebonding model, although the diffusion of H is essential in the H-collision model. Finally, these models predict most of the observed experimental facts but they cannot answer all the questions related to the SW effect yet.

1.1 Thesis Objectives

The density of states (DOS) and the stability are very fundamental properties of a-Si: H thin films with respect to their solar cell applications. Sensitivity to light induced degradation, SWE is known to be an intrinsic property limiting solar cell applications of a-Si: H. Therefore it is necessary to obtain reliable information about the nature of the native and light induced defect states. Improved understanding of the defect states in a-Si: H based materials will lead to further developments in a-Si: H technologies such as solar power generations and LCD displays. Characterization has been essential to the advancement and realization of photovoltaics. Almost every characterization technique that has had application to semiconductor analysis has also had either direct or modified use for photovoltaic investigations. The objective of this thesis is to characterize the effects of native and light induced defect states in the annealed and light soaked states in undoped a-Si: H thin films prepared using different deposition techniques. For this purpose, steady-state photoconductivity measurements will be carried out for different light intensities and temperatures down to 90 K. Then, the results are going to be discussed in terms of existing defect models developed for undoped a-Si: H.

CHAPTER 2

MATERIALS AND METHODS

2.1 Sample Preparation

Hydrogenated amorphous silicon, a-Si:H, thin films used in this study were deposited using DC Glow discharge technique in BP Solarex (Pennsylvania), radio frequency (RF) plasma enhanced chemical vapor depotision (PECVD) at the Pennsylvania State University and United Solar Systems Corporation (USSC) of Michigan, RF magnetron sputtering deposition technique at University of Illinois, Urbana-Champagne, and Hot-Wire CVD technique at the National Renewable Energy Laboratory at Colorado. The samples used in this thesis are listed in Table 2.1.

Table 2-1. Samples used in this thesis

DEPOSITION TECHNIQUE	DEPOSITION PLACE	SAMPLES
RF-PECVD DILUTED	Pennsylvania State University, PA(USA) United Solar Systems Corporation (USSC) of Michigan-USA	Lj-51 L12229 L12231
RF-PECVD UNDILUTED	Pennsylvania State University, PA(USA)	4m Yl-6b SN128
RF MAGNETRON SPUTTERING	University of Illinois, Urbana-Champagne-USA	Sputtered
HOT-WIRE CVD	National Renewable Energy Laboratory at Colorado-USA	H608
DC GLOW DISCHARGE	BP Solarex (Pennsylvania)-USA	SmartB1 SmartB2 SmA1

The deposition conditions used to make the undoped a-Si:H thin films using RF-PECVD system at Penn State University were as follows: the total chamber pressure was 0.5 torr, pure silane(SiH_4) flow was 15 sccm, and the RF power density was

200 MW/cm^2. The substrate temperature, T_s was varied from 180 ^{0}C to 300 ^{0}C. The gas was injected through the cathode and the substrates were mounted on the anode for each film deposition. These were Corning 7059 glass substrates for transmission and reflection measurements and Corning 7059 glass substrate with preevaporated Nichrome coplanar electrodes for dark conductivity, steadystate photoconductivity and sub-bandgap photoconductivity measurements. The thicknesses of the films vary from 0.7μm to 2.0 μm[80].

Undoped a-Si:H films prepared using DC PECVD system at Solarex Thin Film Division have following deposition conditions [81]: pure silane flow was 200 sccm, plasma current was 0.135 mA/cm^2, the pressure was 0.5 torr, and the substrate temperature between 200 ^{0}C and 300 ^{0}C. The film thicknesses ranged from 0.5μm to 1.5μm and were deposited onto quartz substrates for transmission and reflection measurements and 7059 glass substrate with coplanar NiCr electrodes for conductivity measurements.

Deposition conditions[82] used to prepare a-Si:H thin films using RF Magnetron sputterring system in University of Illinois, Urbana-Champagne were deposited in an ultrahigh vacuum chamber; the partial pressures of O_2, CO and H_20 were less than $1x10^{-9}$, $1x10^{-9}$ and $2.5x10^{-9}$ Torr, respectively. The films were grown using high purity argon and hydrogen gases and a high purity 5 x 12 in. Cystalline silicon target. The total C_H of the films was independently controlled by adjusting the hydrogen partial pressure in the discharge at a constant substrate temperature of 230 ^{o}C. The hydrogen partial pressure was increased from 0.2 to 1.2 mTorr and the argon partial pressure was kept constant at 1mTorr. The deposition rate was ~30 to 200 Å/min. and controlled by the cathod current(0.25-0.80A).

The standard conditions[23] for growing a-Si:H film in National Renewable Energy Laboratory were 20-50 sccm of SiH4 and 10 mT pressure. A straight or spiral tungsten filament with a diameter of 0.5 mm and the substrate 4-5 cm above it. A spiral shaped filament had proven to better accommodate to the thermal stress due to the heating and cooling of the filament, enabling an increase in the filament lifetime. The filament was heated by an AC or DC current (14 A) to about 1900 °C.

The deposition systems for DC Glow discharge, RF-PECVD, RF Magnetron sputtering and HW-CVD techniques are shown in Figure 2.1 to Figure 2.4 respectively.

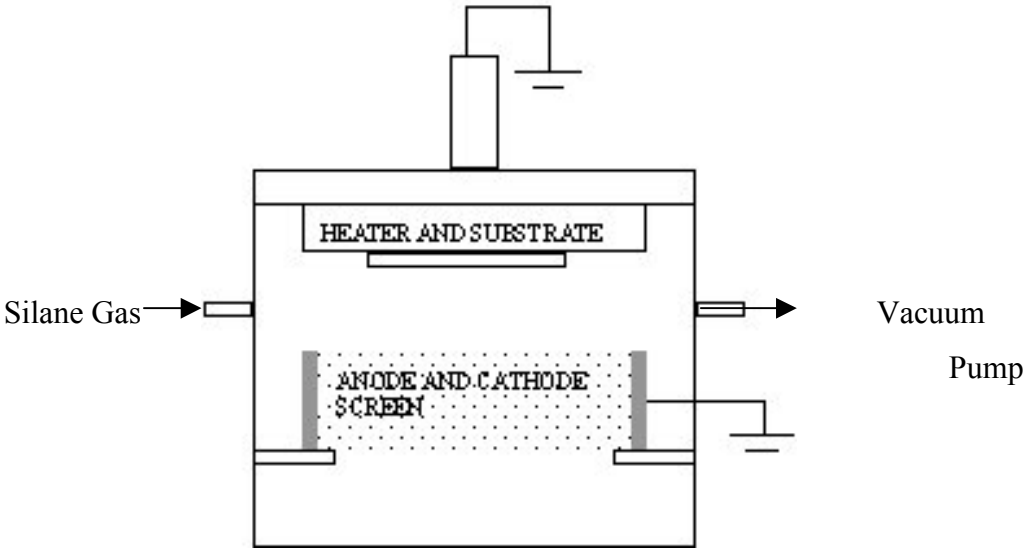

Figure 2.1 DC Glow discharge system.

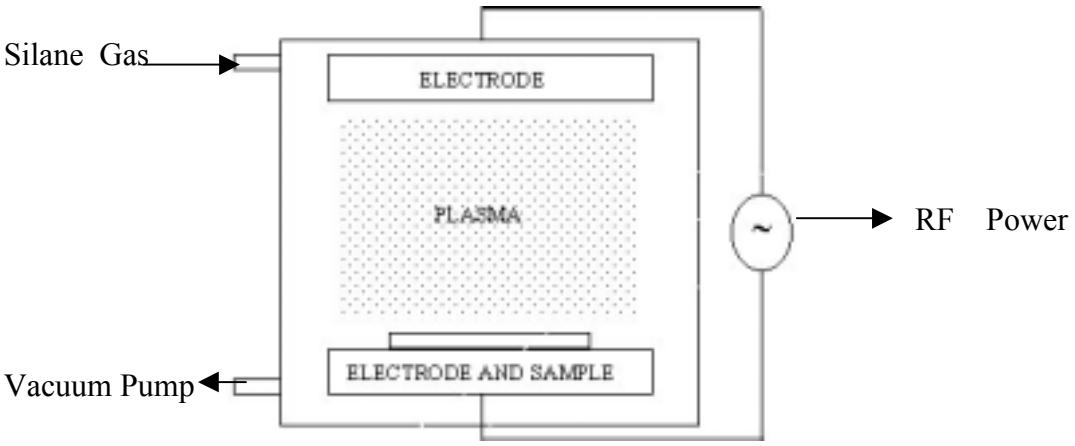

Figure 2.2 Radio Frequency Plasma Enhanced Chemical Vapor Deposition RF PECVD System.

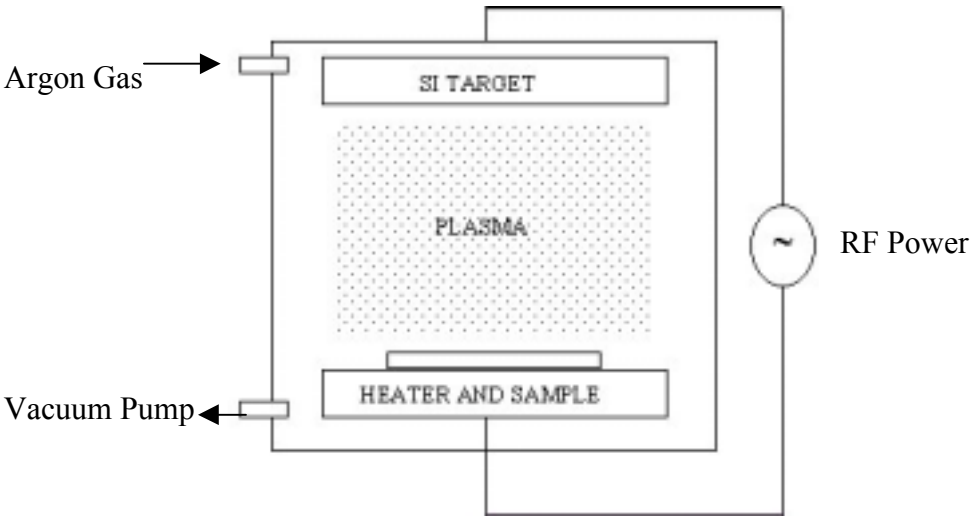

Figure 2.3 RF Magnetron sputtering system.

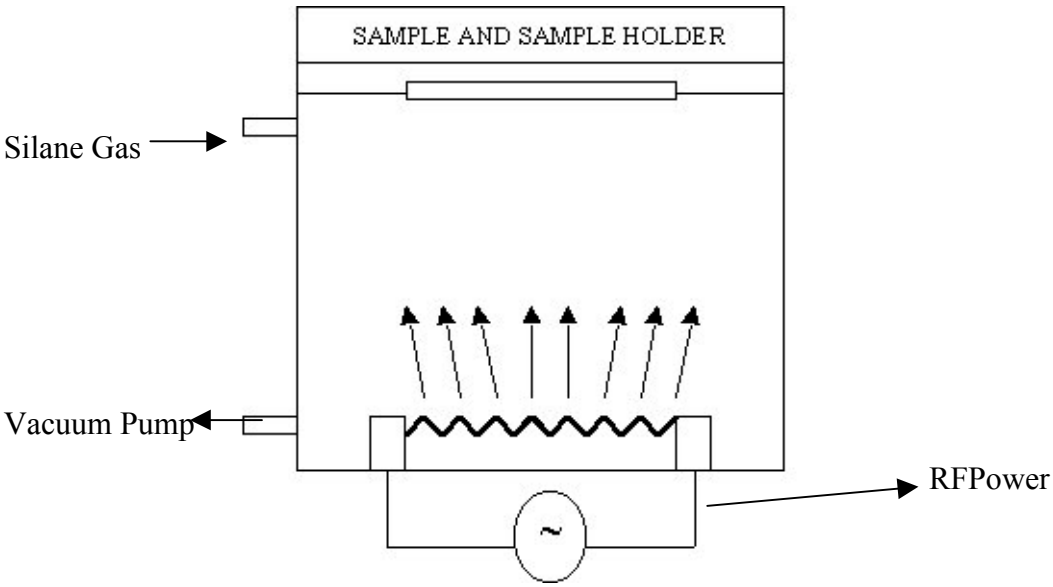

Figure 2.4 Hot-wire chemical vapor deposition sysyem.

2.2 Steady state photoconductivity system

Steady state photoconductivity system was designed for this study at İzmir Institute of Technology(IZTECH). It consists of a measurement box and ENH(Halogen Photo Optic Lamp at 250W) white light source as shown in Figure 2.5. ENH white light source operates under 115V and 2.05A constant current mode. A small fan is fixed to

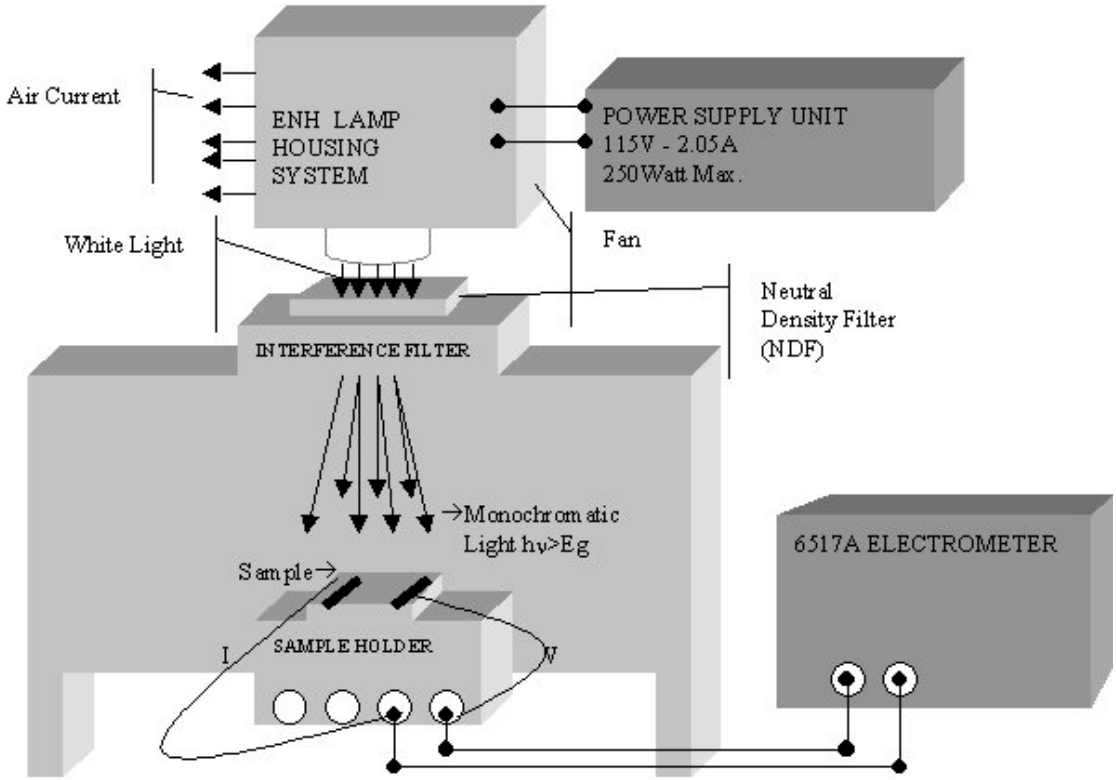

the housing not to

Figure 2.5 Steady State Photoconductivity System

cause overheating of ENH bulb. The monochromatic, uniformly absorbed, light flux was obtained using interference bandpass filters with energy $h\nu=E>E_{optical}$ of the sample studied. The incident white light flux was calibrated using a calibrated silicon detector for the appropriate interference filters. A-Si:H sample is placed over sample holder and electrical connections are obtained using BNC connectors. A constant voltage is applied across the coplanar electrodes and photocurrents were measured using a Keithley 6517A Electrometer. Measurements were carried out in the Ohmic regime of current

voltage curve. Intensity of monochromatic light was changed using neutral density filters whose transmission values changes from 0.1% to 50%. The sample geometry is shown in Figure 2.6a and 2.6b. Steady-state photoconductivity is calculated using the measured photocurrent, applied voltage and sample geometry as shown below.

Using Ohm's law:

$$R = V/I_{ph} = [1/\sigma_{ph}]*[d/(t*l)] \quad \textbf{(Eq. 2.1)}$$

$$\sigma_{ph} = [I_{ph}*d]/[V*t*l]\ (\Omega\text{-cm})^{-1} \quad \textbf{(Eq. 2.2)}$$

where I_{ph} is measured photocurrent, V is the voltage applied across electrodes, d is the seperation between electrodes (the length of conductor), t is the thickness of the film, *l* is the length of electrodes.

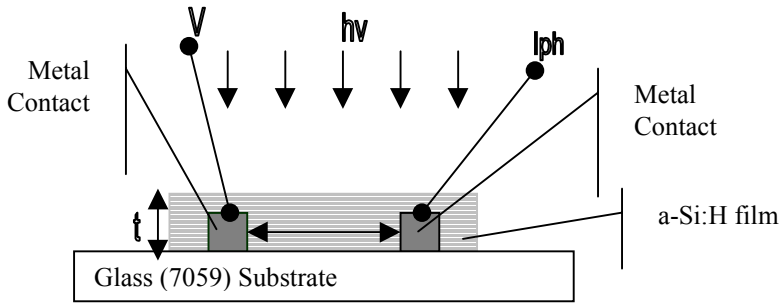

Figure 2.6a Side view of an a-Si:H thin film on glass substrate.

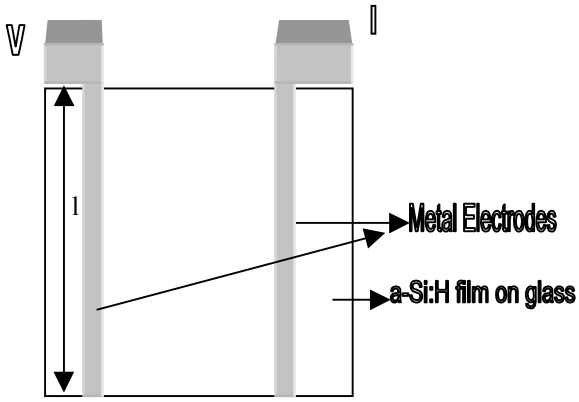

Figure 2.6b Top View of an a-Si:H sample with coplanar geometry.

2.3 Annealing System

A vacuum annealing box was designed and manufactured at IZTECH to anneal the samples and measure the dc dark conductivity. This is schematically shown in Figure 2.7. A vacuum pump connected to the box decreases to the pressure down to 0.5 Torr. Temperature measurement was carried out using Omega CL8500 Meter/Calibrator with a K-type thermocouple mounted on a glass substrate and fixed on copper block as shown in Figure 2.8. A 25 watt heater fixed under the copper block heats the sample. Temperature increases up to 200^0 C from room temperature. The samples are annealed in vacuum about several hours at 180^0 C. The dc dark currents were measured by using Keithley 6517A Electrometer via the electric feed-through connections attached to the annealing box. The dc dark current measurements are carried out from 180^0 C to room temperature. Then, dc dark conductivities are calculated using applied voltage, measured dark current and the sample geometry. By plotting semi-log of dark conductivity versus 1000/T, the slope yields activation energy of dark conductivities, which is almost equal to the position of the dark Fermi level from the conduction band mobility edge as shown below:

$$\sigma_D = e\mu N_c e^{[-(Ec-Ef)/kT]} = \sigma_0 exp^{[-(Ec-Ef)/kT]} \qquad \textbf{(Eq. 2.3)}$$

where the plot of $\log(\sigma_D)$ versus 1000/T (called Arrhenius plot) yields $E_a = E_c - E_f$, the thermal activation energy of the dark conductivity, and $\sigma_0 = e\mu N_c$ is the exponential prefactor obtained.

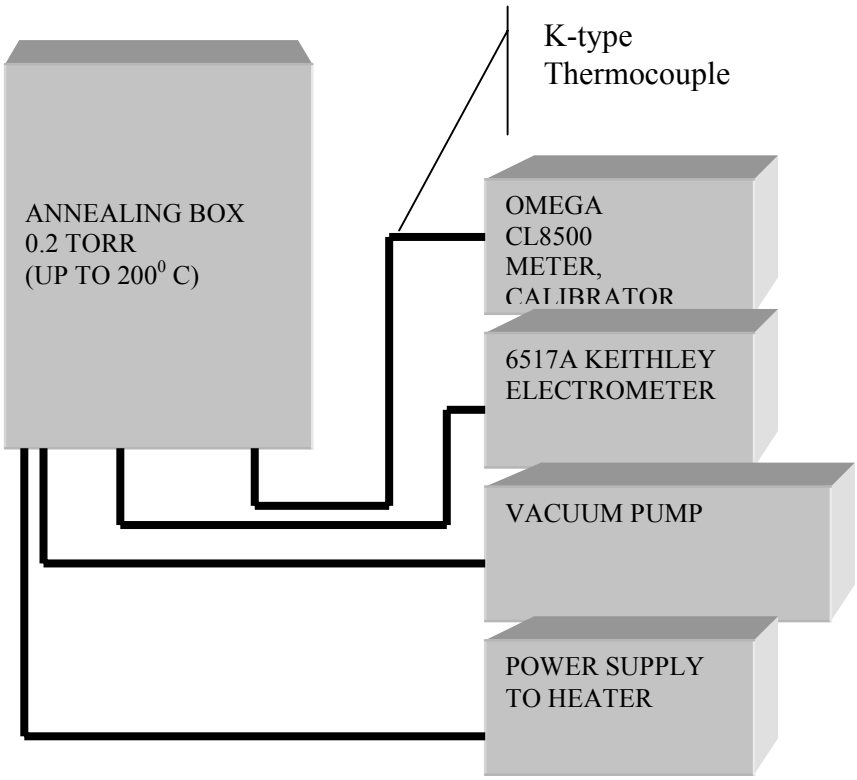

Figure 2.7 Vacuum Annealing System

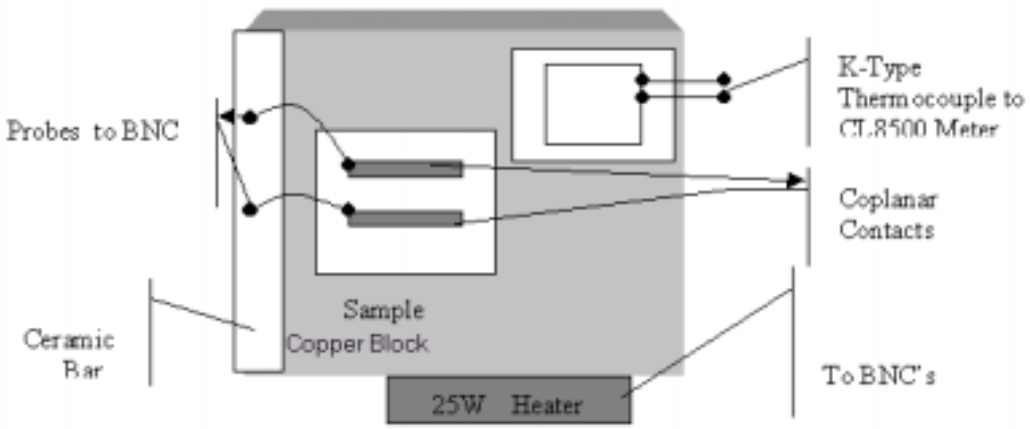

Figure 2.8 Top view of the sample holder and sample in vacuum annealing box

2.4 Light Soaking Station

One of the goals of this study is to investigate the effects of the light induced defect states (Staebler-Wronski defects)[11] on the electrical properties of undoped a-Si:H. For this purpose, an ELH(Halogen Photo Optic Lamp at 300W) white light station was designed and developed at IZTECH as shown in Figure 2.9. White light source uses 300W ELH bulbs and operates under 115V and 2.53A constant current mode. A small fan is attached to the housing to cool the light bulb and improve its lifetime. Light soaking was carried out for 10 hours for all samples under the same light intensity(a few suns). Samples were cooled using two different fans which blow air on the sample not to cause annealing effect during the soaking. The sample temperature was below 50^0 C during the soaking. Same product of ELH lamps were used throughout the study to eliminate any effects from the light output variations. After light soaking, the steady-state photoconductivity at room temperature for different light intensities and low temperature photoconductivity for three different intensities were carried out.

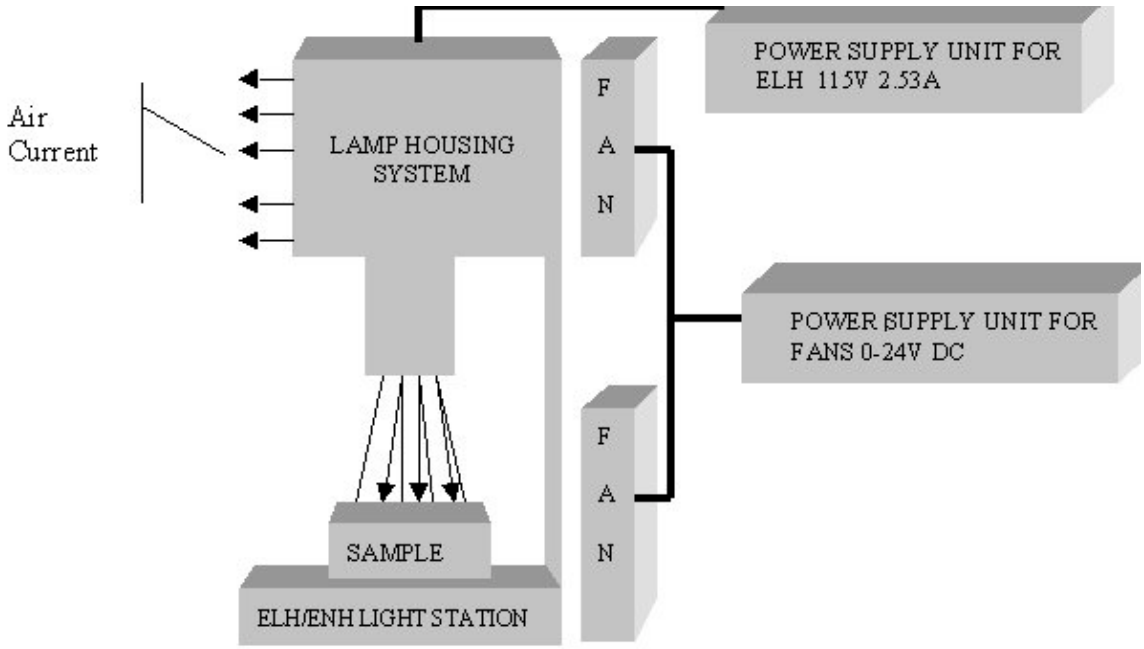

Figure 2.9. ELH Light Soaking Station

2.5 Low Temperature Photoconductivity System

The main goal of this thesis is to investigate the effects of defect states using temperature dependence of steady-state photoconductivity. For this reason, an experimental setup shown in Figure 2.10 has been developed for this study. The system includes a Coolstar Cold Head model 2/9, an Oxford Cryodrive 1.5 down to 10 ^{0}K, a Leybold Trivac Vacuum Pump, Termovac Sensor with tungsten filament for vacuum readings, a water cooling system for Cryodrive. Temperature measurements were done using Rd-Iron Temperature Sensor. Temperature and Helium flow rate were controlled using ITC 502 Temperature Controller unit by setting up P-I-D control parameters. Samples are mounted on a specially designed sample holder. Indium metal flakes were placed between the contacts and probes for better electrical contact. Red light diode arrays with $\lambda \cong 660$nm are used to provide uniform generation of photocarriers in the sample. The photocurrents were measured using a Keithley 6517A Electrometer and a constant voltage was applied from the same unit. Photocurrents were measured in the Ohmic regime of current-voltage curve. All the units were controlled using a computer program for ease of operation written in Object Bench Software which is seen in Appendix B. Illumination intensities were changed by changing applied voltage to the LED's from 3V to 10V.

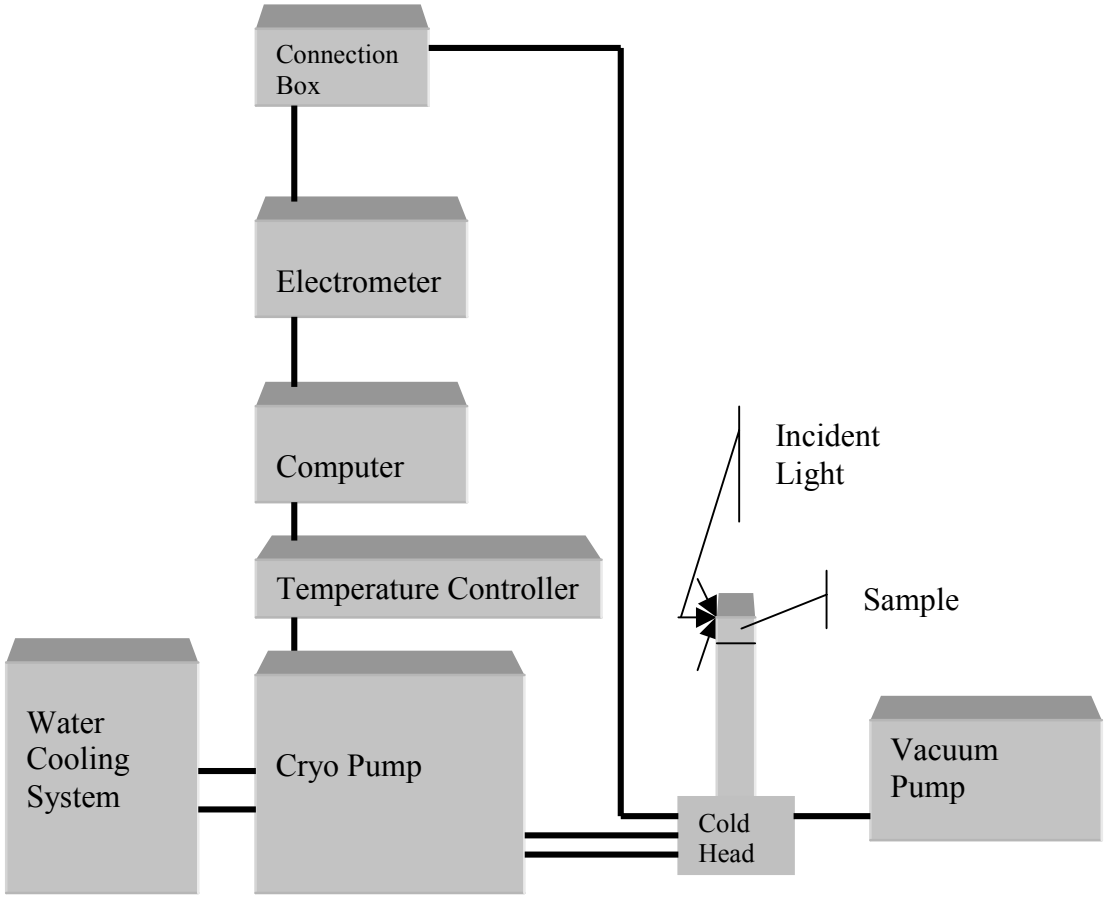

Figure 2.10. Setup used for low temperature photoconductivity measurements.

CHAPTER 3
ANNEALED STATE BEHAVIOUR OF A-Si:H

3.1 Introduction

It is well known that deposition conditions of undoped a-Si:H films change its electrical and optical properties substantially. It shows a wide range of as-grown or annealed state characteristics. In this chapter, undoped a-Si:H films in the annealed state are characterized using temperature dependence of dark conductivity, steady-state photoconductivity versus light intensity at room temperature, and steady-state photoconductivity versus temperatures down to 90 ^{0}K at different light intensities.

3.2. Activation Energy of Dark Conductivity

Undoped a-Si:H films behave like direct bandgap semiconductor with an optical bandgap of 1.70 eV to 1.80 eV and corresponding mobility gap of 1.80 eV to 2.0 eV. The bandgap is easily modified by the hydrogen content of the film during the deposition process. The Fermi levels for undoped a-Si:H films are expected to be around the middle of the bandgap, which indicates its position from the conduction band mobility edge, even though slightly n-type conduction have been occasionally reported in the literature. For the samples studied in this thesis, we have developed a vacuum system as described in Chapter 2 to measure the dark currents through the films as function of temperature. Dark currents of coplanar a-Si:H thin films were measured from 180 C to room temperature. Then, dark conductivities were calculated using applied voltage, measured dark currents and the sample's thickness and contact geometry. Semi-log plot of dark conductivity versus 1000/T, which is called Arrhenius plot, yields a straight line. The slope of this line is used to calculate the position of dark Fermi level in the bulk of the film.

Examples of Arrhenius plots for undoped a-Si:H films prepared under different deposition systems and conditions are summarized in following Figures: DC GD samples are on Figure 3.1, RF Magnetron sputtered and HW-CVD films are on Figure 3.2, undiluted RF PECVD films are on Figure 3.3, and diluted RF PECVD films are on Figure 3.4. Activation energy of dark conductivity, which is equal to the position of

dark Fermi level, E_f , from the conduction band, indicates that most of the films are undoped and Fermi level is around the middle of the badgap. As summarized in Table 3.1, only the sample 4m has activation energy of 0.60 eV, which shows slightly n-type conduction. This type of activation energy values have been occasionally reported for undoped a-Si:H in the literature. These values are also summarized in Table 3.1.

Table 3-1. Activation energy values of the samples obtained from the slope of Arrhenius plots.

DEPOSITION TECHNIQUE	SAMPLES	Activation Energy Ef (eV)
DC GLOW DISCHARGE	SmartB1	0.93
	SmartB2	0.93
	SmartA1	0.93
RF MAGNETRON SPUTTERING	Sputtered	0.96
HOT-WIRE CVD	H608	0.92
RF-PECVD UNDILUTED	4m	0.6
	Yl-6b	0.97
	SN128	0.86
RF-PECVD DILUTED	Lj-51	1.02
	L12229	0.98
	L12231	0.98

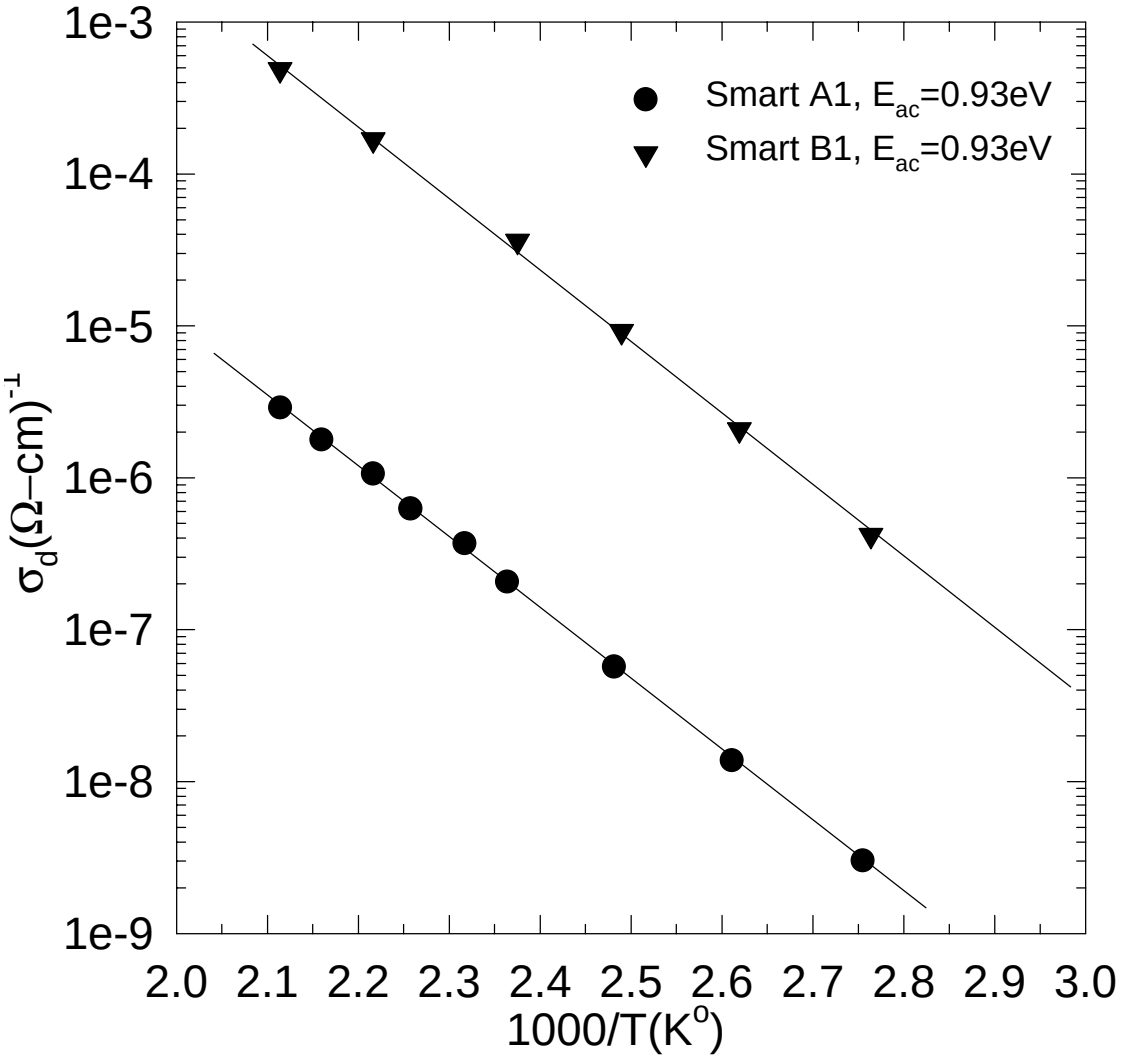

Figure3.1. Arrhenius plot of dark conductivity for a-Si:H films deposited in DC-Glow-discharge system.

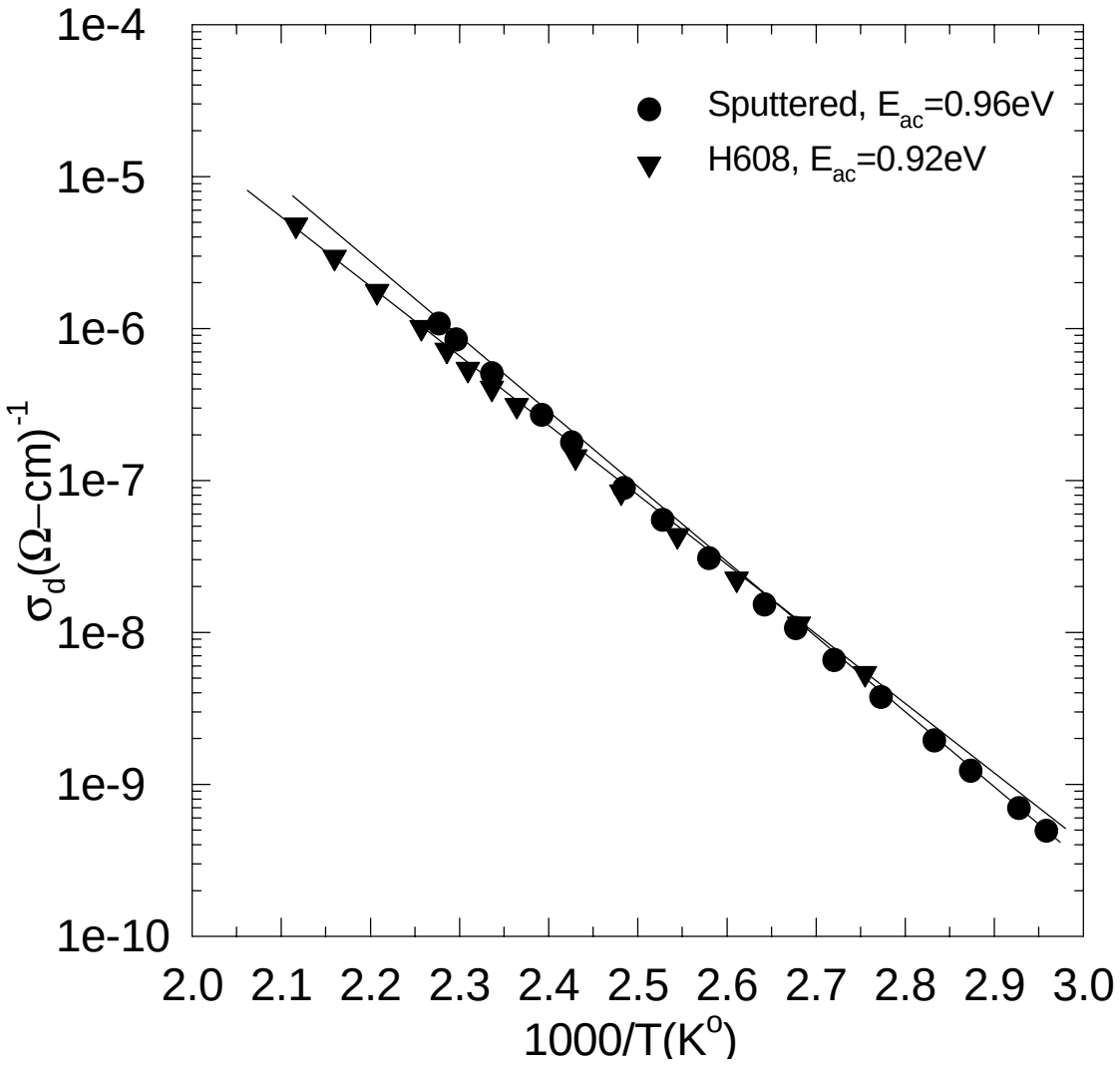

Figure3.2. Arrhenius plot of dark conductivity for a-Si:H films deposited in Hot-Wire CVD and RF-Magnetron Sputtering systems

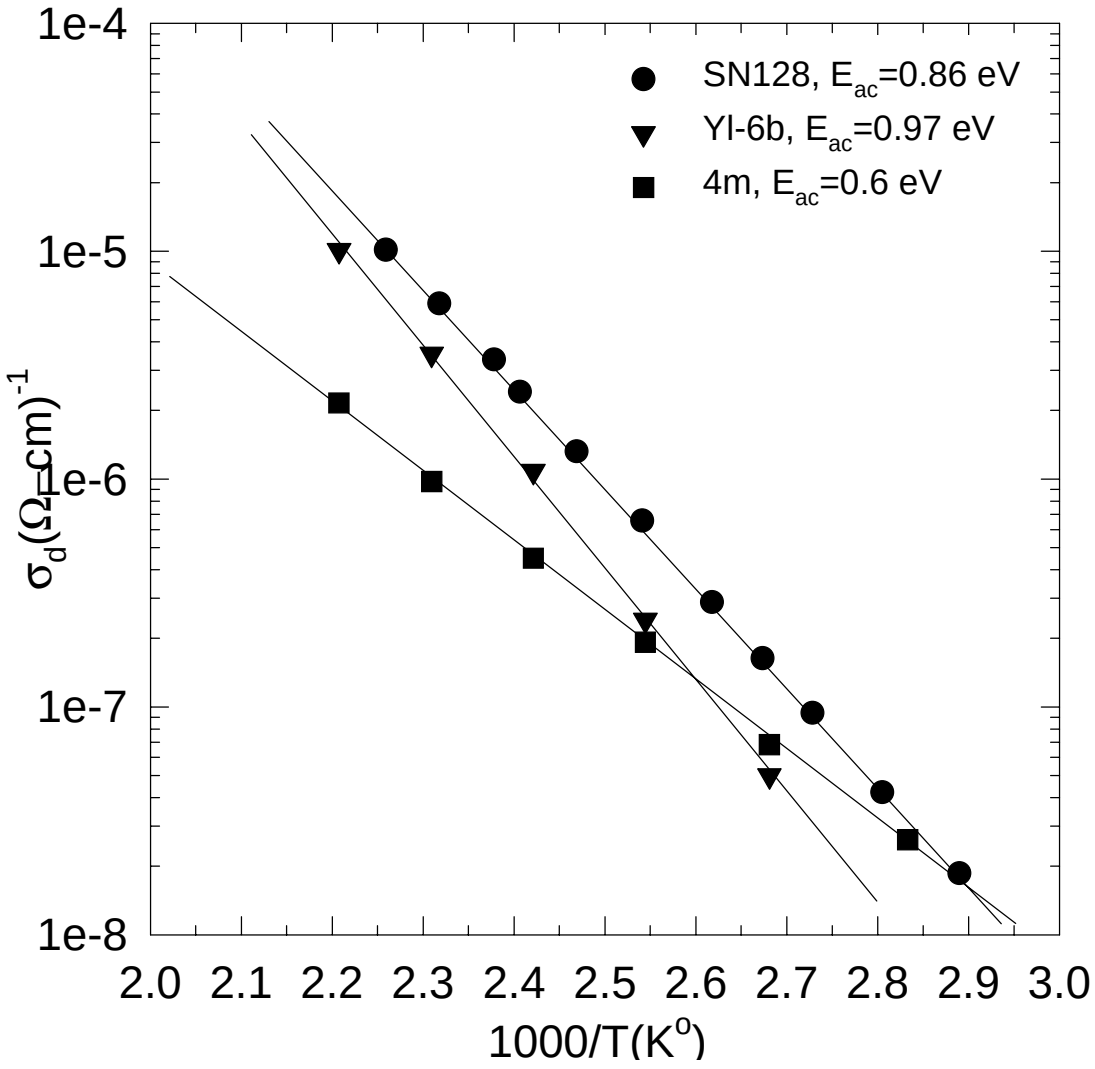

Figure3.3 Arrhenius plot of dark conductivity for a-Si:H films deposited in RF-PECVD system without H–dilution.

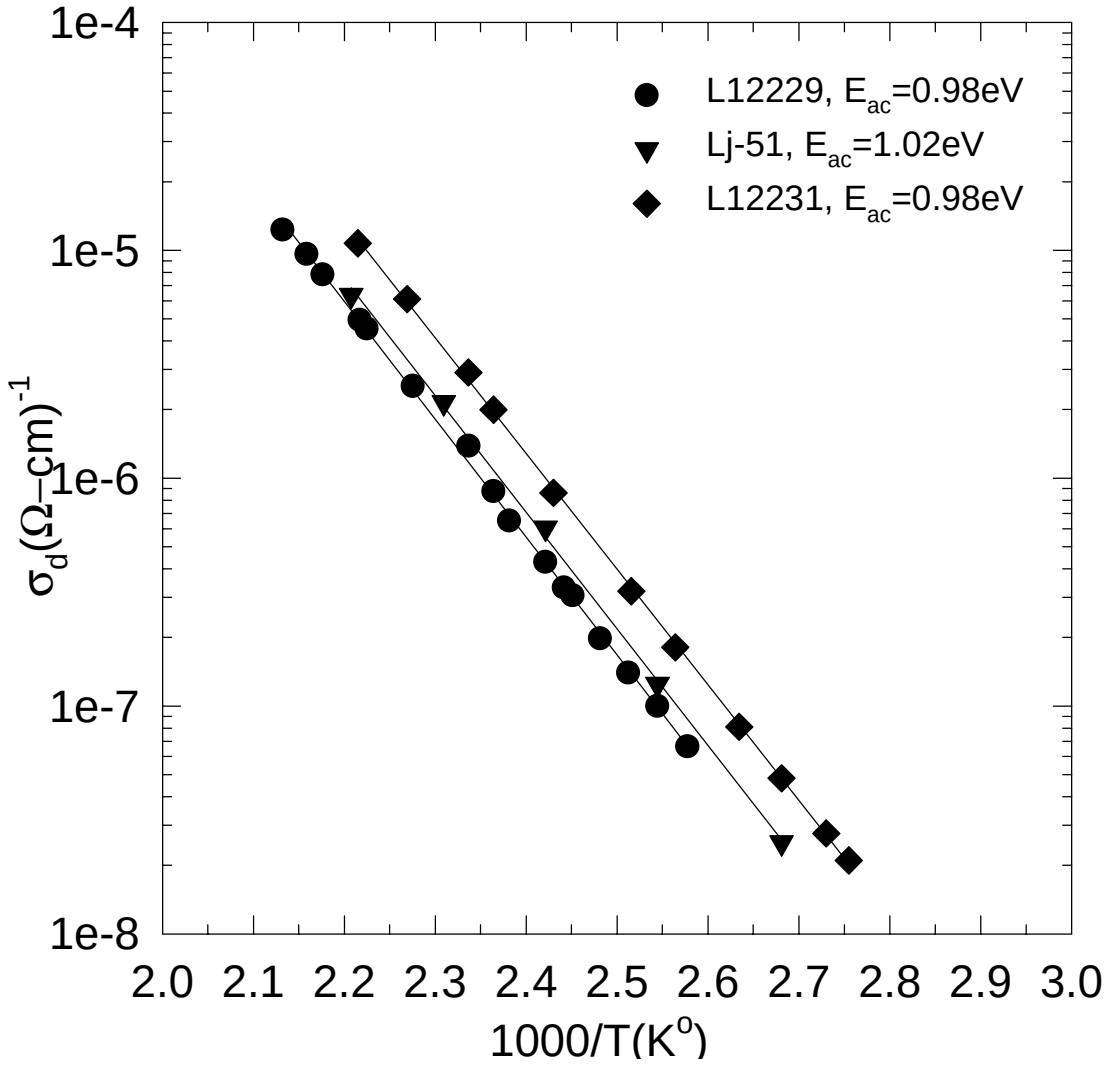

Figure3.4. Arrhenius plot of dark conductivity for a-Si:H films deposited in RF-PECVD reactor using H-dilution of silane.

3.3. Steady-state Photoconductivity

Steady state photoconductivity, σ_{ph}, in a-Si:H thin films shows non-integer power-law dependence on light intensity, F, or generation rate, G, as defined by $\sigma_{ph}=CG^{\gamma}$ where γ is the power and C is a constant. Meaning of γ has been given in Appendix A. It represents the nature of recombination kinetics between free electrons and holes at the extended states. Steady-state photoconductivity measurements at room temperature were carried out using monochromatic red light with energy, E= 1.87 eV, which is greater than the optical gap of films studied here. Maximum intensity of monochromatic light was decreased to lower levels using neutral density filters, then intensity dependence of photoconductivity was obtained for all the samples in the annealed state. Due to variations in the deposition conditions, the magnitude of photoconductivity can show a wide range variations. However, log-log plot of photoconductivity versus light intensity always shows a straight line. The slope of straight line yields the power γ. These experimental results are illustrated in the follwing Figures: DC GD fims in Figure 3.4, HW-CVD and RF Magnetron sputtering films in Figure 3.6, Undiluted RF PECVD films in Figure 3.7, and H-diluted RF-PECVD films in Figure 3.8. It can also be seen from Table 3.2 that γ values are less than unity for all films. They are not equal to 0.5 either, which is a direct indication of recombination of electrons in the conduction band with free holes in the valence band. However, γ values less than unity is still representing the recombination of free electrons in the CB with free holes in the VB through the recombination centers in the bandgap. For this reason, intensity dependence of photoconductivity infers that defect states in the bandgap of a-Si:H is playing the major role. The values of γ change from 0.72 to 0.90, which is very close to unity. That could be due to differences in the density and energy distribution of defect states in the bandgap. It is not possible to obtain further information about these defect states using the power of intensity, γ.

Even though the values of the exponent γ are very close to each other among the films, the magnitude of photoconductivity at 100% intensity of monochromatic light can have a wide range of values. As summarized in Table 3.2, it changes from $1.0\text{x}10^{-7}$ $(\text{ohm-cm})^{-1}$ to $16\text{x}10^{-7}$ $(\text{ohm-cm})^{-1}$. This could be due to differences in the densities of defect states in the bandgap and also differences in the optical gap of samples. Due to incorporation of hydrogen in the films during deposition, optical gap can change from 1.70 eV for undiluted films and 1.82 eV for diluted films. However, all films exhibit

very good photoconductivity as compared with those measured in the dark. Conductivity increase by a few orders of magnitude upon light exposure. Because of that the films will serve very good absorber layer for solar cells. Since photoconductivity depends not only on the densities of defect states in the bandgap, but also their nature, carrier capture cross sections as well as the absorption coefficient and mobility of free carriers, it cannot be a direct tool to get information about these defect states.

Table 3-2. Steady-state photoconductivity in the annealed state

DEPOSITION TECHNIQUE	SAMPLES	σ_D(R.T)$(\Omega\text{-cm})^{-1}$	σ_{Ph}(100%)$(\Omega\text{-cm})^{-1}$	γ values
DC GLOW DISCHARGE	SmartB1	8.0×10^{-10}	1.3×10^{-7}	0.85
	SmartB2	8.3×10^{-10}	1.7×10^{-7}	0.85
	SmartA1	7.0×10^{-10}	1.2×10^{-6}	0.90
RF MAGNETRON SPUTTERING	Sputtered	1.3×10^{-10}	3.4×10^{-7}	0.86
HOT-WIRE CVD	H608	6.1×10^{-10}	2.9×10^{-7}	0.89
RF-PECVD UNDILUTED	4m	3.2×10^{-10}	9.2×10^{-7}	0.86
	Yl-6b	1.1×10^{-9}	2.6×10^{-6}	0.72
	SN128	1.8×10^{-9}	1.5×10^{-6}	0.76
RF-PECVD DILUTED	Lj-51	1.6×10^{-10}	1.0×10^{-6}	0.90
	L12229	1.7×10^{-10}	6.2×10^{-7}	0.90
	L12231	9.2×10^{-10}	1.6×10^{-6}	0.85

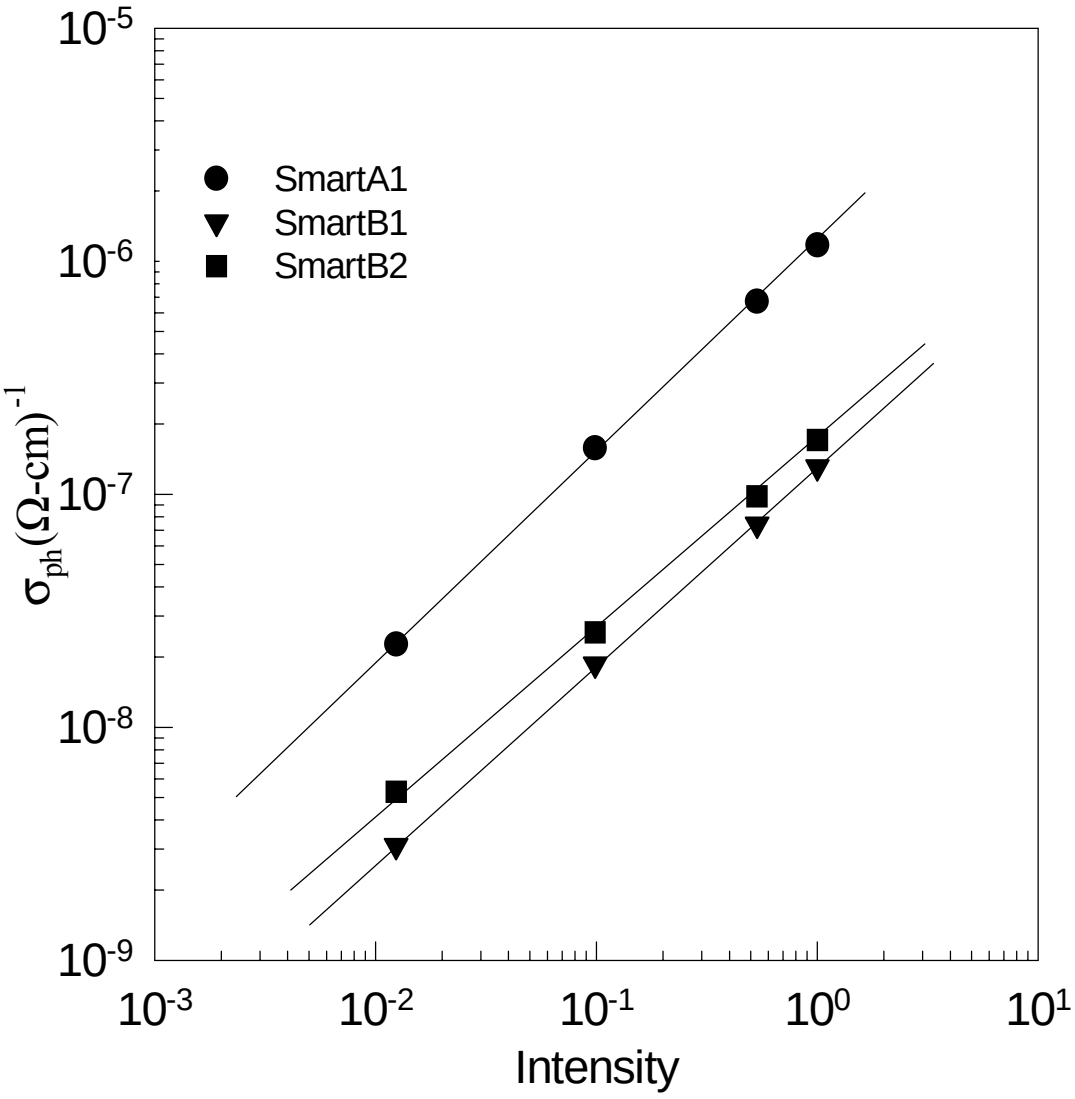

Figure3.5. Steady-state photoconductivity measued with monochromatic light of λ=690nm at different intensities for DC Glow-discharge a-Si:H films in the annealed state.

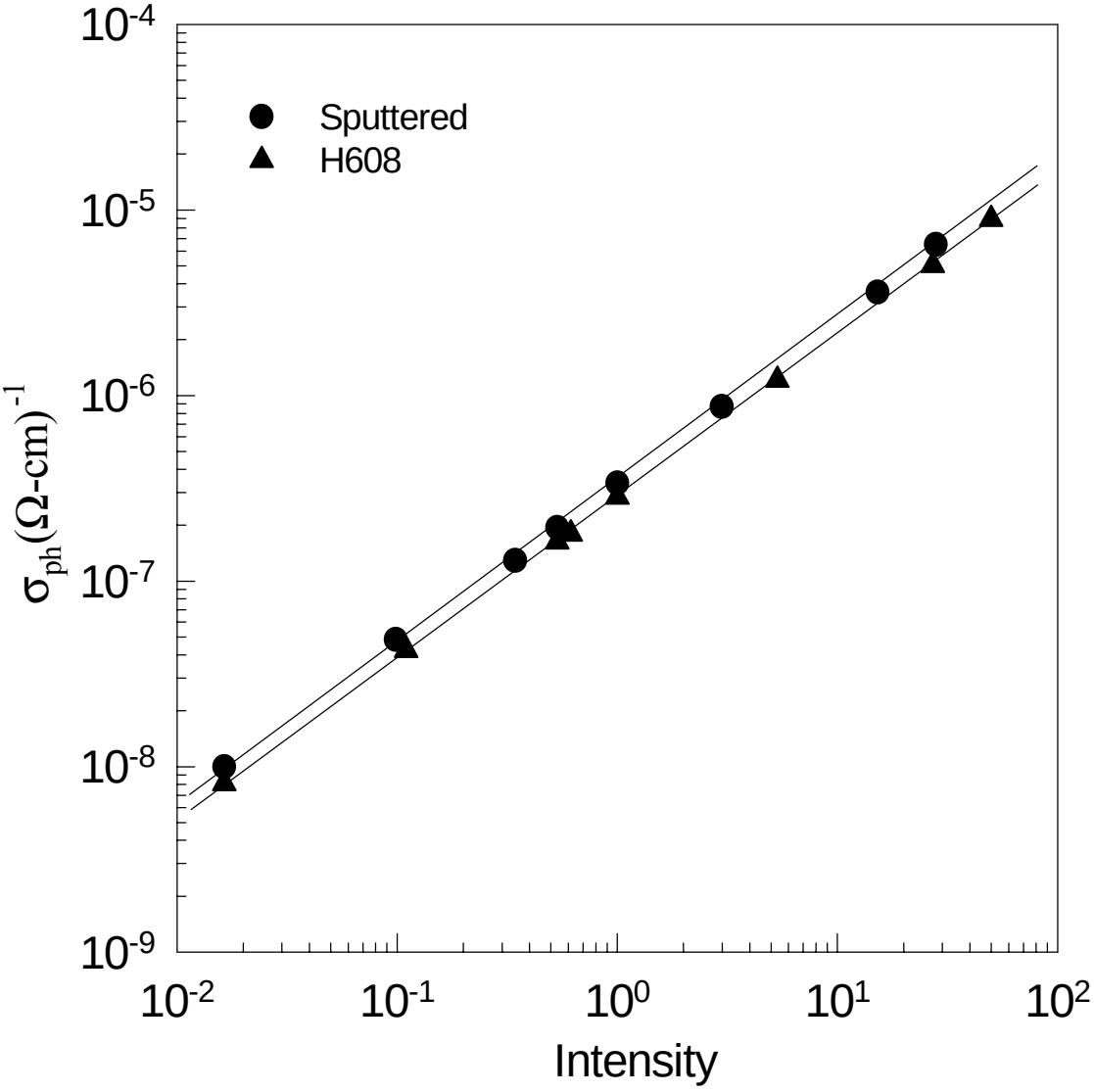

Figure3.6. Steady-state photoconductivity at λ=690nm for Hot-wire CVD and RF-Magnetron Sputtering samples in the annealed state.

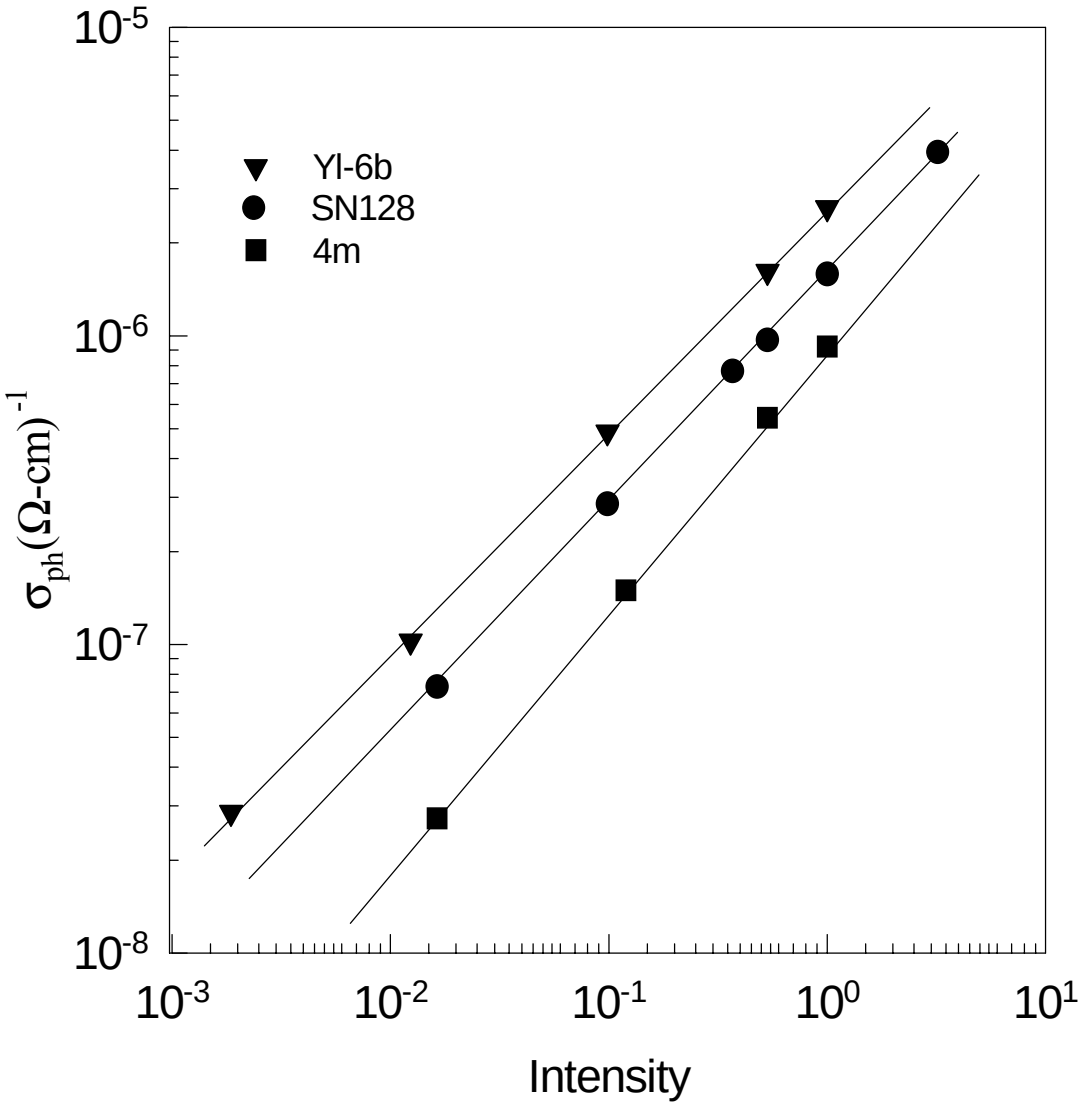

Figure3.7. Steady-state photoconductivity at λ=690nm for undiluted RF-PECVD samples in the annealed state.

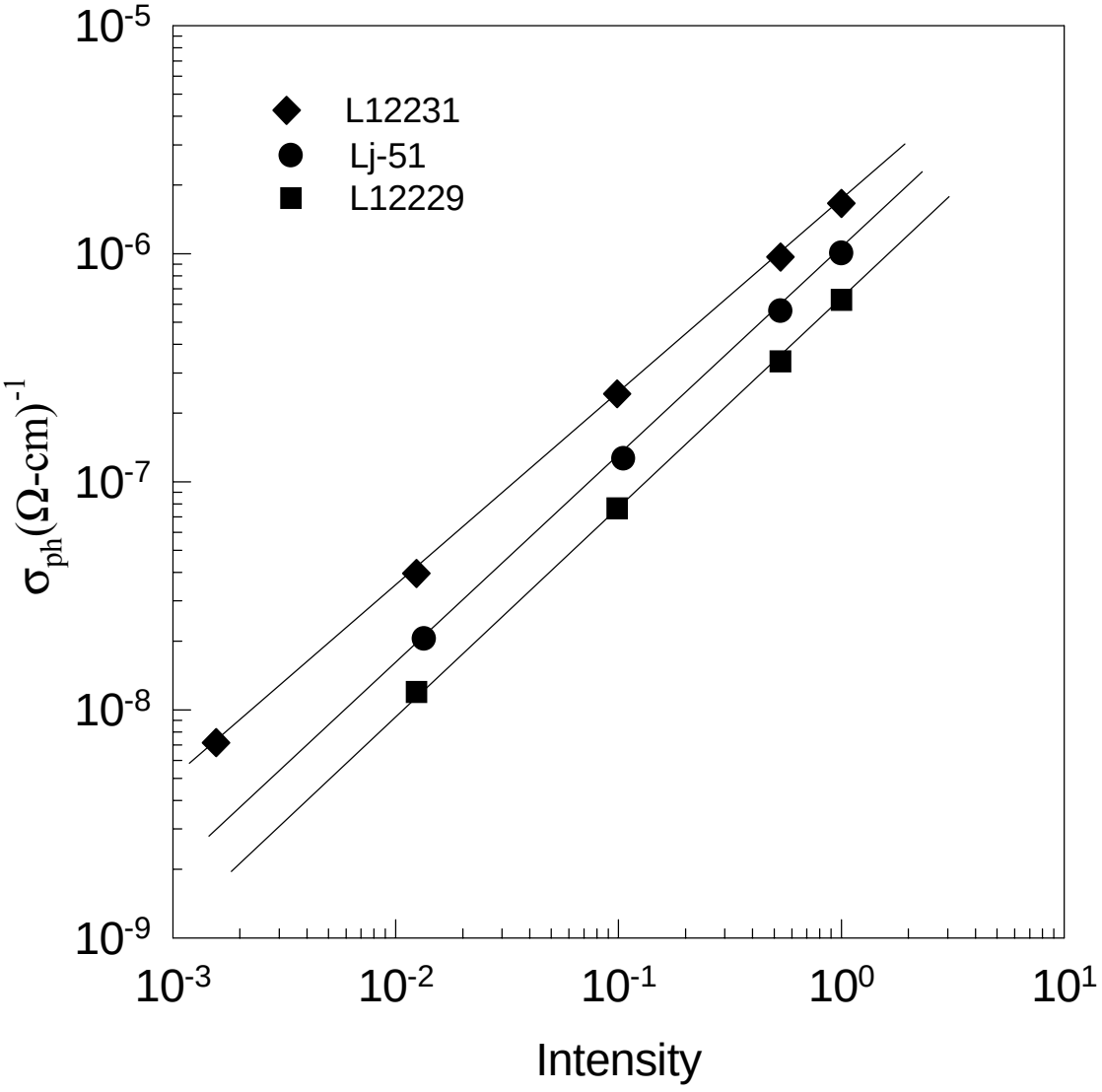

Figure3.8. Steady-state photoconductivity at λ=690nm for diluted RF-PECVD samples in the annealed state.

3.4. Low Temperature Photoconductivity

As described above, intensity dependence of steady state photoconductivity at room temperature allows us to probe the effects of defect states in the bandgap for a certain energy range since the intensity of light cannot be increased more due to experimental limitations. However, alternatively the sample temperature at a constant light intensity can be decreased from room temperature to lower temperatures and the effects of defect states on measured photoconductivity can be detected extensively. For this reason, the samples are mounted in a closed cycle cryostat, which allows light penetration through a window, and cooled to lower temperatures. At every temperature, sample was illuminated with a constant intensity of red light and photocurrents were measured using an electrometer.

An example of low temperature photoconductivity spectra is shown in Figure 3.9 for DC GD a-Si:H sample SmartB2 for three different light intensity. Begining from room temperature, photoconductivity increases with increasing intensity consistent with previous results. Let us consider only the result of highest intensity F3. As temperature decreases, photoconductivity starts decreasing, consistent with an increase in the recombination centers as quasi-Fermi levels move closer to their respective band edges. But this decrease continues until temperature T1, where photoconductivity remains to be constant for a wide range of temperatures. The spectrum becomes flat until temperature $T1^{*}$. This is called photosensitization. It is difficult to explain this effect with increasing mobility, which is one of the determining parameter of photoconductivity. But rather it is due to free electron density, n, and therefore free electron lifetime, $\tau_{n.}$. This is unlikely for a defective material , which has continuous defect distribution in energy throughout the bandgap. As temperature decreases, quasi-Fermi levels for free electrons and holes move through their respective band edges and more defect states are converted to recombination centers as defined by Simmons-Taylor statistics in Appendix A. The increase in the density of recombination centers must decrease free electron lifetime for a constant light intensity if there are same kind of recombination centers present in the bandgap. Furthermore, lifetime of free electrons are not only controlled by the density of recombination centers but also their carrier capture cross sections. If there are more than one type of defect states, each has different carrier capture cross sections but second type ,new defects, has very low capture cross-

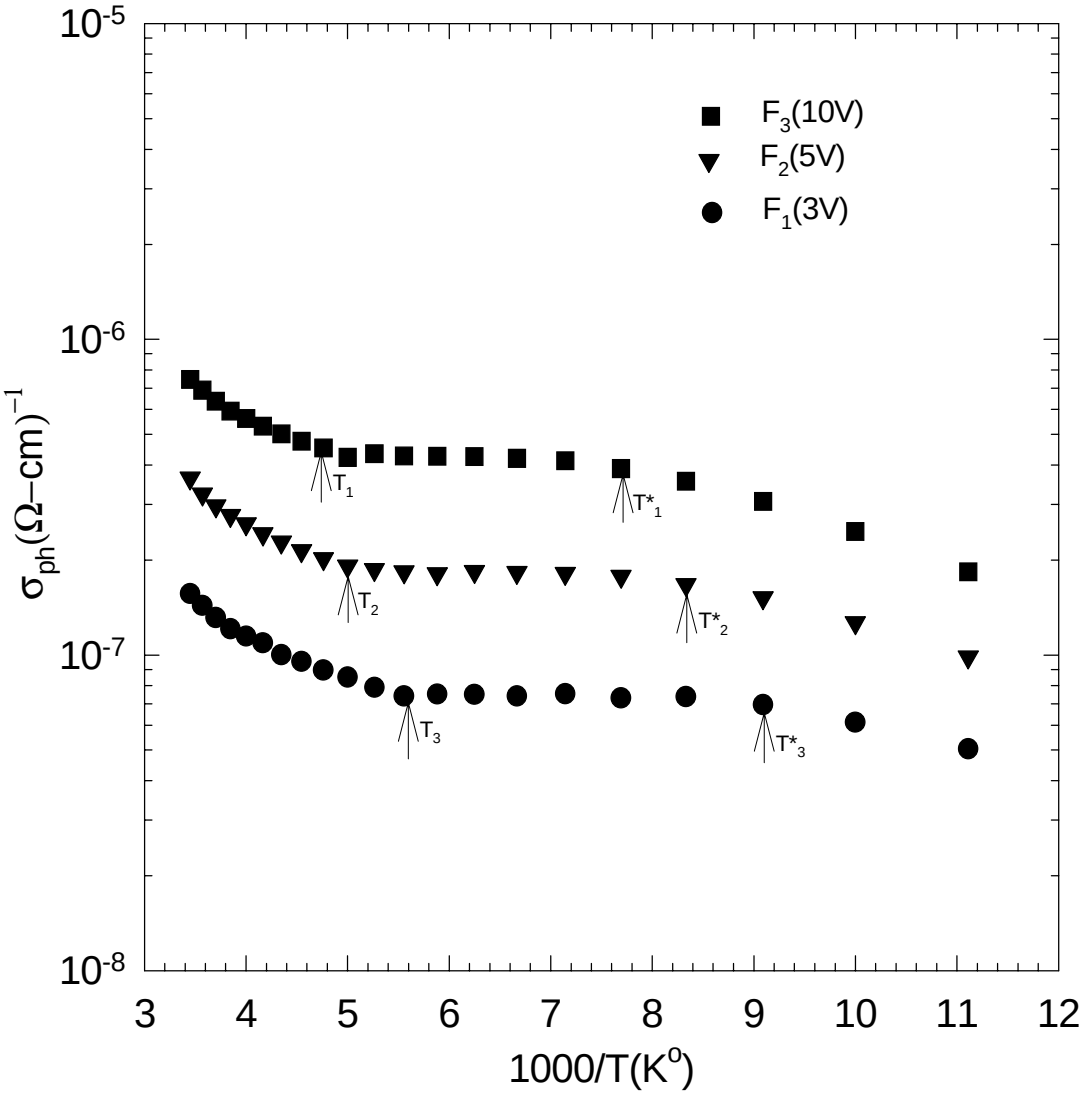

Figure3.9.σ_{pc} versus 1000/T graph for different intensities for sample SmartB2 in the annealed state.

sections for electron, then free electron lifetime will increase as more second type new defects become recombination centers. The degree of improvement in free electron lifetime is also proportional to the density of second type defect states as well. At temperature T1 the photosensitization starts for the highest intensity F3. As we go to lower intensity F2, photoconductivity decreases from room temperature down to temperature T2, which is lower than T1. Then it becomes flat again. It means that at intensity F2, quasi-fermi levels reach to new type defect states at lower temperature since F2 is lower than F3. Similarly, at the lowest intensity F1, photoconductivity decreases until temperature T3, which is lower than T2, then becomes flat. These transition temperatures are thermally activated. The turning point in temperature is consistent with the theory of Simmons-Taylor, indicating that quasi-Fermi levels reach to a new type defect states, which have very small capture cross-section for electron than first type defect states and act as photosensitizing states. This effect is also called thermal quenching.

Quasi-Fermi levels can be moved by either light intensity at constant temperature or by temperature at a constant light intensity. This effect is also seen in other DC GD a-Si:H films. The summary of low T photoconductivity at a constant intensity F2 is illustrated in Figure 3.10 for three DC GD samples. The samples SmartB1 and SmartB2 are from the same deposition run made at 215 ^{0}C substrate temperature and SmartA1 was made at 260 ^{0}C substrate temperature with similar other deposition parameters. The results of SmartB1 and SmartB2 are almost identical within the experimental error but SmartA1 has factor 5 higher photoconductivity at room temperature due to differences in defect structure and optical gap. However, they all show the same type of low T photoconductivity spectrum. Initially photoconductivity decreases to a certain temperature, then it becomes flat. It later starts decreasing again at lower temperatures. At the lower temperatures around 100 ^{0}K, quasi-Ferimi levels move so apart and reach to high density of the conduction and the valence band tail states. They introduce very large recombination centers between quasi-fermi levels and electron lifetime will decrease continuously. Transition temperature ,T^{*}, at lower temperature part of the spectrum is different for SmartA1 and SmartB1. It is an indication that SmartA1 has lower optical gap ,1.70eV, than SmartB1 ,1.80eV. Due to the fact that the onset of exponential band tails in recombination kinetics is detected much higher temperature for SmartA1. It is indicated by TA^{*} and TB^{*} on Figure 3.10 for clarity. The

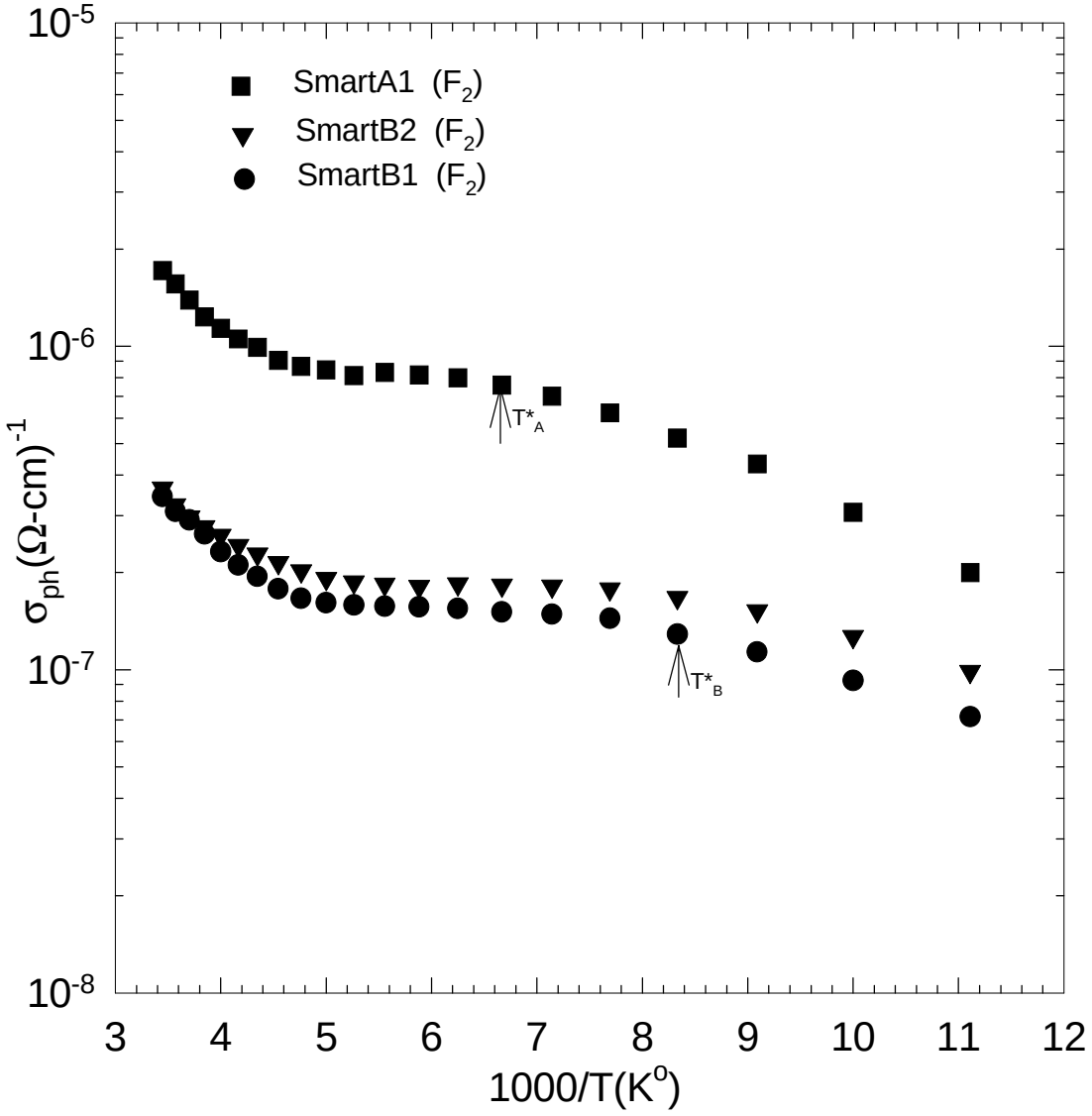

Figure3.10. Low temperature photoconductivity of DC Glow-discharge samples in the annealed state.

turning temperatures are not same for each film due to differences in defect density and distribution in energy and optical gap of samples but the shape of spectrum is consistent for all three samples indicating similar defects distributions throughout the bandgap.

As seen from the activation energy data and room temperature photoconductivity results, similar device quality a-Si:H films are also produced using a RF-PECVD system. An example of low temperature photoconductivity spectrum of undoped a-Si:H sample 4m prepared without hydrogen dilution of silane gas is shown in Figure 3.11 for three different light intensities. As intensity icreases from F1 to F3, spectrum shows a parallel shift to higher values keeping the same shape. Photoconductivity initially decreases from room T to 250 ^{0}K for intensity F3, then it starts increasing and peaks around temperature 155 ^{0}K. The feature of minimum and maximum points at the spectrum are clearly seen for three different intensities. In each one, these points correspond to different temperatures consistent with the theory of Simmons-Taylor. Photosensitization in this sample is more significant and sets in at higher temperatures than those observed in DC GD samples. For example; for intensity F3, undiluted a-Si:H films has transition at 250 ^{0}K, however, it happens around 200 ^{0}K for DC GD samples. This effect indicates that new type of defect states resulting in photosensitization are closer to midgap in undiluted RF-PECVD films and their density must be higher to cause a peak in low T spectrum. As temperature is decreased further below the peak temperature ,$T1^*$, photoconductivity exhibits a sharp decrease, where free electron lifetime decreases due to onset of exponential bandtail states as recombination centers. In addition, the results of other undiluted RF-PECVD films are summarized in Figure 3.12. Even though they were made in the same deposition system, they can exhibit different photosensitization than the sample 4m in Figure 3.11. Other two undiluted films have characteristics more similar to DC GD samples. Photoconductivity at highest intensity F2 decreases down to 200 ^{0}K, then little photosensitization sets in. It decreases with much smaller slope than higher temperature part of the spectrum. Here, new defect states could be closer to band edges burried under the tail states or their densities might be lower. But their presence is obvious that slope shows a change.

Undiluted a-Si:H films deposited using RF-PECVD system generally show significant photosensitization like the sample 4m in Figure 3.11 and suffer great amount

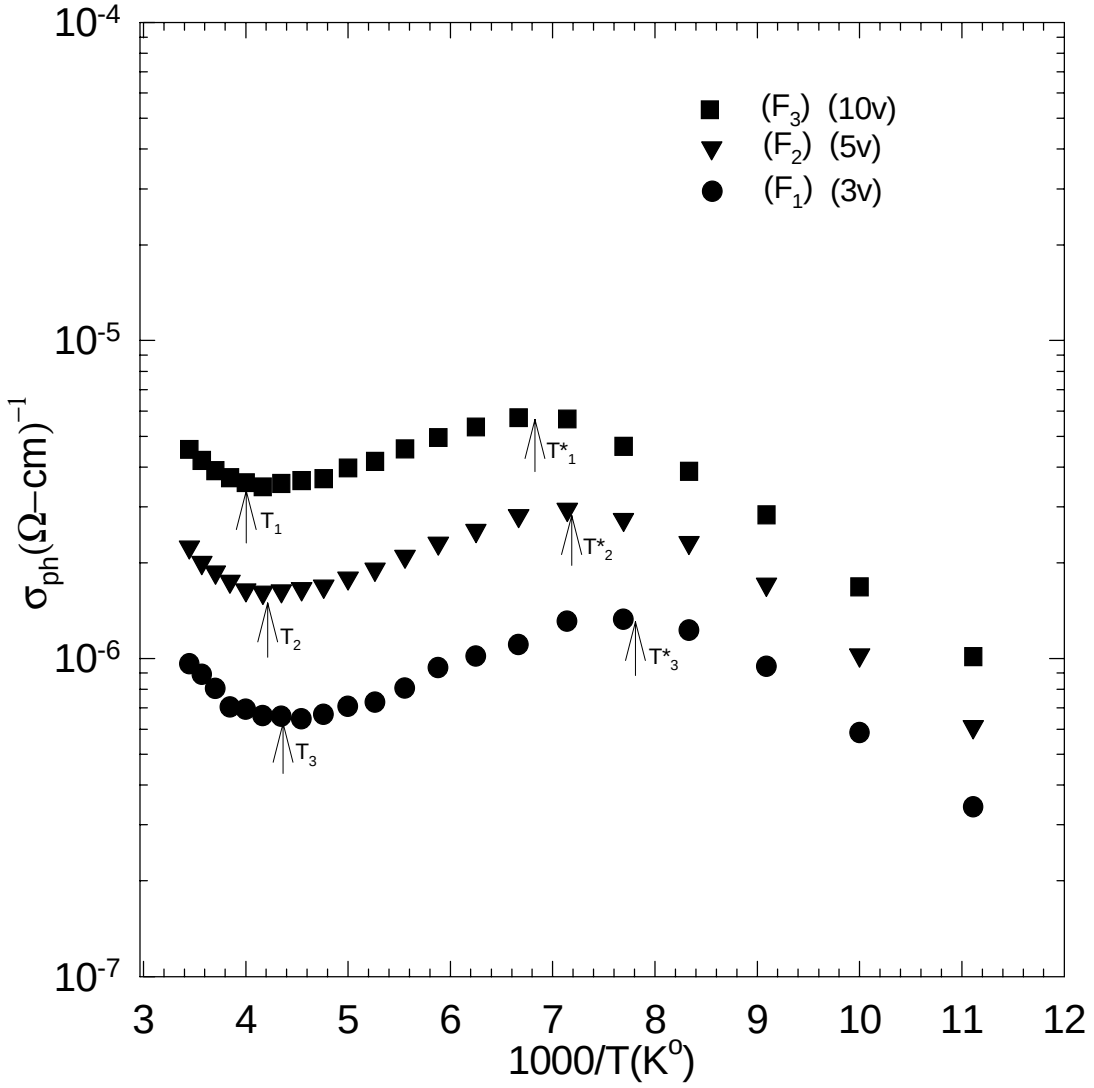

Figure3.11.σ_{pc} versus 1000/T graph for different intensities for undiluted RF-PECVD sample 4m in the annealed state.

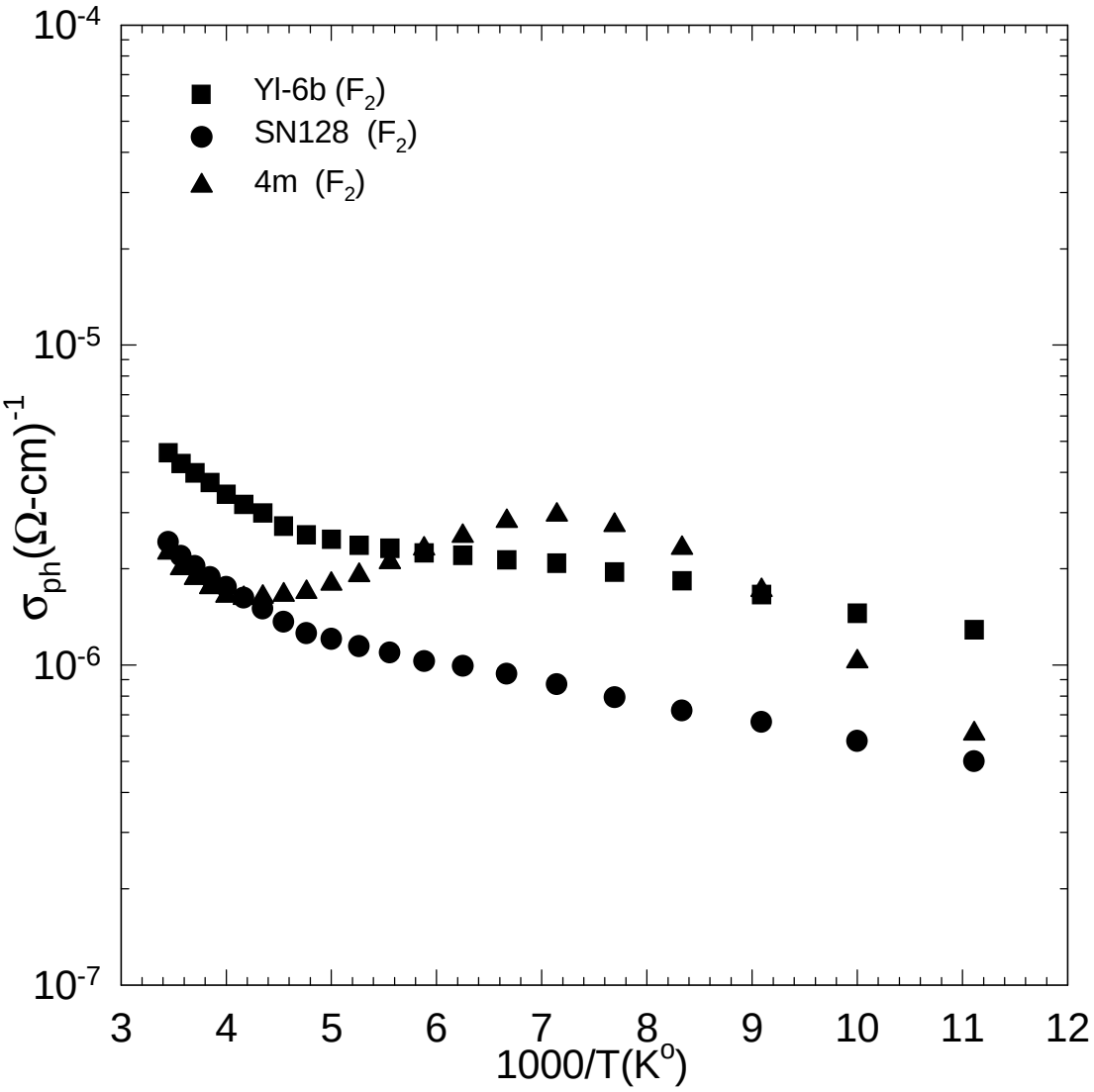

Figure3.12.Low temperature photoconductivity of undiluted RF- PECVD samples in the annealed state.

of degradation upon light soaking. To prepare more stable and lower stabilized defect density material, hydrogen dilution technique was developped[20,21]. In this technique, silane gas is diluted with hydrogen at different ratios (H_2 / (SiH_4 + H_2) =R) from 0 to 40 until material changes phase from amorphous to microcrystallinity. To investigate the effects of hydrogen dilution process on the defect distribution in the bandgap, low temperature photoconductivity measurements were carried out in three diluted a-Si:H films. The spectra for the sample LJ-51 prepared for R=10 at Penn State University are illustrated in Figure 3.13 for three different intensities. Consistent paralel shift in photoconductivity spectra is seen as intensity increases from F1 to F3. However, there are significant differences from previous results. First, photoconductivity at intensity F3 starts decreasing from room T to 250 ^{0}K by only 15%. It was around 30-40% for undiluted sample 4m. Second, it does not show a peak. It rather stays constant until 166 ^{0}K, then it starts decreasing again with a constant slope. Other two lower intensities also show the same trend and transitions at temperatures consistent with the analysis of Simmons-Taylor. These transition temperatures are indicated by arrows on the figure for clarity.

Similar results are also obtained for other diluted a-Si:H films prepared by low-hydrogen dilution (exact ratios are not publicised by the Company) at USSC as shown in Figure 3.14. Diluted sample LJ-51 and low-hydrogen diluted sample L12229 exhibit almost the same transition temperatures and magnitudes of photoconductivity. The only difference is that photoconductivity decreases gradually faster in low H-diluted film. As seen from Figure 3.14, high hydrogen dilution significantly changes the spectrum. Photosensitization in temperature dependence of photoconductivity starts much earlier in temperature. It is almost at room temperature. It remains to be flat until 200 ^{0}K then it starts to decrease continuously. This type of behavior is not observed in DC GD and undiluted RF-PECVD films. Onset of photosensitization at room temperature indicates that photosensitizing defect states are located much closer to midgap in diluted a-Si:H films, especially in high H-diluted sample, than those in undiluted and DC GD samples. Because of that the effects of exponential tail states as recombination centers starts at temperatures as high as 200 ^{0}K. Furthermore, high H-diluted films have a factor of 3 higher photoconductivity due to these photosensitizing defect states than other diluted films.

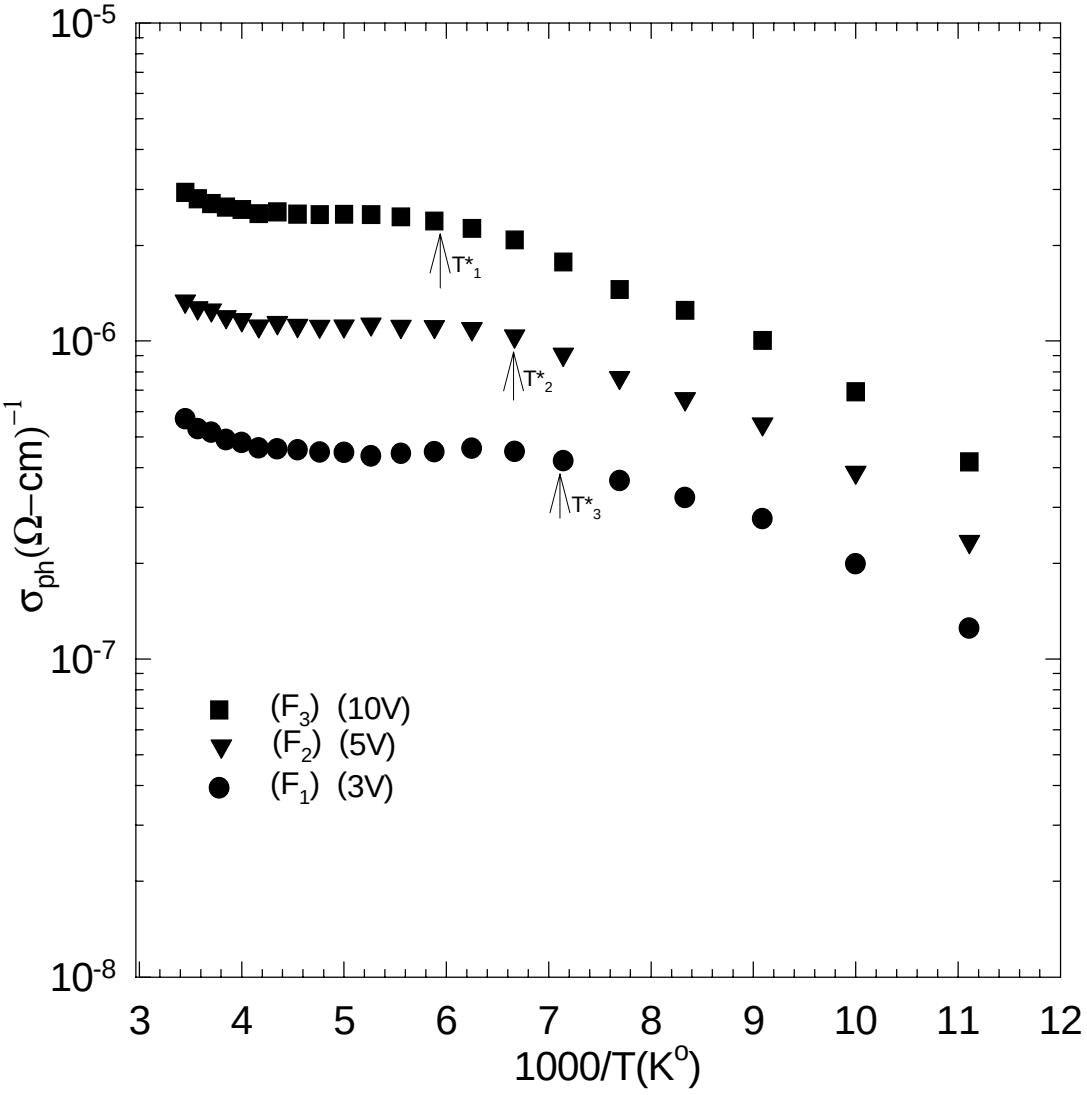

Figure3.13.σ_{ph} versus 1000/T graph for different intensities for diluted RF-PECVD sample Lj-51 in the annealed state.

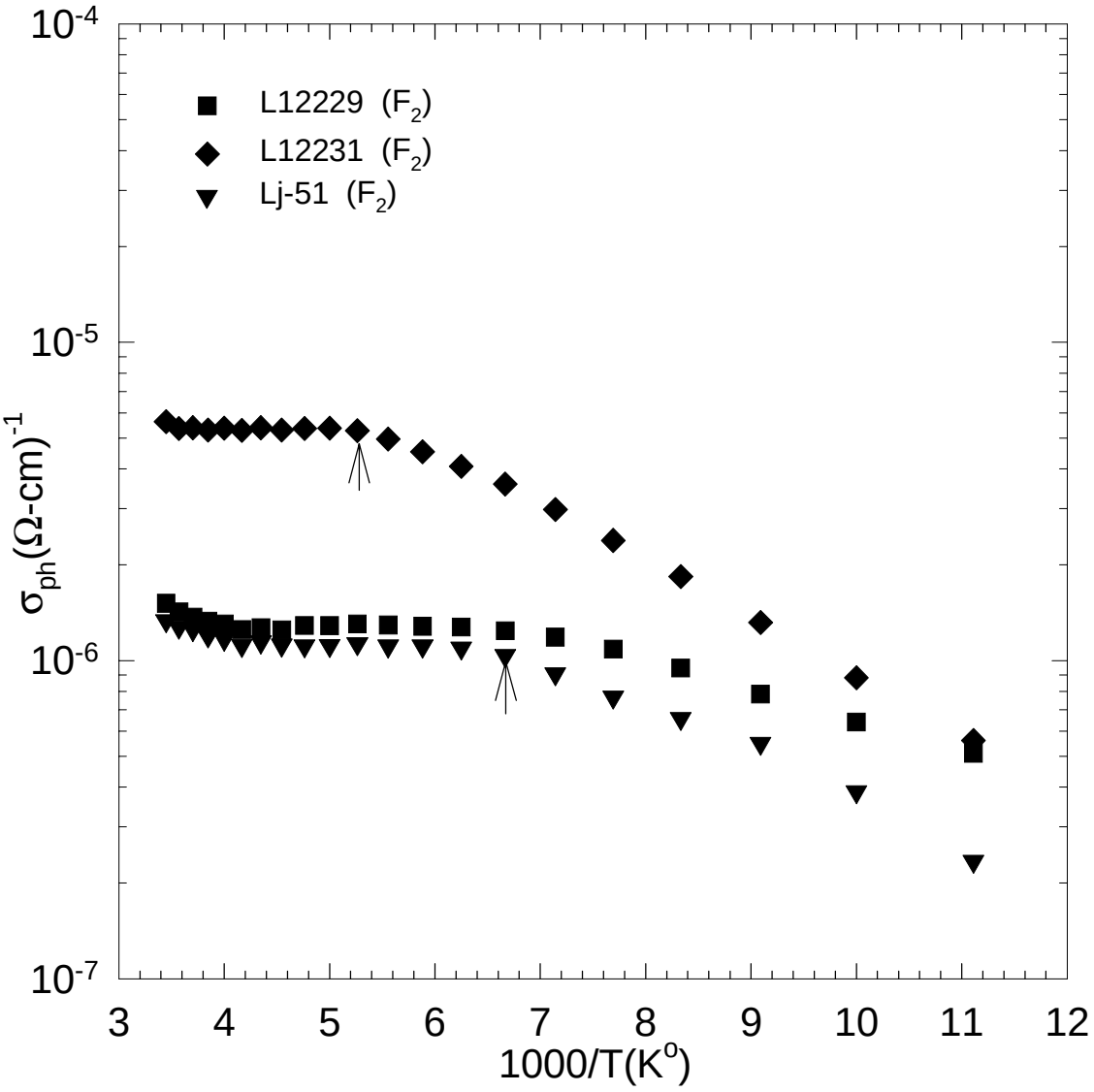

Figure3.14.Low temperature photoconductivity of diluted RF-PECVD samples in the annealed state.

Finally, similar results were obtained for the device quality a-Si:H films deposited using HW-CVD and RF magnetron sputtering techniques as given Figure 3.15. Photoconductivity starts decreasing from room T down to 250 ^{0}K for sputtered sample and to 200 ^{0}K for HW-CVD film. Then, photosensitization sets in as observed in previous films. It establishes a slight peak at 150 ^{0}K for sputtered film, then gradually decreases to lower temperatures. However, HW-CVD sample shows much wider photosensitization and peaks around 100 ^{0}K. The onset of exponential tail states is barely seen at 90 ^{0}K. This is observed only in HW-CVD samples, indicating that photosensitizing states are deep in the bandgap, further away from the midgap, and closer to band edges.

As a conclusion, it is found in this thesis that undoped a-Si:H films prepared using different deposition conditions and systems have dark Fermi level positions 0.6 eV to 1.0 eV from the conduction band edge. Steady-state photoconductivity measured at 100% intensity of monochromatic red light shows variation from $1x10^{-7}$ (ohm-cm)^-1 to $16x10^{-7}$ (ohm-cm)^-1. Its power dependence on light intensity, γ, has a values between 0.72 and 0.90. Temperature dependence of photoconductivity exhibits three different regions: Region I is the effect of defect states around midgap, which cause decrease of photoconductivity as temperature decreases; Region II is the onset of photosensitization until certain temperature. Depending on its effect, there could be a peak in the spectrum, a flat region or much slower decrease with temperature; Region III is the onset of exponential band tail states, where free electron lifetime and therefore photoconductivity gradually decreases with temperature.

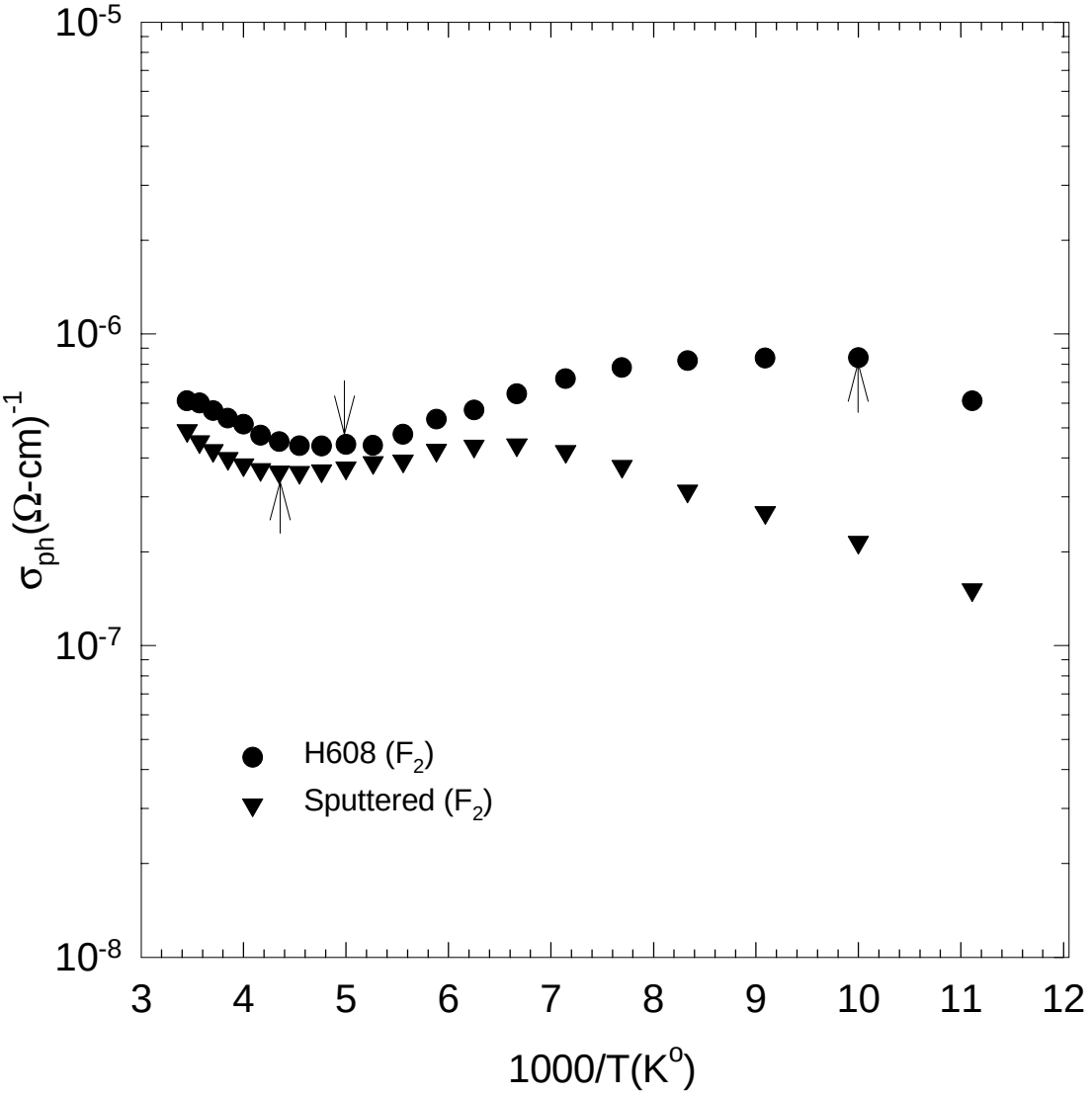

Figure3.15.Low temperature photoconductivity of Hot-Wire CVD and RF Magnetron Sputtered samples in the annealed state.

CHAPTER 4
STAEBLER-WRONSKI EFFECT

4.1 Introduction

The Staebler-Wronski effect(SWE)[11] is known to be an intrinsic property limiting solar cell applications of a-Si:H. Electrical properties of a-Si:H deteoriate when it is illuminated by sun light. Dark and photoconductivity decrease and the density of paramagnetic defects in the films increases[13,65]. In this chapter, a-Si:H thin films were studied in the light soaked state to investigate the effect of Staebler-Wronski defects. The results of annealed state described in Chapter 3 were compared with light soaked state results to see the consequences of the SWE in different device quality films. The SWE was monitored with dark conductivity, steady-state photoconductivity versus light intensity at room temperature, and steady-state photoconductivity versus temperatures down to 90 ^{o}K at different light intensities.

4.2 Dark Conductivity

After 10 hours white light illumination, σ_D measured at room temperature show a slight degradation from its annealed value. Some films show greater degradation than others as indicated in Table 4.1. As given in Chapter 3 that σ_D is determined by the dark Fermi level E_f. Degradation of σ_D corresponds to a shift of E_f towards midgap. Activation energy data showed that E_f is very close to the middle of the bandgap in most of the samples. After light soaking, samples become more intrinsic as E_f move closer to the midgap. This is one of the consequences of SWE in a-Si:H films. More significant degradation have been observed in samples SN128 and sputtered a-Si:H films.

Table 4-1. Room temperature darkconductivity σ_D (R.T)$(\Omega\text{-cm})^{-1}$ values for the annealed and light soaked state.

Samples	σ_D (R.T)(Annealed)	σ_D (R.T)(Soaked)	$\sigma_D(A) / \sigma_D(S)$
SmartB1	$8.0x10^{-10}$	$2.0x10^{-10}$	4
SmartB2	$8.3x10^{-10}$	$1.7x10^{-10}$	4.88
SmartA1	$7.0x10^{-10}$	$1.8x10^{-10}$	3.8
Sputtered	$1.3x10^{-10}$	$8.9x10^{-12}$	14.6
H608	$6.1x10^{-10}$	$3.0x10^{-10}$	2
4m	$3.2x10^{-10}$	$1.1x10^{-10}$	2.9
Yl-6b	$1.1x10^{-9}$	$8.6x10^{-10}$	1.28
SN128	$1.8x10^{-9}$	$5.3x10^{-11}$	33.9
Lj-51	$1.6x10^{-10}$	$1.1x10^{-10}$	1.45
L12229	$1.7x10^{-10}$	$1.1x10^{-10}$	1.54
L12231	$9.2x10^{-10}$	$2.0x10^{-10}$	4.6

4.3 Steady-state Photoconductivity

The room temperature steady-state photoconductivity, σ_{ph}, in undoped a-Si:H thin films in the light soaked state were measured following a few suns of high intensity light soaking. The Staebler-Wronski effect in steady-state photoconductivity is illustrated in Figure 4.1 for DC GD a-Si:H film SmartA1. Log-log plot of σ_{ph} versus light intensity obeys a power law as observed in the annealed state. The power γ is 0.90, which is close to unity and shows no significant change from that of annealed value. The magnitude of σ_{ph} measured at 100% light intensity decrease from 1.2 x 10^{-6} $(\Omega\text{-cm})^{-1}$ to 7.2 x 10^{-8} $(\Omega\text{-cm})^{-1}$. It shows a degradation by a factor of 16. The Steabler-Wronski effect is seen as a parallel shift in log-log plot of σ_{ph} vs light intensity with a significant degradation in the magnitude of σ_{ph}. This degradation is due to decrease in the free electron density, n, in the soaked state. The main parameter determining the free electron density is the increase in the density of recombination centers, which reduce the free electron life time τ_n. This is direct effect that long time white light illumination of a-Si:H film creates new defect state in the bangap of a Si:H. However, it is not possible to obtain detailed information about the defect states by just monitoring the degradation of σ_{ph}. Now, these defect states are generally named as the Staebler-Wronski defects or light induced defects.

The effects of the Staebler-Wronski defects were also studied in other undoped DC GD a-Si:H films under the same period of white light soaking. They are shown in Figure 4.2 for both annealed and light soaked state. The exponent γ is almost 0.90 for Smart B1 and Smart B2, which show a slight increase from its annealed value. Both films show almost identical degradation in σ_{ph}. It decreases from its annealed state value of 1.7 x 10^{-7} $(\Omega\text{-cm})^{-1}$ to 2.6 x 10^{-8} $(\Omega\text{-cm})^{-1}$. They show a factor of 5 degradation in σ_{ph}, which is much less than that of sample Smart A1. However, they are still less photoconductive than sample Smart A1. They have similar γ values indicating that distribution of light induced defect states present in the bandgap is similar for all three samples. But their densities and energy distributions cannot be determined by looking at the degradation of σ_{ph} curves.

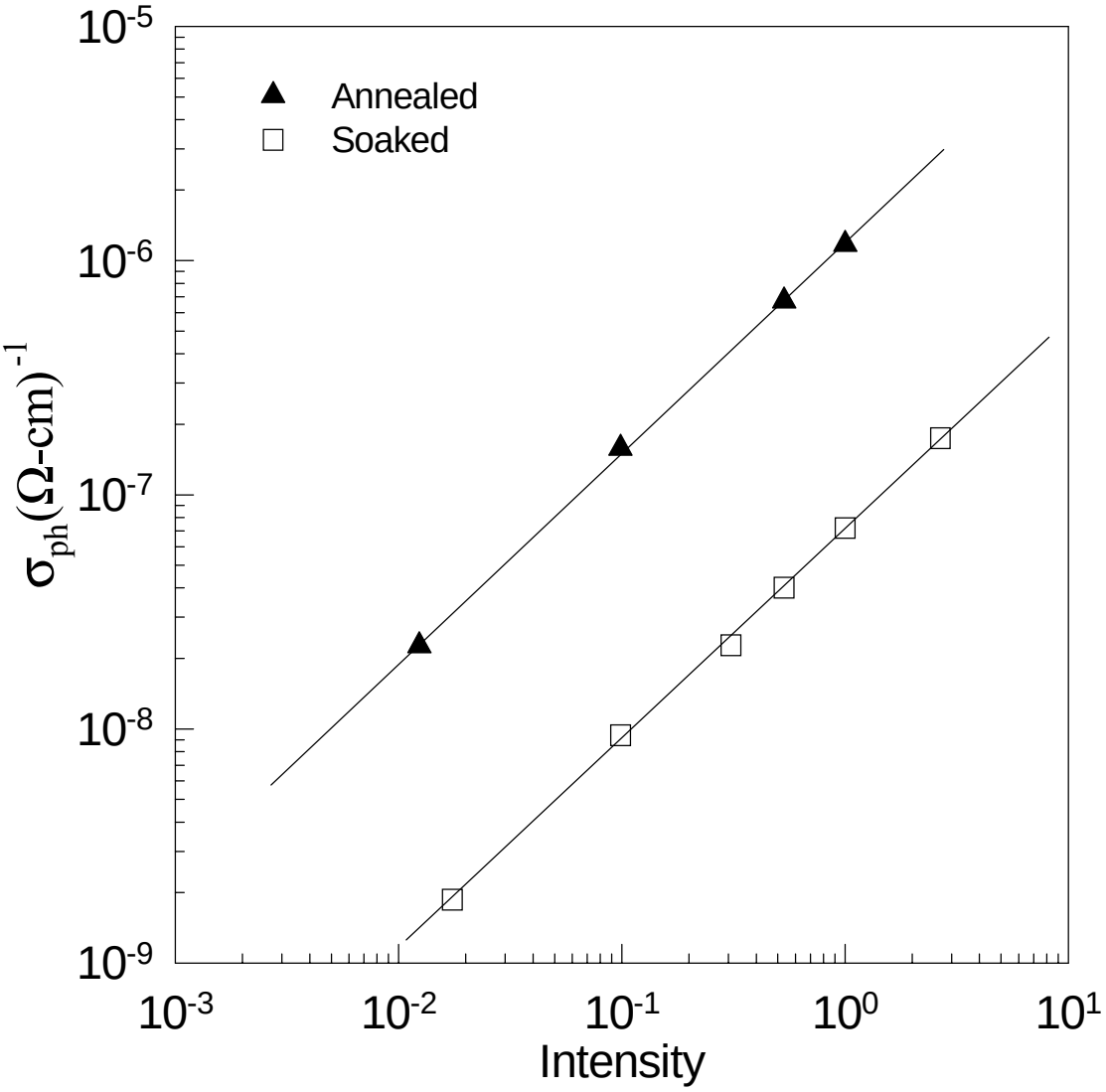

Figure4.1. Steady-state photoconductivity measured with monochromatic light of λ=690nm at different intensities for Smart A1 in the annealed and light soaked state.

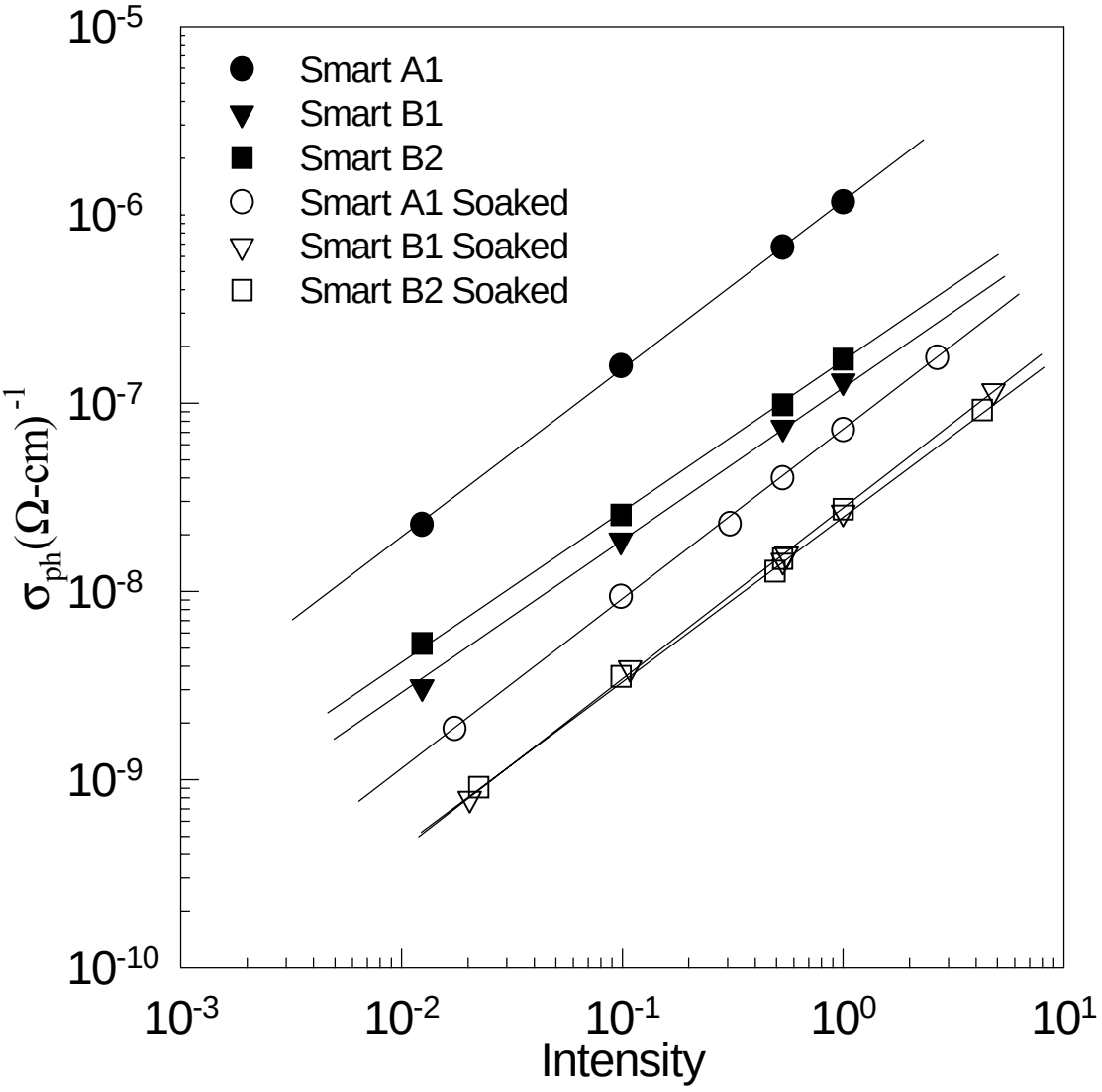

Figure4.2. Steady-state photoconductivity measured with monochromatic light of λ=690nm at different intensities for DC Glow-discharge a-Si:H films in the annealed and light soaked state.

Furthermore, the Staebler-Wronski effect in σ_{ph} are summarized in Table 4.2 and changes in σ_{ph} for other samples are shown in following figures: HW-CVD and sputtered films in Figure 4.3, undiluted RF-PECVD films in Figure 4.4, and Diluted RF-PECVD films in Figure 4.5. The exponent γ is close to unity in soaked state and has a value between 0.85 to 0.90 for all films. It increases from 0.70 to around 0.90 for undiluted RF-PECVD films and shows almost no change for others. The similar γ values indicate that all samples have similar Staebler-Wronski defect distribution in light soaked state even though they had drastically different native defect profiles due to differences in the deposition conditions in the annealed state.

The consequences of the Staebler-Wronski effect is clearly seen in the magnitude of σ_{ph} measured at 100% of light intensity. HW-CVD film shows a degradation in σ_{ph} by a factor of 5 and sputtered film by a factor of 10. However, more degradation is observed in undiluted RF-DECVD samples YL-6B and SN128. Even though each has different annealed state value, σ_{ph} is reduced to the values between 2 - 7 x 10^{-8} $(\Omega\text{-cm})^{-1}$ after 10 hrs of white light soaking. If samples are illuminated longer under the light, this degradation will continue until a saturation in σ_{ph}. However, this procedure takes very long periods of times which was not an intention in this thesis.

Table 4-2. Steady-state photoconductivity in the annealed(A) and light soaked state(S)

Samples	σ_{Ph}(100%)A $(\Omega\text{-cm})^{-1}$	γ (A)	σ_{Ph}(100%)S $(\Omega\text{-cm})^{-1}$	γ (S)	$\frac{\sigma_{Ph}\,(A)}{\sigma_{Ph}\,(S)}$
SmartB1	1.3×10^{-7}	0.85	2.6×10^{-8}	0.90	5
SmartB2	1.7×10^{-7}	0.85	2.7×10^{-8}	0.88	6.3
SmartA1	1.2×10^{-6}	0.90	7.2×10^{-8}	0.90	16.67
Sputtered	3.4×10^{-7}	0.86	3.5×10^{-8}	0.84	9.72
H608	2.9×10^{-7}	0.89	5.8×10^{-8}	0.89	5
4m	9.2×10^{-7}	0.86	7.0×10^{-8}	0.92	13.15
Yl-6b	2.6×10^{-6}	0.72	5.2×10^{-8}	0.90	50
SN128	1.5×10^{-6}	0.76	5.0×10^{-8}	0.87	30
Lj-51	1.0×10^{-6}	0.90	7.5×10^{-8}	0.92	13.33
L12229	6.2×10^{-7}	0.90	5.7×10^{-8}	0.86	10.87
L12231	1.6×10^{-6}	0.85	5.3×10^{-8}	0.81	30.19

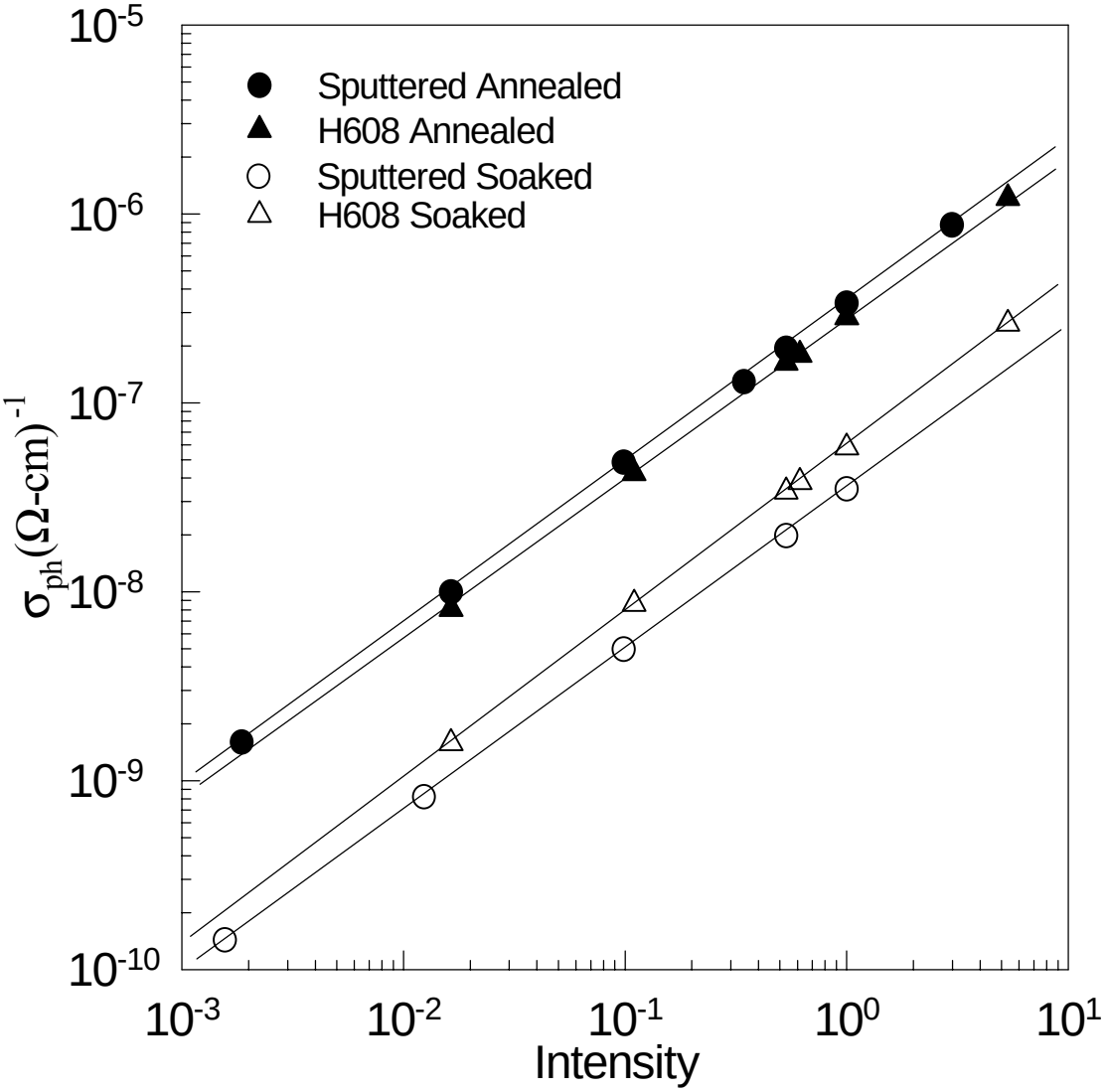

Figure4.3. Steady-state photoconductivity measured with monochromatic light of λ=690nm at different intensities for HW-CVD and RF-Magnetron Sputtering a-Si:H films in the annealed and light soaked state.

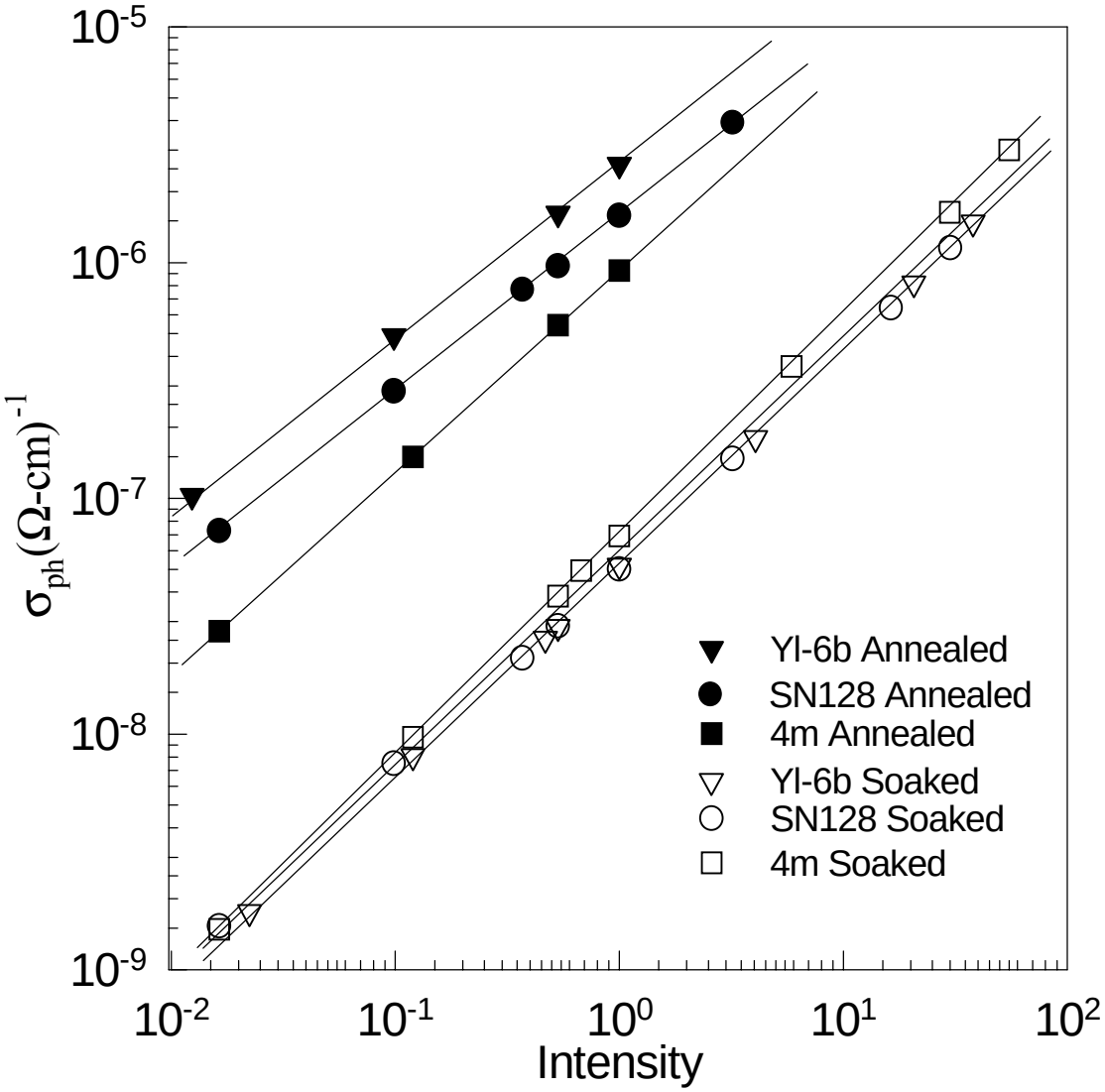

Figure4.4. Steady-state photoconductivity measured with monochromatic light of λ=690nm at different intensities for undiluted RF-PECVD a-Si:H films in the annealed and light soaked state.

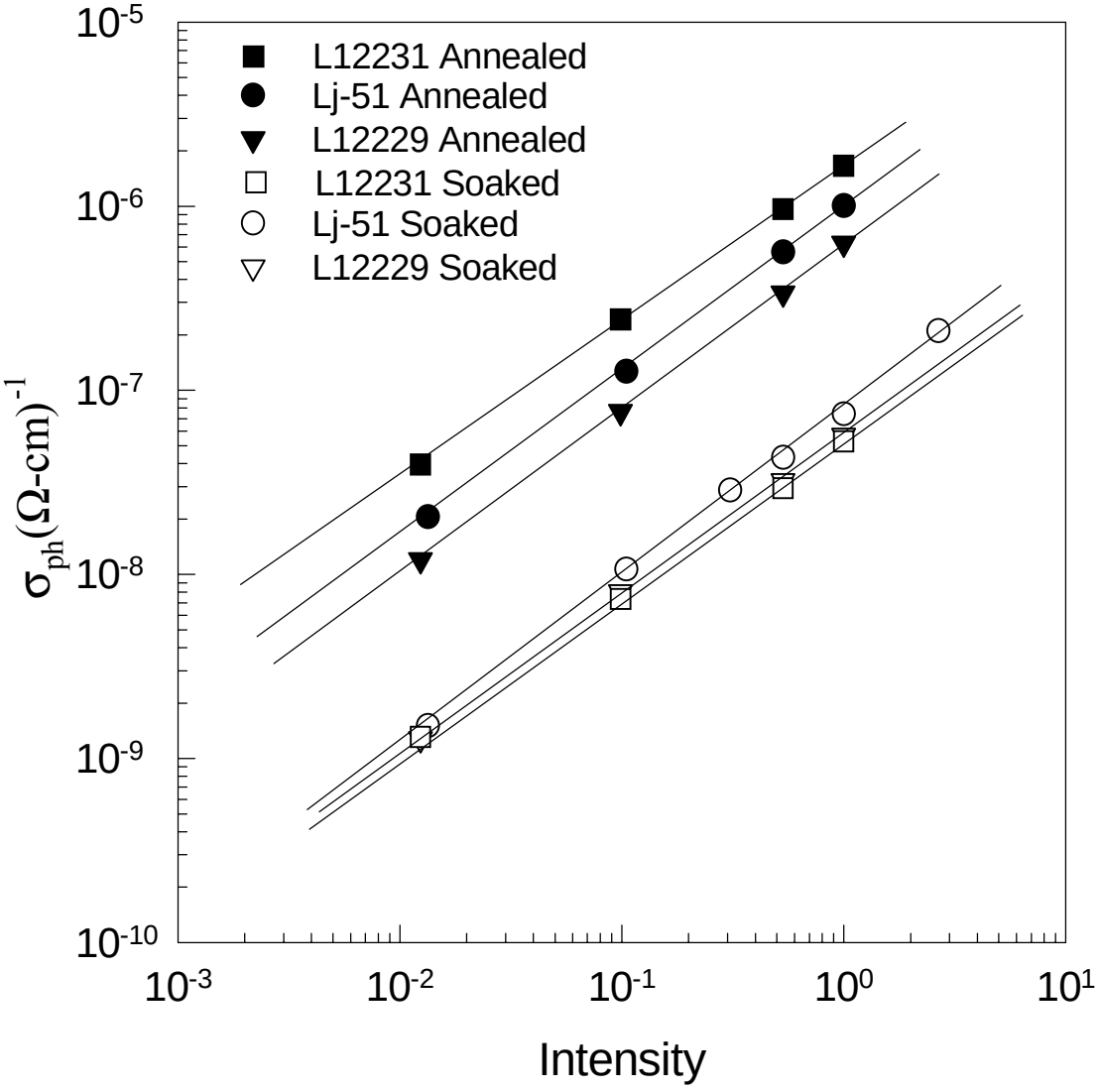

Figure4.5. Steady-state photoconductivity measured with monochromatic light of λ=690nm at different intensities for diluted RF-PECVD a-Si:H films in the annealed and light soaked state.

4.4 Low Temperature Photoconductivity

Steady-state photoconductivity measured at room temperature shows a great deal of decrease after 10 hours of white light soaking. Its power dependence on light intensity becomes almost similar for all samples with a value between 0.85 and 0.90. Those results indicate that new defects states, the Staebler-Wronski defects, are created by light in a continuous distribution of energy in the bandgap. However, it is not possible to understand the nature of the Staebler-Wronski defects from those results. It can only be possible to infer that there is an increase in continuous defect states in the bandgap.

To understand the Staebler-Wronski effect in these a-Si:H thin films, the investigation was extended to the measurement of σ_{ph} at several constant intensities for a wide range of temperatures. Low temperature photoconductivity spectra of DC Glow Discharge a-Si:H sample SmartB2 for three intensities after 10 hours of light soaking are shown in Figure 4.6 together with those measured in the annealed state for the same light intensities. As seen from the Figure, each spectrum shifts to higher photoconductivity values as light intensity increases from F1 to F3, which is consistent with those of annealed spectra. For the same light intensity, such as F3, σ_{ph} (F3) spectrum degrades substantially to lower values due to the Staebler-Wronski effect. The shape of spectrum also shows differences and similarities from that of annealed state. For example, σ_{ph} (F3) starts decreasing from room temperature as temperature decreases. That indicates that at constant intensity F3, the number of recombination centers between the quasi-Fermi levels increases as temperature goes down. This is similar to what observed in the annealed state for high temperature region. However, at a certain temperature, region II in spectrum sets in, where σ_{ph} remains to be insensitive to temperature even though the density of recombination centers increase with decreasing temperature. In light soaked spectrum, region II sets in at lower temperatures. It was around 208 ^{0}K in the annealed state but region II sets in at 178 ^{0}K in the light soaked state.

It can be inferred that light soaking created defects which have the similar nature as native defect states. Their density increased. Because of this, quasi-Fermi levels move slower in energy in the light soaked state. It cannot reach to region II, where photosensitization becomes dominant, until 178 ^{0}K. After this transition temperature,

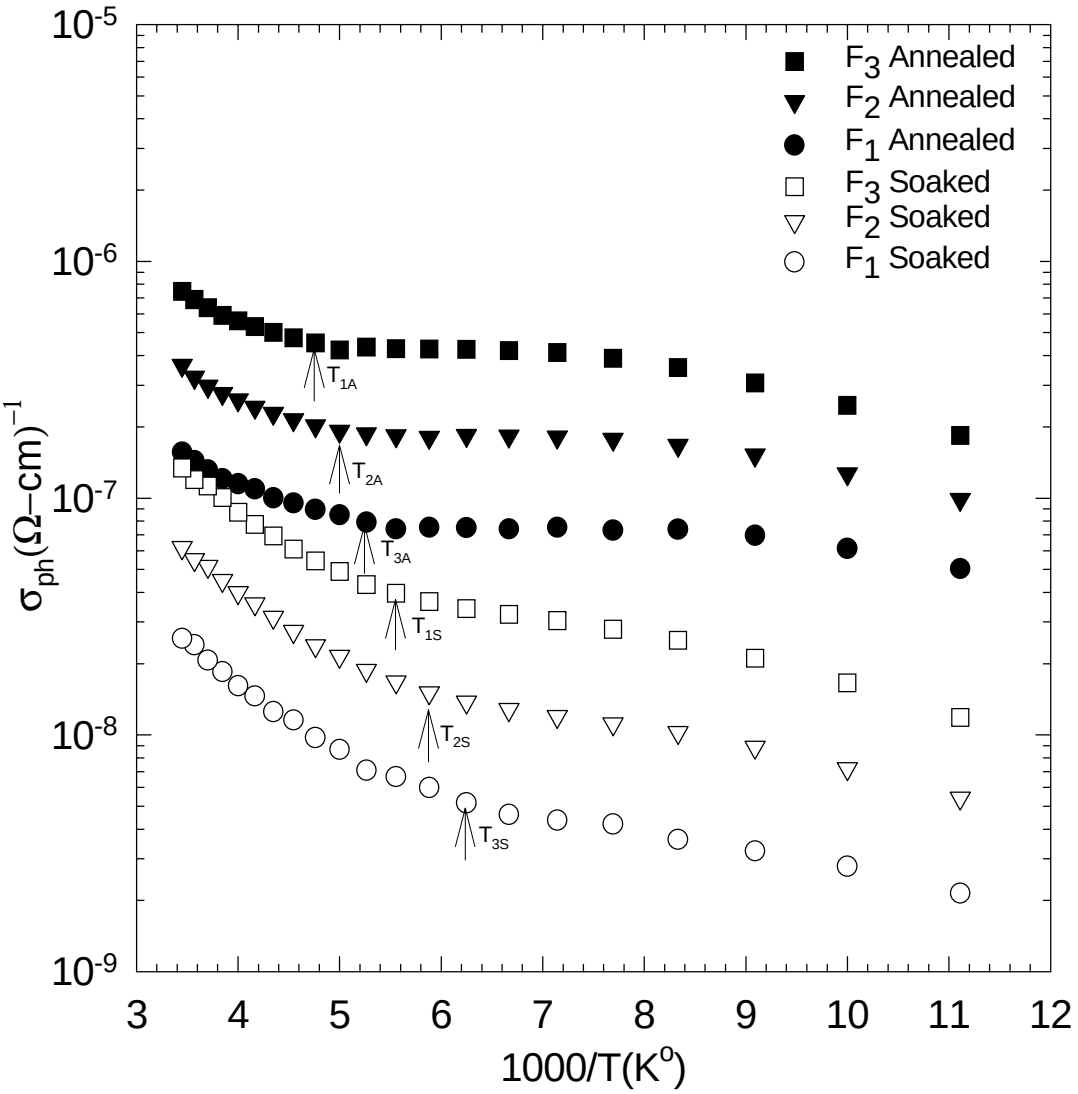

Figure 4.6. σ_{ph} versus 1000/T graph for different intensities for sample SmartB1 in the annealed state and light soaked state.

σ_{ph} does not show significant decrease but slightly becomes constant until 110 ^{0}K. After that temperature, it is decreasing again with a certain slope. The lowest temperature region could be the onset of exponential tail state recombination due to wide opening of quasi-Fermi levels. This onset had started at higher temperatures for the annealed case, which was around 130 ^{0}K.

As the light intensity is decreased rom F3 to F2, room temperature σ_{ph} decreased to $6.5x10^{-8}$ $(\Omega\text{-cm})^{-1}$. It then decreases when temperature decreases until 166 ^{0}K, where a transition to region II begins. This transition temperature is lower than that of intensity F3 and consistent with the analysis of Simmons-Taylor. Again, σ_{ph} remains almost constant after 166 ^{0}K until 100 ^{0}K. The onset of region III is barely seen at the last point. The behavior of the σ_{ph} spectrum at the lowest intensity is similar to previous ones that σ_{ph} decreases in region I until 156 ^{0}K. After that temperature, σ_{ph} remains to be constant and the onset of tail state recombination cannot be detected in the limit of lowest temperature. The temperature needs to be decreased further to detect the region III in the spectrum. As a result, these spectra measured in the light soaked state indicate that Staebler-Wronski defects are present in the material. There could be more than one type of Staebler-Wronski defects created by light. First type defects are created around the midgap, which are also present in the annealed state and responsible for region I. Second type defects are created closer to the band edges and they are detected at lower temperatures. They give photosensitizing behaviour and cause no change in σ_{ph} as temperature decreases.

The effect of Staebler-Wronski defects were also observed in the low temperature photoconductivity spectrum of other DC Glow Discharge a-Si:H films. The results for intensity F2 are shown in Figure 4.7 both in the annealed and light soaked state. Samples SmartB1 and SmartB2 exhibit almost identical results since they are made from the same deposition run. Sample SmartA1 show sligthly higher σ_{ph} values. But in general they show similar spectra. Transition temperature to region II is around 170 °K for all samples and only region II can be observed until 90 °K for ligth intensity F2. These results can lead to a conclusion that DC Glow Discharge films have similar Staebler-Wronski defect distributions after ligth soaking.

It was demonstrated that some of undiluted RF-PECVD films have completely different photoconductivity versus temperature spectra in the annealed state. The effects of photosensitizing states were much more substantial that σ_{ph} showed a peak at

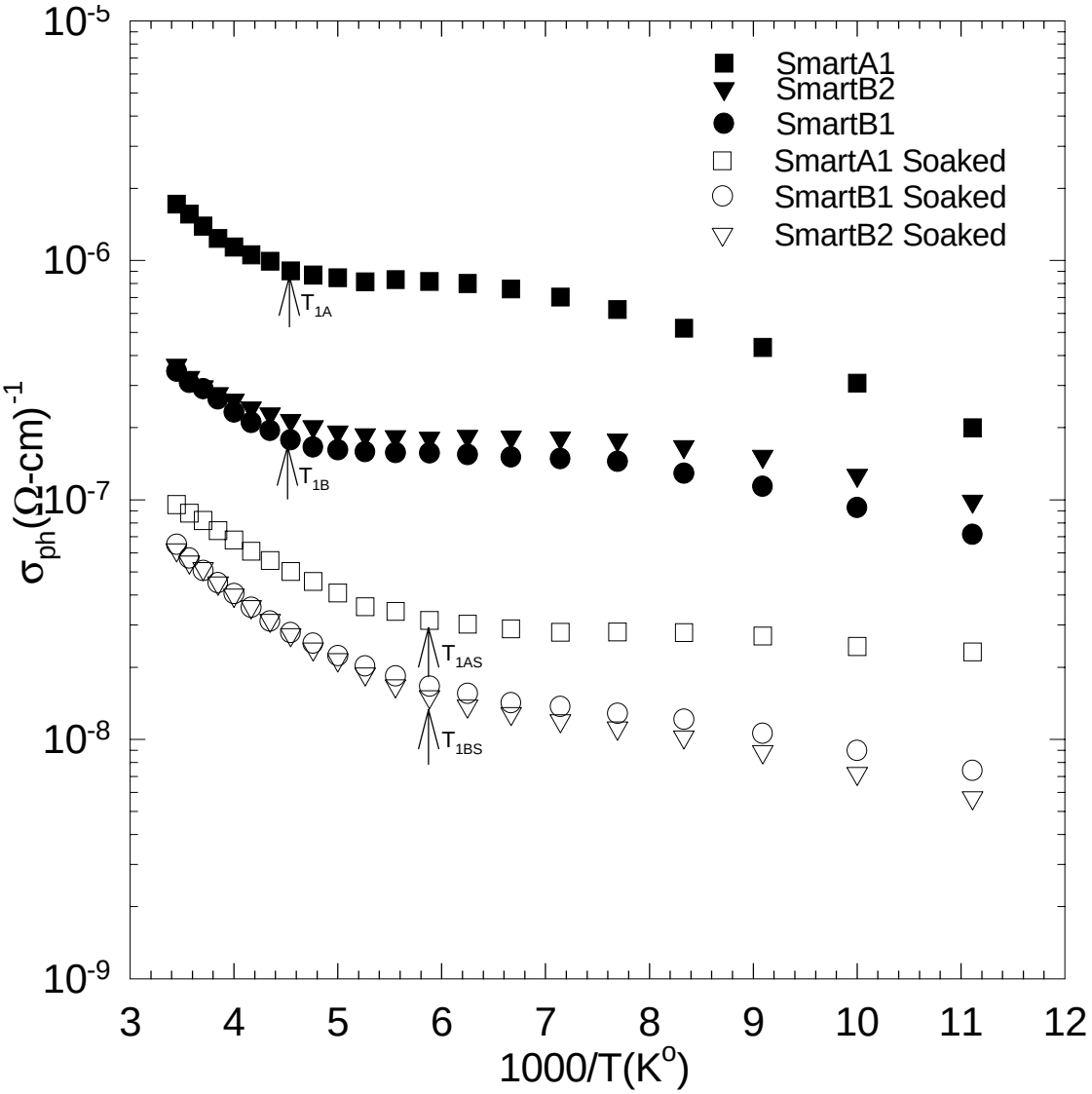

Figure 4.7.Low temperature photoconductivity of DC Glow-discharge samples in the annealed and light soaked state at constant intensity F_2.

lower temperatures. These samples were also subjected to the same light soaking process and Staebler-Wronski effect was investigated in low temperature σ_{ph} spectra. The results of undiluted RF-PECVD sample 4m are shown in Figure 4.8. σ_{ph} at room temperature for each intensity decreased substantially from the corresponding annealed state value. Further decrease in temperature at constant intensity decreases σ_{ph} with a constant slope. It decreases until 170 °K for intensity F2 similar to that observed in DC Glow Discharge samples. Then, σ_{ph} remains to be constant. This behaviour of σ_{ph} in the soaked state is an important change from that of annealed state. Because σ_{ph} decreased to 250 °K, then it started to increase again and peaked around 140 °K. This peak completely disappeared after light soaking, then σ_{ph} spectrum becomes similar to that observed in DC Glow Discharge samples. Mainly two regions in σ_{ph} spectrum can be observed at temperatures down to 90 °K. Even though the native defect density and distribution were substantially different in the annealed state, the defect distributions due to Staebler-Wronski effect seem resemble to that of DC Glow Discharge samples. Both shape and transition temperatures are very close to that of DC Glow Discharge and undiluted RF PECVD sample.

To see the characteristics of other undiluted RF PECVD samples in the light soaked state, σ_{ph} data for lower temperatures were also measured for three different ligth intensities. Since these undoped RF-PECVD samples were displaying similar annealed state characteristics to that of DC Glow Discharge films. As seen from Figure 4.9, these undoped RF-PECVD samples show large degradation of σ_{ph} due to creation of Staebler-Wronski defects by light. Their σ_{ph} spectrum shifts downward in magnitude and displays two regions. σ_{ph} initially decreases from room temperature until transition temperature around 170 °K, then it becomes either constant or shows very slight decrease for a wide temperature region. In region II, photosentisizing defect states play more dominat role that they improve free electron life time τ_n , instead of decreasing it. In the first region, defect states acting as recombination center increases as temperature decreases and resulting in a decreased electron life time and σ_{ph}. It can be inferred that ligth soaking process removes the photosensitizing peaks from low temperature σ_{ph} spectrum if it is present in the annealed state. All samples gain similar defect distribution after ligth soaking process.

The photosensitizing states were more dominant and become effective at higher temperatures in the annealed state of a-Si:H films prepared by hydrogenated dilution

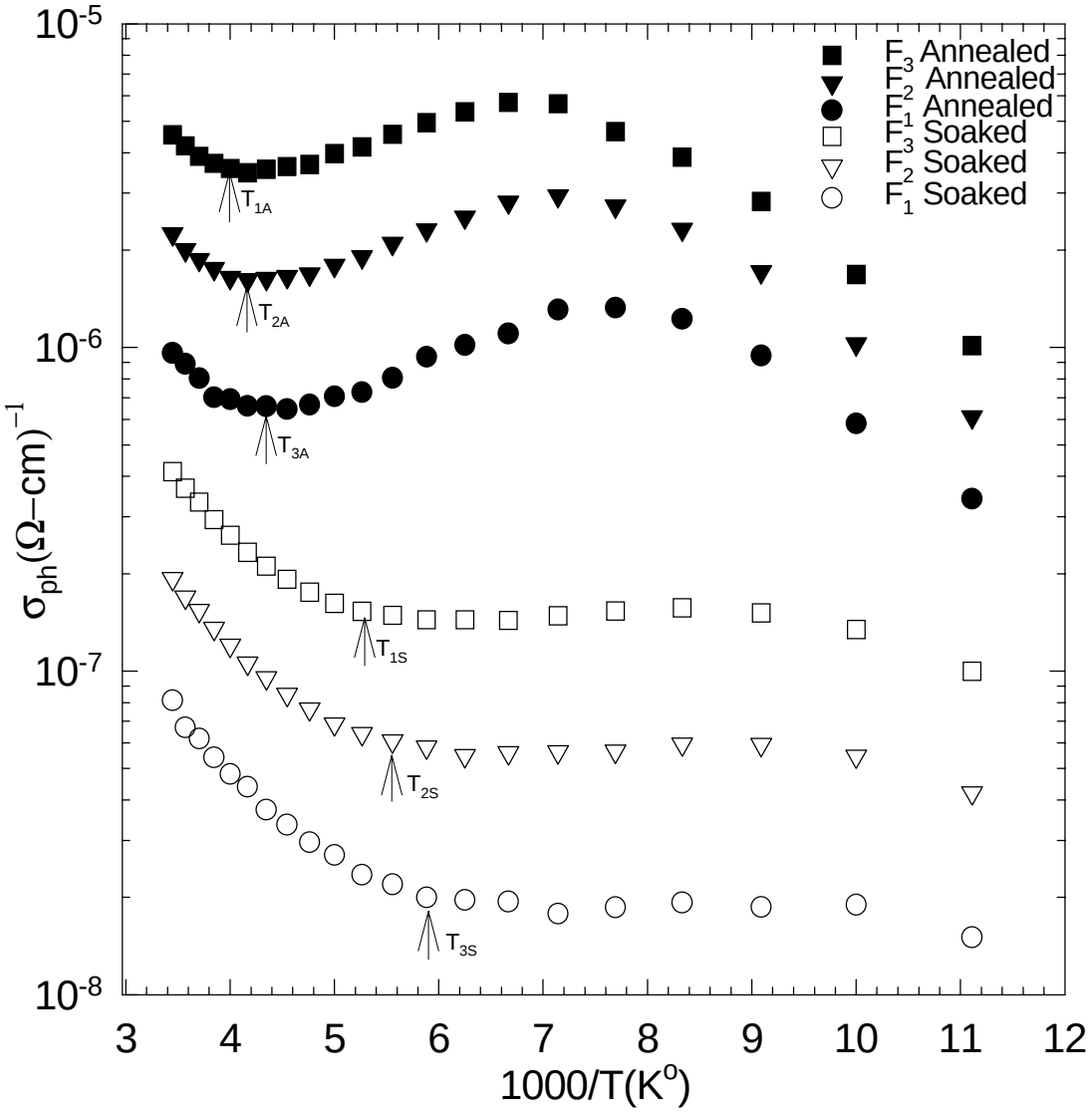

Figure 4.8. σ_{ph} versus 1000/T graph for different intensities for undiluted RF-PECVD sample 4m in the annealed state and light soaked state.

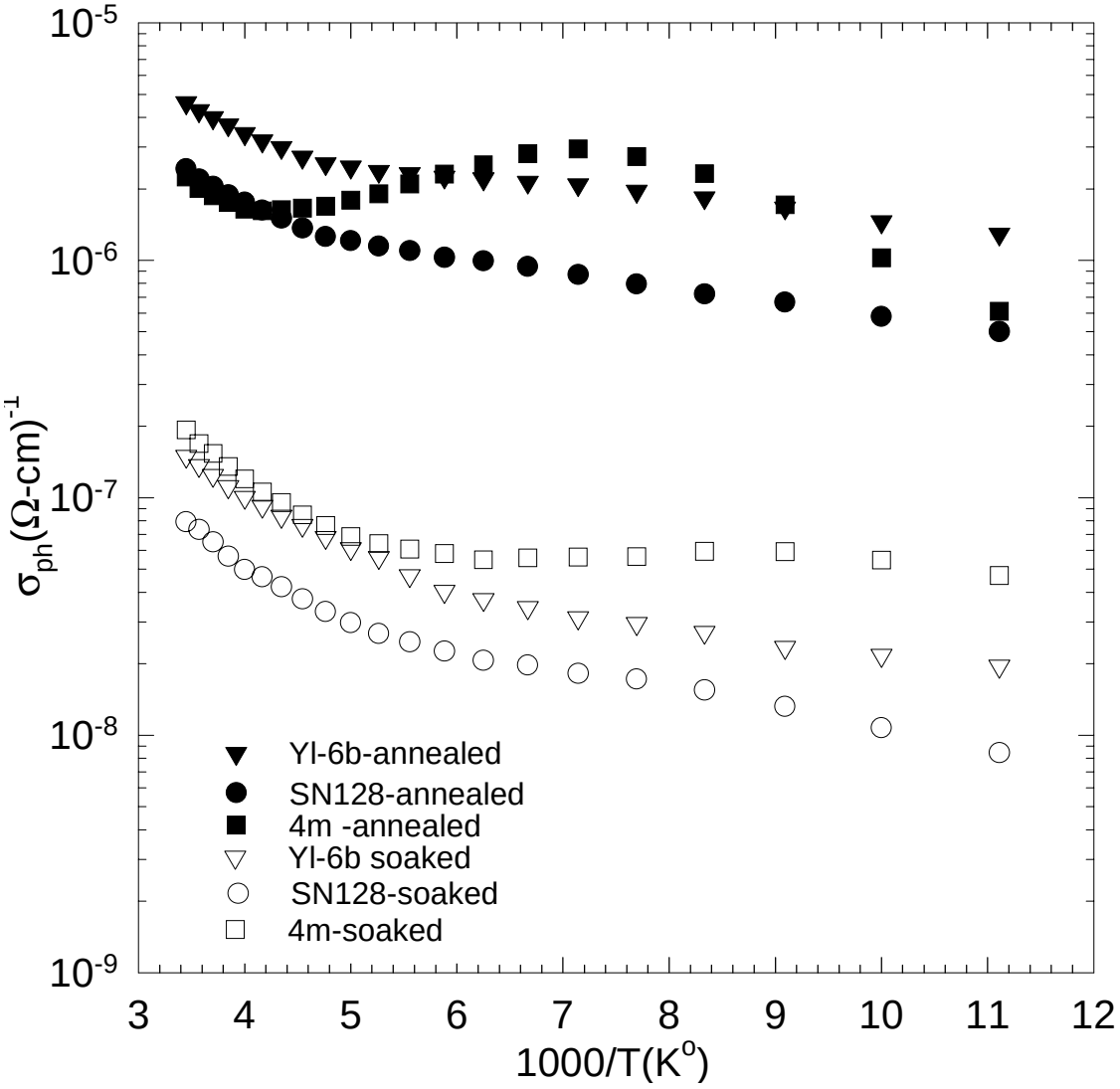

Figure 4.9.Low temperature photoconductivity of undiluted RF- PECVD samples in the annealed and light soaked state at constant intensity F_2.

technique as seen in previous chapter. The effects of the Staebler-Wronski defects on diluted RF-PECVD films were investigated under identical light soaking process. Example of the results for diluted a-Si:H sample LJ-51 is shown in Figure 4.10 for both annealed and light soaked state. As clearly seen from the figure, σ_{ph} was almost constant from room temperature to 160 °K in the annealed state. However, this behavior at higher temperature region disappears after ligth soaking. Instead of having constant σ_{ph}, there is decreasing σ_{ph} as temperature decreases similar to that observed in previous DC Glow Discharge and RF-PECVD films in the light soaked state. σ_{ph} decreases from room temperature down to temperature of 170 °K, exactly the similar transition temperature of previous films, then it becomes to be unchanged for lower temperatures. At transition temperature, photosensitization effect becomes dominant. Again transition temperature decreases as ligth intensity decreases from F3 to F1. For the diluted RF-PECVD sample LJ-51, it is 192 °K, 172 °K, and 154 °K for F3, F2 and F1 respectively. This is an indication that the quasi Fermi levels reach to photosensitizing state at much lower temperatures for lowest light intensity as described Simmons-Taylor statistics. Therefore, these transition temperatures are thermally activated.

The results of low temperature σ_{ph} for other two diluted RF-PECVD films and that of LJ-51 are summarized in Figure 4.11 for intensity F2. It is conclusive that all diluted films show similar characteristic low temperature σ_{ph} spectrum in light soaked state. The effects of photosensitizing states in region II shifts to much lower temperatures contrary to that observed in the annealed state. Region I becomes apparent, the same as soaked state of other samples. Only region I and II can be observed from room temperature to 90 °K although region II and III were observed in the annealed state. These diluted a-Si:H films clearly indicate that more Staebler-Wronski defects are created around the midgap, which effectively reduces the electron life time and finally σ_{ph} and hence photosensitizing Staebler-Wronski defects are created away from midgap. Due to increased density of Staebler-Wronski defects, quasi-Fermi levels E_{fn} and E_{fp} cannot reach to exponential tail states and a sharp decrease in σ_{ph} have not been observed until 90 °K at intensity F2. However, at intensity F3, the onset of exponential tail state recombination is observed below 90 °K.

Finally, the results of device quality a-Si:H films made using HW-CVD technique and RF magnetron sputtering are shown in Figure 4.12. for both annealed and ligth soaked states. For both samples, significant photosensitization effect was observed in the annealed state. It was much more significant in HW-CVD sample. After 10 hours

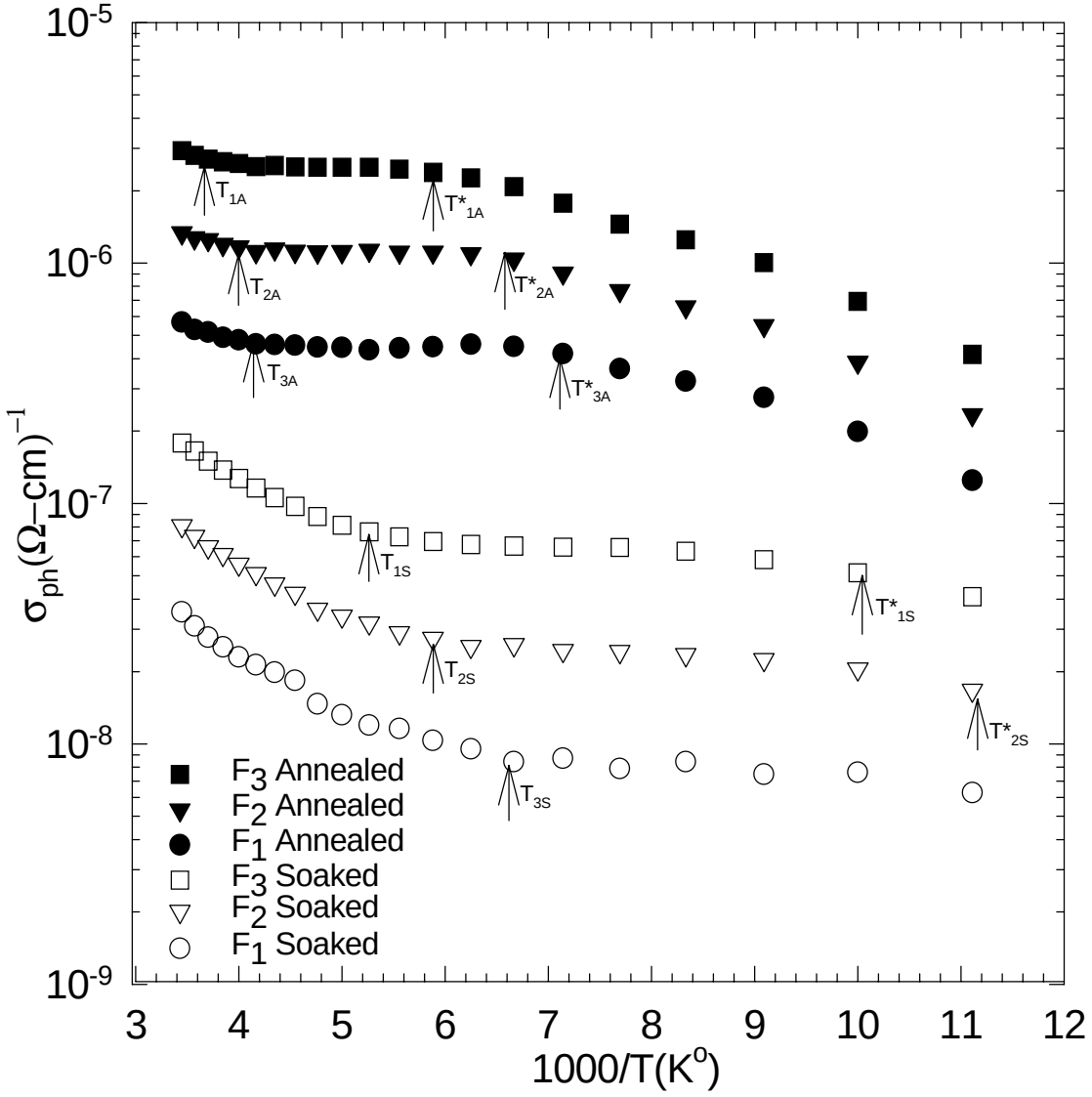

Figure 4.10. σ_{ph} versus 1000/T graph for different intensities for diluted RF-PECVD sample Lj-51 in the annealed state and light soaked state.

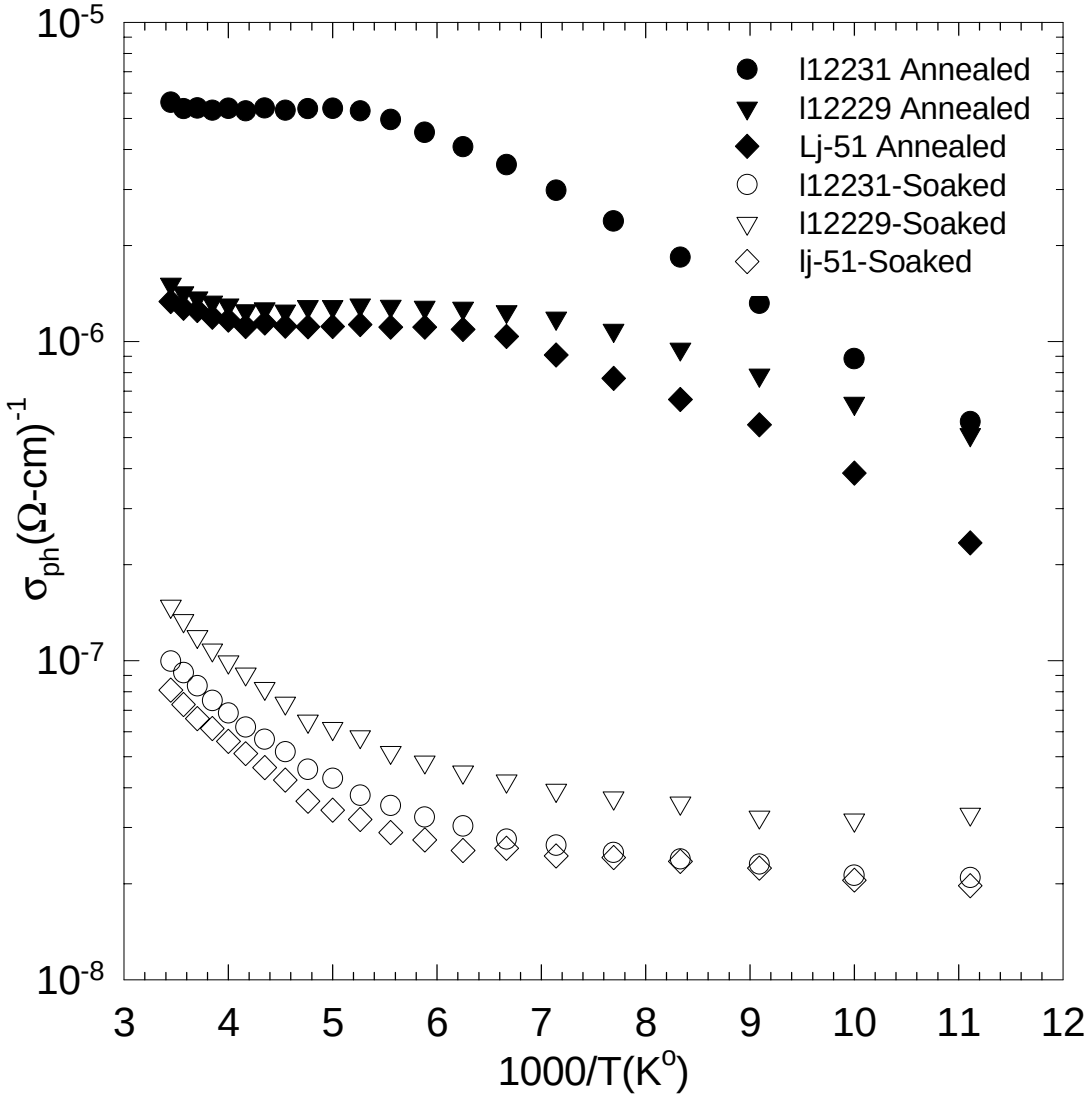

Figure 4.11.Low temperature photoconductivity of diluted RF-PECVD samples in the annealed and light soaked state at constant intensity F_2.

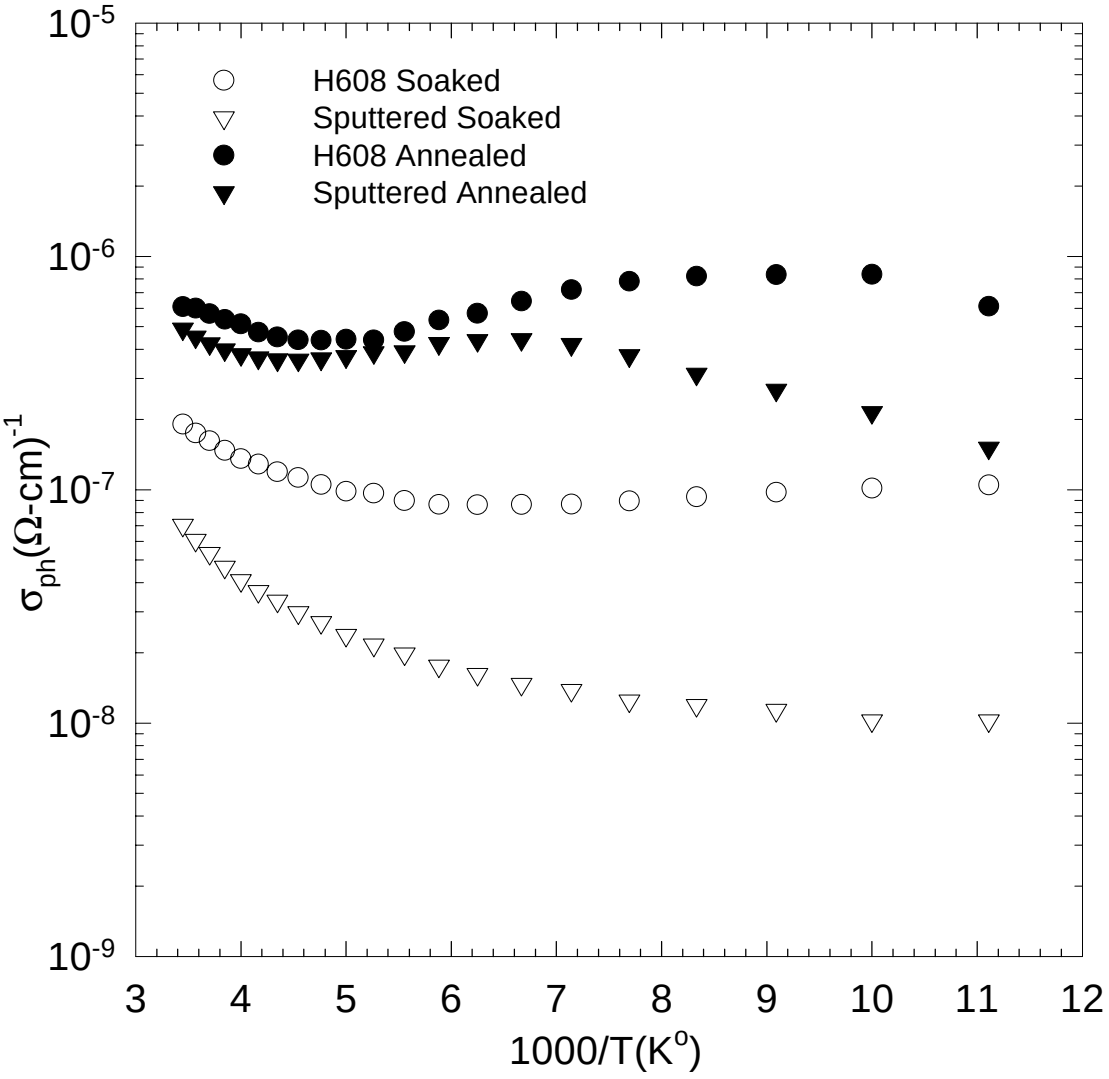

Figure 4.12. Low temperature photoconductivity of Hot-Wire CVD and RF Magnetron Sputtered samples in the annealed and light soaked state at constant intensity F_2.

of white ligth soaking, more significant Staebler-Wronski effect is seen in sputtered film that σ_{ph} at room temperature decreased by factor of 10. However, it is only factor of 5 for HW-CVD sample. As temperature decreases, σ_{ph} in region I starts decreasing until transition temperature. Then photosensitization sets in. Transition temperature is around 178 °K for HW-CVD sample and 150 °K for sputtered sample. σ_{ph} remains to be constant in region II for sputtered film but it is slightly increasing until 90 °K for HW-CVD sample. This increase in σ_{ph} in region II is less significant than that observed in annealed state. This type of behaviour in soaked state is observed only in HW-CVD sample indicating that both photosensitizing defects and free electron lifetime killer defects are created in a certain proportion; electron lifetime killer defects are around midgap and electron lifetime sensitizing defects closer to band edges. This is important difference from other films that more electron life time killer defects around midgap and less photosensitizing defects closer to band edges are created by light. The Staebler-Wronski effect results in creation of at least two different types of defect states. Their effects are only seen in low temperature σ_{ph} spectrum as region I and region II in light soaked state.

In conclusion, a wide range of variations in photoconductivity at room temperature have been measured, indicating the effects of deposition conditions on film properties. The slope of log-log plot of photoconductivity versus intensity changes from 0.70 to 0.90 in the annealed state and becomes close to unity for all films in the soaked state. In the annealed state, low temperature photoconductivity spectra show three regions for DC GD, Sputtered, HW-CVD, and undiluted RF-PECVD films. H-Diluted RF-PECVD films show only two regions. Region I in the spectra is due to defect states around the midgap, where free electron lifetime decreases by temperature; Region II is due to new type of defect states, different from region I, which are closer to the band edges. In region II, free electron life time and photoconductivity increases or remain to be constant as temperature decreases; Region III is due to the onset of the exponential tail states, where free electron lifetime decreases continuously. H-Diluted a-Si:H films do not show the region I even at room temperature but starts from region II and ends with region III. In the light soaked state, substantial decrease in photoconductivity due to Staebler-Wronski defects are observed in all films. All films show almost the same shape low temperature photoconductivity spectra. Region I is extended to lower temperatures down to 170^0K, then region II with a constant photoconductivity dominates until 90^0K. Region III can barely be detected at temperatures below 90^0K and

intensities higher than used in the study. These results indicate that there are at least two types of defect states present in the annealed state: neutral silicon dangling bond, D^0, states and non-D^0 states, possibly charged defect states. Light soaking creates more D^0 states around the midgap, as well as non-D^0 states closer to the band edges.

CHAPTER 5
DISCUSSION AND CONCLUSIONS

Undoped hydrogenated amorphous silicon thin film materials prepared using different deposition systems have been characterized both in the annealed and light soaked states. The characterization includes dark conductivity as a function of temperature, steady-state photoconductivity versus light intensity at room temperature and steady-state photoconductivity versus temperature for three different intensities. A qualitative comparison of these results have been carried out to understand the effects of native and Staebler-Wronski defect states in the bandgap of a-Si:H thin films prepared under different deposition conditions.

In the annealed state, undoped a-Si:H films were kept at 180 ^{o}C for a few hours, then dark conductivity was measured as a function of temperature. Dark conductivity versus 1000/T, also called Arrhenius plot, plots were obtained. The slope of these plots yields the position of dark Fermi level in the bandgap. As we have explained in Chapter 3, all films show higher activation energy values. It is well established that undoped a-Si:H have optical gap of 1.70eV to 1.86eV depending on the hydrogen content in the material. However, electron transport in dark and recombination processes of free electrons and holes are subject to higher bandgap than the optical gap defined from optical measurements. This higher bangap was first measured by Wronski et al. in 1989 and defined as “Mobility gap” and later others called it as “Recombination bandgap”. Mobility gap of a-Si:H is greater than optical bandgap by 0.1eV to 0.2eV. Our samples used in this thesis have optical gaps of 1.70eV to 1.82eV and corresponding mobility gaps varies from 1.90eV to 2.02eV. For undoped a-Si:H films dark Fermi level is expected to be in the middle of the bandgap which should be around 0.95eV to 1.0eV. Our experimental results agree very well with this expectation. Only for the samples 4m and SN-128 prepared using RF-PECVD deposition system without hydrogen dilution, activation energy of dark conductivity is 0.60eV and 0.85eV respectively. These values show that dark Fermi level is positioned above the middle of the bandgap. Even though these films are undoped, the impurity concentration levels are very low to cause such kind of 0.1 to 0.4eV shift in the Fermi level. The reason for having lower activation energies in undoped films is due to charge distribution of defect state in the bandgap, which totally determine the position of dark Fermi level. Many reported

results on undoped a-Si:H film for dark Fermi level show variations from 0.6eV to 0.90eV for the activation energy. The results of dark conductivity as a function of temperature are consistent for the expected values of dark Fermi level for an undoped film.

Position of dark Fermi level is an important determining factor for occupation of midgap defect states in dark. Presence of the midgap defect states can be detected by measuring steady-state photoconductivity at room temperature using a monochromatic light with energy greater than the optical gap. Monochromatic light $E = h\nu > E_{opt}$, results in excitation of free electrons from the valence band to the conduction band. This process involves the extended states at higher energies. However the excited free electrons in the conduction band cannot stay longer over there. They must recombine with free holes in the valence band in a certain time. Therefore this recombination process must go through certain steps. They might directly recombine with holes in the valence band or recombination could be through the midgap defect states. Depending on the dominant recombination process, measured steady-state photoconductivity shows certain dependence on the intensity of the excitation. To understand the dominant recombination process, steady-state photoconductivity for different intensities were measured for all films in the annealed state using the same monochromatic red light. As given in Chapter 3, the results of σ_{ph} are proportional to light intensity ($\sigma_{ph} \alpha F^{\gamma}$). The power γ has values of close the unity for all the samples studied here. In Appendix A, several theoretical models for the recombination process in photoconductivity have been presented. The values of γ is a direct indication of recombination in photoconductivity. If γ=0.5, called bimolecular recombination, free electron in the conduction band recombine directly with the free holes in the valence band. Midgap defect states are not involved in this recombination process. However, experimental results for the samples do not show such γ values excluding this type of recombination in undoped a-Si:H. If γ=1.0 which is called monomolecular recombination, free electron in the conduction band recombine with the holes in valence band through recombination centers in the bandgap. It is direct indication that midgap defect states around dark Fermi level are involved in the photoconductivity. γ=1.0 means that mobility lifetime product ($\mu\tau$) is constant as intensity increases. According to Simmons-Taylor statistics the number of recombination centers will increase as intensity of excitation increases. Therefore, $\mu\tau$ product must show a decrease correspondingly. This type of behavior can only be valid in films with a very low

constant density of midgap defects at discrete energies as shown by Rose[83]. In undoped a-Si:H, measured values of power γ is close to unity between 0.70 and 1.0. This type of behavior is not a mixture of two different recombination proceses but rather an indication of continuous distrubition of defect states in the bandgap, where the recombination of free electrons take place.

Experimental results in the annealed state show values of γ from 0.8 to 0.95, which are very close to unity. Again only films prepared with RF-PECVD without hydrogen dilution exibit γ values around 0.70. This is an indication that density and distribution of midgap defect states are slightly different in these films. However, the power γ for all films show that midgap defects states are involved in the recombination of free electrons in the conduction band with the free holes in the VB. Their distribution is continuous throughout the bandgap. Due to the differences in their densities, magnitude of photoconductivity shows large variations. Even though films are prepared in the same deposition sytem, they can have wide range of photoconductivities. For example samples prepared at Penn State University using RF-PECVD, those prepared at USSC using the same deposition system and DC GD films, they are showing the variations. This behavior was reported in detail by SMART group that there is no unique undoped a-Si:H films with a well defined electrical and optical properties like single crystalline silicon[19]. The results obtained in the annealed state are consistent with the generally reported magnitudes of σ_{ph} in the literature.

Steady-state photoconductivity in the annealed state which is measured for different intensities gives very limited information about the native midgap defect states since intensity of light is limited to probe the effects of the defects in the bandgap. Alternatively, temperature can be used for wider range of defect involvement in the recombination process. As given in Appendix A, Simmons-Taylor Statistics predicts the effects of continuous midgap defect states as tempareture decreased at constant light intensity. In the measured photoconductivity both density and nature of midgap defect states are involved through the carrier capture cross sections. For better understanding of the continuous midgap defect states, steady-state photoconductivity at three different light intensity were measured as temperature decreased from room temperature to 90 ^{0}K. It is expected that at a constant intensity, quasi-Fermi levels for electrons and holes are fixed in energy in the bandgap. Only certain part of midgap defect states around the dark Fermi level are involved in recombination process. It was clearly measured that $\gamma<1.0$ represents active role of these recombination centers. By

decreasing temperature, quasi-Fermi levels move through their respective band edges, electron quasi-Fermi level E_{fn} moves to the conduction band edge E_c and hole quasi-Fermi level E_{fp} moves through the valance band edge E_v. As a result of this, new midgap defect states are converted to recombination centers. Their density and nature are reflected in measured photoconductivity. Low temperature photoconductivity spectra measured on undoped films show certain characteristic features. Some samples show similar spectra even though they are made in different deposition systems. The others exhibit obvious differences in temperature scale.

There are three distinct regions in low tempareture photoconductivity spectra. Region I is between room temperature and 250 ^{0}K which is sample dependent. In this region, σ_{ph} decreases with decreasing temperature. It is consistent with increasing density of recombination centers between quasi-Fermi levels. There is only one type of dominant recombination center determining free electron lifetime. In region II, σ_{ph} remains to be constant or increases as temperature decreases. This region is called Thermal quenching region or photosensitization region. Transition temperature to region II is thermally activated. In region II, dominant recombination centers are different from those in region I. This type of behavior has been also reported before in the literature[24,43,54]. It is an indication that new types of defect states are converted to recombination centers between quasi-Fermi levels and they have much lower capture cross-sections for electrons from those of defects dominating in region I. Rose called this type of defects "sensitizing states" or Mc Mahon and Crandall labeled them as "safe hole traps" in the valence band tails. Region II is definitely due to the effects of second type of defect states in the bandgap of a-Si: H. It is believed that dominant defect center around the midgap is neutral silicon dangling bond, D^0 states. They are dominating the region I of low T spectrum. However, region II is controlled by non-D^0 defect states, which could be charged defect states or other type of unknown defects. It is only possible that defect models predict charged silicon dangling bonds or floating bonds present in the annealed films.

Third region seen in the low temperature photoconductivity spectrum is detected at lower temperatures below 100 ^{0}K. In this region, σ_{ph} decreases continuously. It is more likely that σ_{ph} decreases due to the onset of high density of recombination centers dominating over defects around the midgap. These defects are exponential conduction and valance band tail states. At this lower temperature, quasi-Fermi levels move very

close to band edges and hit in the band tail states. The behavior of low temperature σ_{ph} spectra are similar for all DC GD films, sputtered sample, and RF-PECVD samples SN-128 and YL-6B. The degree of thermal quenching or photosensitization is more substantial in sample 4m deposited by RF-PECVD and also for HW-CVD sample. This is an indication that non-D^0 defect states have higher density in these samples. The effects of these photosensitizing states are clearly seen in H-diluted samples prepared in different laboratories. They are more dominating and closer to the middle of the bandgap. Their effects are seen even at room temperature. Therefore, H-diluted samples show only region II and region III. H-dilution technique results in more non-D^0 defect states in the material. Even though the magnitude of σ_{ph} is different in films, the shape of low T spectrum is similar for the undiluted films. Transition temperatures are sample dependent and show good agreement among different samples. These transition temperatures from region I to region II and from region II to region III are thermally activated as intensity of light changes. As a conclusion, there are exponential tail states dominating region III at very low temperatures below 100 ^{0}K, and there are at least two different types of midgap defect states in the bandgap of a-Si:H in the annealed states. These defects states could be neutral silicon dangling bond defects, D^0, and non-D^0 defect states; charged defect states or floating bond defect states predicted by the recent defect models proposed for a-Si:H[67,68,74,78].

In the light soaked state, samples show great deal of degradation in dark and photoconductivity. Dark conductivity decreases from its annealed value indicating that dark Fermi level moves slightly through the midgap. Degradation of photoconductivity shows that more defect states created by light soaking. These defect states are called Staebler-Wronski defects. They are annealed out at higher temperature and annealed state values are restored at temperature above 150 ^{0}C. As seen in Chapter 4, HW-CVD sample and DC GD sample show the least degradation in σ_{ph} and others show a degradation factor from 6 to 50. In the intensity dependence of photoconductivity, $\sigma_{ph} \alpha F^{\gamma}$, the power γ becomes almost similar for all films. It is close to unity between 0.85 to 0.95, within the experimental error. This indicates that distribution of defect states after light soaking becomes almost similar for all films even though they had wide range differences seen in the annealed state characteristics.

The effects of Staebler-Wronski effect in the light soaked samples are also characterized using low temperature photoconductivity study. Even though, large

differences in the shape of low temperature spectra were detected in films deposited under different conditions, all samples now show almost the same shape of spectra. Mainly region I and region II are dominating the spectrum until 90 ^{0}K. Region III can be detected at higher intensity and lower temperatures than 90 ^{0}K. Region I becomes dominant until 170 ^{0}K which is lower than that observed in the annealed state. That means that more defects are created around midgap and they are same type that present in the annealed state. Transition temperature at different light intensities is thermally activated. This behavior is consistent with the analysis of Simmons-Taylor Statistics. In region II, σ_{ph} remains to be constant for almost all samples independent of deposition conditions. Region II dominates until 100^{0}K. In this region, there is still photosensitization not to decrease σ_{ph} as temperature decreases. This can only be possible by having defect states with very low capture cross sections for electrons than the defect states dominating in region I. They must be non-D^0 defect states. They were present in the annealed state and were more dominant in some samples like sample 4m. But their effects are reduced by the defects created by light. The spectrum of sample 4m in the soaked state becomes the same as others. Similarly, diluted a-Si:H films showed the effects of non-D^0 states in the annealed state, showing only region II and III in the annealed state. However, light soaked spectra changed significantly from that of annealed state and become similar to that of other a-Si:H films. That clearly shows that more D^0 states are created by light around midgap and less non-D^0 states are created closer to the band edges. Staebler-Wronski defects created by light are at least two types of defects. More D^0 defect states are created around midgap, which determine region I in the spectra and less non-D^0 defects are created away from the midgap. They act as photosensitizing defects since σ_{ph} remains to be constant in region II. These defect states can be detected at temperatures below 160K. They cannot be detected using σ_{ph} at room temperature even at the highest light intensity.

As a conclusion, light soaking creates Staebler-Wronski defects in the bandgap. They decrease dark and photoconductivity. There are at least two different types of Staebler-Wronski defects created by light. One type is more dominant in density and located around midgap. They are more likely that neutral silicon dangling bond defect states, D^0. Second type of Staebler-Wronski defect states are created away from midgap and closer to band edges. They act as electron sensitizes. They are different from D^0 states. They are non-D^0 defect states; charged silicon dangling bond

defects, D^+ and D^-, or floating bond defects. These kinds of defects are resulted from the new defect models proposed for SWE in a-Si:H. These defect models are “defect pool model”, “H-collision model” and “silicon rebonding model”. From these experimental results, only qualitative understanding of these defects and their effects are observed. Exact analysis of results requires self-consisting analysis of these results using a detailed numerical modeling based on the Simmons-Taylor Statistics. Then, it can be possible to obtain their densities, nature and energy distributions in the bandgap of a-Si:H.

5.1 Future Proposed Research

In this thesis, only qualitative understanding of Staebler-Wronski defects and native defects on steady-state photoconductivity for different light intensities and temperatures were carried out. For better understanding, light calibration with a better detector will be necessary to quantify flux and generation rate. Furthermore, a detailed numerical simulation program must be developed to analyze the results. This will illuminate the picture of native and light induced defect state located in the bandgap of a-Si:H.

REFERENCES

[1] La van Hove, Phys. Rev. **89**, 1189 (1953).

[2] H. Fritzsche, " Density of states in noncrystalline solids," in Physical Properties of Amorphous Materials, edited by D. Adler, Plenum Press, New York, 1985.

[3] S. M. Sze, Physics of Semiconductor Devices , Second Edition, Wiley-interscience Publication, New York, 1981.

[4] R.C. Chittick, J.H. Alexander, and H.F. Sterling, " The preparation and properties of amorphous silicon, " J. Electrochem. Soc. **116**, 77 (1969).

[5] W. E. Spear and P. G. LeComber, " Substitutional doping of amorphous silicon, " Solid State Comm. **17**, 1193(1975).

[6] D. E. Carlson and C. R. Wronski, " Amorphous silicon solar cells, " Appl. Phys. Lett. **28,** 671 (1976).

[7] Davied E. Carlson and Sigurd Wagner, " Amorphous silicon photovoltaic systems," in Renewable Energy-Sources for Fuels and Electricity, edited by T. B. Johansson, H. Kelly, A. K. N. Reddy and R. H. Williams,Island Press, Washington, 1991.

[8] M. Pinarbasi, M.J. Kushner, J.R. Abelson, J. Vac. Sci. Technol. A, **8 (3)**, 1369 (1990).

[9] A.H. Mahan and M. Vanecek, Amer. Inst. of Phy. Conf. Proc. **234**, 195 (1991).

[10] D. Adler, Solar Cells, **9**, 113 (1983).

[11] D. L. Staebler and C. R. Wronski, " Reversible conductivity changes in discharge produced amorphous Si," Appl. Phys. Lett. **31,** 292 (1977).

[12] K. Morigaki, I. Hirabayashi, N. Nakayama, S. Nitta and K. Shimakawa, Solid State Commun. **33**, 851 (1980).

[13] H. Dersch, J. Stuke and and J. Beichler, Appl. Phys. Lett. **38**, 456 (1981).

[14] A. Skumanich, N. M. Amer and W. B. Jackson, Bull. A.P.S. **27**, 146 (1982).

[15] J. Desner, B. Goldstein and D. Szostak, Appl. Phys. Lett. **38**, 998 (1980).

[16] Lawrence L. Kazmerski, " Photovoltaic characterization: A survey of diognastic measurements," J. Mater. Res. **13**, 2684 (1998).

[17] M. H. Tanielian, N. B. Goodman and H. Fritzche, J. De Phys. **42**, Suppl. 10, C4-375 (1981).

[18] D. Han and H. Fritzche, J. Noncryst. Solids **59&60**, 397 (1983).

[19] C. R. Wronski, N. Maley, T. M. Peterson, J. R. Abelson, M. B. Bennett, P. K. Bhat, R. Biswas, V. L. Dalal, A. E. Delahoy, S. J. Fonash, C. M. Fortmann, S. Guha, W. Luft, T. McMahon, D. Redfield, P. C. Taylor and S. Wagner, "Findings and plans of the stable materials adisory research team," in European Photovoltaic Solar Energy Conference, (1992).

[20] S. Guha et al., J. Appl. Phys. **52**, 859 (1981).

[21] Y. Ziegler, V. Daudrix, C. Droz, R. Platz, N. Wyrsch and A. Shah, " More stable low gap a:Si:H layers deposited by PE-CVD at moderately high temperature with hydrogen dilution," Solar Energy Materials&Solar Cells, **66**, 413-419, (2001).

[22] S. Bauer, B. Schroder and H. Oechsner, " The effect of hydrogen dilution on the microstructure and stability of a-Si:H films prepared by different techniques," J. Noncryst. Solids **227-230**, 34-38 (1998).

[23] M. Vanecek, A.H. Mahan, B.P. Nelson, and R.S. Crandal, Proc. 11th European PV Solar Energy Conf. Edited by L. Guimaraes, W. Palz, C. Dereyff, H.Kiess, and P. Helm (Harwood Acad. Publ.,Switzerland, 1993), p. 96.

[24] Qi Wang, Brent P. Nelson, E. Iwaniczko, A. H. Mahan, R. S. Crandall, and J. Benner," The influence of charge effect on the growth of hydrogenated amorphous silicon by the hot-wire chemical vapor deposition technique," 2nd World Conference and Exhibition on Photovoltaic Solar Energy Conversion Presentation, Vienna, Austria, 1998.

[25] B. Schroder and S. Bauer, J. Noncryst. Solids **266-269**, 115-119 (2000).

[26] Brent P. Nelson, Yueqin Xu, A. Harv Mahan, D.L. Williamson and R.S. Crandall, Mat. Res. Sos. Symp. Proc. **609,** A22.8.1(2000).

[27] G. D. Cody, C. R. Wronski, B. Abales, R. Stephens , and B. Brooks, Solar Cells, **2**, 227(1980).

[28] R. W. Collins, J. Koh, H. Fujiwara and C. R. Wronski, " Application of real-time spectroscopic ellipsometry for characterizing the structure and optical properties of microcrystalline component layers of amorphous semiconductor solar cells," Solar Energy Materials and Solar Cells, **49**,135-142, (1997).

[29] Sheng, Shuran; Sacher, Edward; Yelon, Arthur; Branz, Howard M.; Masson and Denis P., " Structural changes in a-Si:H studied by X-ray photoemission spectroscopy," Materials Research Society Symposium - Proceedings, **557**, 359-364, (1999).

[30] J. D. Cohen and F. Zhong, " Transient modulated photocurrent studies in hydrogenated amorphous silicon: A new look at defect relaxation dynamics," J. Noncryst. Solids, **190**, 123-132 (1995).

[31] M. Gunes, Y. M. Li, R. M. Dawson, C. M. Fortmann, and C. R. Wronski, "Investigation of intrinsic defect states in hydrogenated amorphous silicon films using steady-state photoconductivity and sub-bandgap absorption," in Proc. of IEEE XXIII Photovoltaic Specialists Conference (IEEE,New York, 1993), p.885.

[32] Mehmet Gunes and Christopher R. Wronski, "Differences between light induced and native midgap states in intrinsic hydrogenated amorphous silicon obtained from detailed modeling of photoconductivity and sub-bandgap absorption," Appl. Phys. Lett. **61**, 678(1992).

[33] S. Lee, M. Gunes , C. R. Wronski, N. Maley, and M. Bennett, "Effects of midgap states in intrinsic hydrogenated amorphous silicon on sub_bandgap photoconductivity," Appl.Phys. Lett.**59**, 1578(1991).

[34] H. Dersch, L. Schweitzer and J. Stuke, Phys. Rev. B, **28**, 4678(1983).

[35] R. M. Dawson, C. R. Wronski, M. Bennett, " The density of states below midgap determined from the space charge limited currents of holes in intrinsic hydrogenated amorphous silicon, " Appl. Phys. Lett. **58**, 272 (1991).

[36] J. D. Cohen, " Density of states from junction measurements in hydrogenated amorphous silicon," in Hydrogenated Amorphous Silicon, vol. **21**, Semiconductors and Semimetals, edited by J. I. Pankove (Akademic Press, New York, 1984),p.9.

[37] C. R. Wronski and R. E. Daniel, Phys. Rev. B, **23**, 794(1981).

[38] W. B. Jackson, and N. Amer, in AIP Conf. Proc. **73**, 263 (1981).

[39] M. Vanecek, J. Kocka, J. Stucklik, Z. Kozisek, O. Stika, and, A. Triska, Solar Energy Materials, **8**, 411 (1983).

[40] K. Pierz, H. Mell, J. Terukov, J. Non-Crst. Solids **77&78**, 547(1985).

[41] H. Curtins and M. Favre, " Surface and bulk states determined by photothermal deflection spectroscopy," in Amorphous Silicon and Related Materials, vol. **A**, (World Scientific, New Jersey, 1989), p. 329.

[42] P. E. Vanier, " Reversible photoinduced changes in the low-temperature photoconductivity of hydrogenated amorphous silicon," Appl. Phys. Lett. **41**, 986(1982).

[43] P. E. Vanier, A. E. Delahoy, and R. W. Griffith, " New features of the temperature dependence of photoconductivity in plasma deposited hydrogenated amorphous silicon alloys, " J. Appl. Phys. **52**, 5235 (1981).

[44] T. J. McMahon and A. Madan, " Photoconductivity and electronic doping effects in hydrogenated amorphous silicon," J. Appl. Phys. **57**,5302(1985).

[45] D. Mendoza and W. Pickin, " Density of states and temperature dependence of the exponent in the light-intensity behavior of a-Si:H photoconductivity," Phys. Rev. B **40**, 3914 (1989).

[46] W. E. Spear , R. J. Loveland and A. Al-Sharbaty, J. Noncryst. Solids, **15**, 410, (1974).

[47] P. D. Persans, Phil. Mag. B, **46**, 435 (1982).

[48] A. Arena and J. Baixeras, Phys. Rev. B **30**, 2016 (1984).

[49] T.J. Mcmahon and J.P. Xi, Phys. Rev. B **34**, 2475 (1986).

[50] M. Zhu and H. Fritzsche, Phil. Mag. B, **53**, 41 (1986).

[51] J.K. Yoon, J. Jaug and C. Lee, J. Appl. Phys. **64**, 6591 (1988).

[52] T. Smail and T. Mohammed-Brahim, Phil. Mag. B, **64**, 675 (1986).

[53] K.V. Koughia, E.I. Terukov, V. Fuhs, Semiconductors **32**, 824 (1998).

[54] B. Gu, D. Han, C. Li and S. Zhao, Phil. Mag. B, **53**, 321 (1986).

[55] R.H. Bube, J. Phys. Chem. Solids. **1**, 234 (1957).

[56] H.-J. Hoffman and F. Stöckmann, Advances in Solid State Physics **19**, 271 (1979).

[57] R.W. Griffith, F.J. Kampas, P.E. Vanier and M.D. Hirsch, J. Noncryst. Solids, **35/36,** 391 (1980).

[58] H. Okamato, H. Kida and Y. Hamakawa, Phil. Mag. B, **49**, 321 (1984).

[59] F. Vaillant, D. Jousse and J.C. Bruyere, Phil. Mag. B, **57**, 649 (1988).

[60] T. Tiedje and A. Rose, Solid State Commun. **37**, 49 (1980).

[61] J. Oreinstein and M..A. Kastner, Phys. Rev. Lett. **48**, 1241 (1981).

[62] R.A. Street and D.K. Biegelsen, J. Noncryst. Solids, **15**, 416, (1980).

[63] J.D. Cohen, J.P. Harbison and K.W. Wecht, Phys. Rev. Lett. **48**, 109 (1982).

[64] M. H. Cohen, H. Fritzsche, S. R. Ovshinski, Phys. Rev. Lett. **22**, 1065 (1969).

[65] M. Stutzmann, W. B. Jackson, C. C. Tsai, " Light induced metastable defects in hydrogenated amorphous silicon: A systematic study," Phys. Rev. B, **32**, 23 (1985).

[66] Y. Bar-Yam and J. D. Joannapoulos, Phys. Rev. Lett. **56**, 2203 (1986).

[67] S. T. Pantelides, " Defect dynamics and the properties of amorphous silicon -a new perspective," Mat. Res. Soc. Proc. **95**, 23 (1987).

[68] H. M. Branz and M. Silver, " Potential fluctuations due to inhomogeneity in hydrogenated amorphous silicon and the resulting charged dangling bond defects," Phys. Rev. B, **42**, 7420 (1990).

[69] G. Schumm and G. H. Bauer, " Thermodynamical equilibrium gap-state distribution in undoped a-Si:H," Phil. Mag. B, **64**, 515 (1991).

[70] M. J. Powell and S. C. Dean, " Improved defect pool model for charged defects in amorphous silicon," Phys. Rev. B, **48**, 10815 (1993).

[71] J. Ristein, J. Hautala, and P. C. Taylor, " Excitation energy dependence of optically induced ESR in a-Si:H," Phys. Rev. B, **40**, 88 (1989).

[72] S. Yamasaki, H. Okushi, A. Matsuda, and K. Tanaka, " Origin of optically induced electron spin resonance in hydrogenated amorphoous silicon," Phys. Rev. Lett. **65**, 756 (1990).

[73] J. Isoya, S. Yamasaki, H. Okushi, A. Matsuda, and K. Tanaka, Phys. Rev. B, **47**, 7013 (1993).

[74] Howard M. Branz, “Hydrogen collision model: theory and experiment,” J. Noncryst. Solids **266-269**, 391-396 (2000).

[75] Howard M. Branz, “Hydrogen collision model: quantitative description of metasitability in amorphous silicon,” Phys. Rev. B. **59**, 5498 (1999).

[76] Howard M. Branz, “Hydrogen collision model of light-induced metasitability in hydrogenated amorphous silicon,” Solid State Commun. **105**, 387 (1998).

[77] R. Biswas and Y.-P. Li, “Hydrogen flip model for light-induced changes of amorphous silicon," Phys. Rev. Lett. **82**, 2512 (1999).

[78] R. Biswas, Y.-P. Li and B. C. Pan, “Mechanism for metasitability in hydrogenated amorphous silicon,” Mat. Res. Soc. Proc. **609**, A3.5.1 (2000).

[79] A Yelon, H. Fritzsche and H. M. Branz, J. Noncryst. Solids (1999).

[80] S. S. Nag. “ Fabrication and control of properties in intrinsic and doped hydrogenated amorphous silicon layers,” Dissertation, The Pennsylvania State University, 1992.

[81] C. M. Fortmann, J O’Down, N. Newton and J. Fischer, “ Light-induced degredation and structure of high efficiency a-Si:H, a-SiGe:H and a-SiC:H soalr cells,” AIP Conf. Proc. **No:157** (American Institute of Physics, New York, 1987), p.103.

[82] M. Pinarbasi, L.H. Chou, N.Maley, A.Myers, D.Leet and J.A.Thornton, Superlat. Microstruc. **3**, 331 (1987).

[83] A. Rose, " Recombination in insulators and semiconductors,” Phys. Rev.B, **97**, 322 (1955).

[84] J. G. Simmons and G. W. Taylor, " Non-equilibrium steady-state statistics and associated effects for insulators and semiconductors containing an arbitrary distribution of traps,” Phys. Rev. **B,** 4, 502 (1971).

[85] W. Shockley and W.T. Read, Jr., " Statistics of the recombinations of holes and electrons,” Phys. Rev.B, **87**, 835 (1952).

APPENDIX A

Simmons-Taylor Statistics and Photoconductivity in a-Si:H

Photoconductivity and its recombination kinetics are used extensively to study the effects of the density and nature of gap states in semiconductors and insulators. Because of continuous distribution of gap states in amorphous semiconductors, in particular hydrogenated amorphous silicon(a-Si:H), the trapping, detrapping and recombination processes under steady-state illumination condition are more complex than those in crystalline semiconductors. In this chapter, the Simmons-Taylor statistics developed for the recombination kinetics of an arbitrary distribution of gap states and their effects on photoconductivity are revisited.

A.1 Simmons-Taylor Statistics

A.1.1 Recombination Kinetics

The recombination statistics for an arbitrary distribution of gap states under steady-state illumination condition was first envisioned by Rose [83] in a phenomenonlogical approach and later formulated by Simmons and Taylor [84]. Because of the continuous distribution of states in the bandgap, Simmons-Taylor statistics is particularly useful to study a-Si:H thin films. This recombination statistics lays the foundation for our understanding of various phenomena and plays a critical role in modeling the experimental data measured in a-Si:H films. In this part, a summary of Simmons-Taylor statistics is given and its application to a-Si:H is also discussed.

Single level recombination statistics was derived by Schockley and Read[85] and applied to crystalline semiconductors successfully. For a single trap level at energy E_t in the band gap, four recombination processes, as shown in Fig.A.1, are possible to determine the occupancy of that discrete trapping level. r_a is the rate at which electrons are captured into traps from the conduction band, r_b is the rate at which electrons are thermally emitted to conduction band from a trap, r_c is the rate at which holes are captured into a trap from the valence band and r_d is the rate at which holes are thermally emitted to the valence band from a trap.

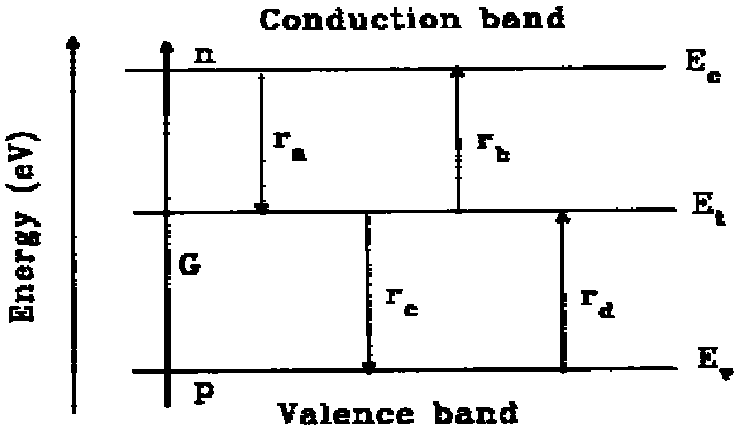

Figure A1. Four recombination processes for a single trap level at energy E_t. E_v represents the valance band edge and E_c is the conduction band edge. Free carriers n and p are created by the light of generation rate G.

These four rates are given as:

$r_a = \upsilon \sigma_n n N_t (1-f)$ **(Eq. A.1)**

$r_b = f N_t e_n$ **(Eq. A.2)**

$r_c = \upsilon \sigma_p p f N_t$ **(Eq. A.3)**

$r_d = N_t e_p (1-f)$ **(Eq. A.4)**

where n: free electron concentration in the conduction band, p: free hole concentration in the valence band, σ_n: carrier capture cross section for electrons, σ_p: carrier capture cross section for holes, υ : thermal velocity of free carriers, e_n: thermal emission probability for electrons, e_p: thermal emission probability for holes, N_t: the density of trapped level at energy E_t per unit volume, f: probability of occupation for a given trap level. Thermal emission probabilities are given :

$$e_n = \upsilon \sigma_n N_c \exp\left(\frac{E_t - E_c}{kT}\right) \quad \textbf{(Eq. A.5)}$$

$$e_p = \upsilon \sigma_p N_c \exp\left(\frac{E_v - E_t}{kT}\right) \quad \textbf{(Eq. A.6)}$$

where N_c and N_v are effective density of states in the conduction and valance band respectively.

In the thermal equilibrium:

$r_a = r_b$ *and* $r_c = r_d$ **(Eq. A.7)**

and occupation function is the Fermi-Dirac function, f(E):

$$f(E) = \frac{1}{1 + \exp\left(\frac{E_t - E_f}{kT}\right)} \quad \textbf{(Eq. A.8)}$$

where E_f is the thermal equilibrium Fermi level.

In a distribution of gap states, each type of state can have different carrier capture cross sections for electrons and holes which then requires its own occupation function. A *species* of states is defined by a particular group of states characterized by a constant ratio, *R(S),* of carrier capture cross sections:

$$R(S) = \frac{\sigma_n(S,E)}{\sigma_p(S,E)} \quad \textbf{(Eq. A.9)}$$

where S represents the type of state (S=1,2,3,….), $\sigma_n(S,E)$ *and* $\sigma_p(S,E)$ are the capture cross sections of electrons and holes at energy E for a specific species of gap states S respectively. A-Si:H can be modeled as having multiple species of defects, such as band tail states and dangling bonds, each different species being characterized by the ratio of the capture cross sections for electrons and holes. The occupancy function of a particular type gap states can be derived by setting the net increase of occupancy of that particular state to be zero in the steady state, i.e., *dn/dt=0*

then

$0 = dn/dt = r_a - r_b - r_c + r_d$ **(Eq. A.10)**

$$0 = \nu\sigma_n(S,E)nN(S,E)(1-f(S,E)) - f(S,E)N(S,E)e_n(S,E)$$
$$-\nu\sigma_p(S,E)pf(S,E)N(S,E) + N(S,E)e_p(S,E)(1-f(S,E)) \quad \textbf{(Eq. A.11)}$$

Thus the probability of occupation, *f(S,E)*, of a state level at any energy *E* is obtained as:

$$f(S,E) = \frac{v\sigma_n(S,E)n + e_p(S,E)}{e_n(S,E) + v\sigma_n(S,E)n + v\sigma_p(S,E)p + e_p(S,E)} \qquad \textbf{(Eq. A.12)}$$

It should also be noted that this occupancy function is of the same form as that originally derived by Shockley and Read [85] for a discrete level state. This does not come as a surprise since an arbitrary distribution of gap states can be considered as an ensemble of single-level states and should obey the same statistics for discrete level states at the same energy. However, it should be noted that this occupancy function is independent of energy distribution of the gap states.

The occupancy function can be expressed as a combination of two modulated Fermi-Dirac functions at $E_{ft}^{\ n}$ and $E_{ft}^{\ p}$ above and below dark Fermi level E_f, respectively:

$$f(S,E) = \begin{cases} \dfrac{R(S)n}{R(S)n+p}\left\{\dfrac{1}{1+\exp\left[\dfrac{(E-E_{ft}^{n}(S))}{kT}\right]}\right\} & \mathrm{E} > \mathrm{E_f} \\ 1-\dfrac{p}{R(S)n+p}\left\{\dfrac{1}{1+\exp\left[\dfrac{-(E-E_{ft}^{p}(S))}{kT}\right]}\right\} & \mathrm{E} < \mathrm{E_f} \end{cases} \qquad \textbf{(Eq.A.13)}$$

Thus an approximate occupancy function can be derived for the entire energy range of the gap:

$$f(S,E) = \begin{cases} \dfrac{R(S)n}{R(S)n+p}\exp\left[\dfrac{-(E-E_{ft}^{n}(S))}{kT}\right] & E > E_{\mathrm{ft}}^{\mathrm{n}} \\ \dfrac{R(S)n}{R(S)n+p} & E_{\mathrm{ft}}^{\mathrm{p}} < E < E_{\mathrm{ft}}^{\mathrm{n}} \\ \left\{1-\dfrac{p}{R(S)n+p}\exp\left[\dfrac{-(E_{ft}^{p}(S)-E)}{kT}\right]\right. & E < E_{\mathrm{ft}}^{\mathrm{p}} \end{cases} \qquad \textbf{(Eq.A.14)}$$

E_{ft}^{n} and E_{ft}^{p} are called the quasi-Fermi levels for trapped electrons and trapped holes, respectively, which are defined as follows:

$$E_{ft}^{n}(S) = Ec + kT \ln\left[\frac{R(S)n + p}{R(S)Nc}\right] \qquad \textbf{(Eq.A.15)}$$

$$E_{ft}^{p}(S) = Ev - kT \ln\left[\frac{R(S)n + p}{Nv}\right] \qquad \textbf{(Eq.A.16)}$$

Two demarcation levels E_{dn} and E_{dp}, as defined by Rose[83], are the energy levels where the tapped carriers has the same probability for thermal re-emission and recombination.

These four energy levels are of great importance in our understanding in the recombination kinetics of photogenerated carriers in a-Si:H and the interpretation of our experimental results. E_{ft}^{n} and E_{ft}^{p} establish the distribution of carriers in the gap states and E_{dn} and E_{dp}, determine these gap states should behave either as recombination centers or shallow traps. A comparison with quasi-Fermi levels for free carriers E_{fn} and E_{fp} reveals that:

$E_{ft}^{n}(S) > E_{fn}(S)$ and $E_{ft}^{n}(S) > E_{dn}(S)$ **(Eq.A.17)**

$E_{ft}^{p}(S) < E_{fp}(S)$ and $E_{ft}(S) < E_{dp}(S)$ **(Eq.A.18)**

at all time under steady-state illumination conditions. The position of E_{dn} and E_{dp} relative to E_{fn} and E_{fp} will, however, depend on the $v\sigma_n(S, E)n$ and $v\sigma_p(S, E)p$:

$E_{fn} < E_{dn}$ and $E_{fp} < E_{dp}$ if R(S)n < p **(Eq.A.19)**

$E_{fn} > E_{dn}$ and $E_{fp} > E_{dp}$) if R(S)n > p **(Eq.A.20)**

It should also be noted that both E_{ft}^{n} and E_{ft}^{p} , E_{dn} and E_{dp} are associated with a specific species of states in the gap. Each species of gap states has its own demarcation levels and quasi-Fermi levels for trapped carriers as illustrated in Fig. A.2.

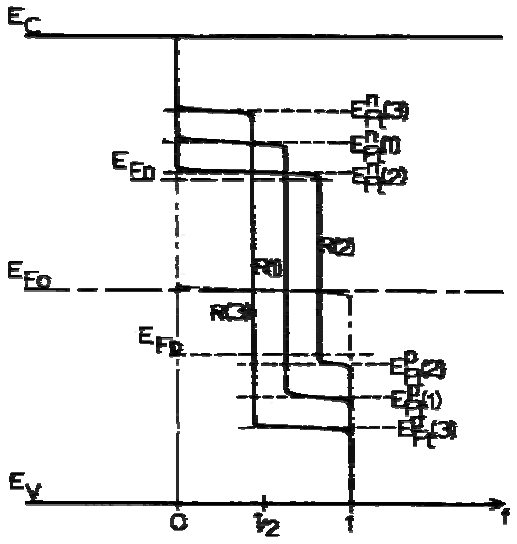

Figure A2. Schematic diagrams of occupancy function as a function of different species.

For insulators or intrinsic semiconductors with $\upsilon\,\sigma_n(S, E)n \sim \upsilon\,\sigma_p(S, E)p$, $E_{fn} \cong E_{dn} \cong E_{ft}^{n}$ and $E_{fp} \cong E_{dp} \cong E_{ft}^{p}$. For intrinsic semiconductors with $R(S) \sim 1$, the difference between these two quasi-Fermi levels, $E_{ft}^{n} - E_{fn}$ and $E_{fp} - E_{ft}^{p}$ are in the order of ~kTln2 (18meV at room temperature). Therefore E_{fn} and E_{fp} are good approximations to E_{ft}^{n} and E_{ft}^{p}, respectively.

Since a-Si:H is highly photoconductive, it is almost always operated under the condition of n , p > > no,po The above equations can be simplified to:

$$f(S,E) = \begin{cases} \dfrac{R(S)}{R(S)+1}\left\{\dfrac{1}{1+\exp\left[\dfrac{(E-E_{ft}^{n}(S))}{kT}\right]}\right\} & E > E_f \\ 1-\dfrac{p}{R(S)+1}\left\{\dfrac{1}{1+\exp\left[\dfrac{-(E-E_{ft}^{p}(S))}{kT}\right]}\right\} & E < E_f \end{cases} \qquad \textbf{(Eq.A.21)}$$

$$E_{ft}^{n}(S) = Ec + kT\ln\left[\frac{(R(S)+1)n}{R(S)Nc}\right] \quad \textbf{(Eq.A.22)}$$

$$E_{ft}^{p}(S) = Ev - kT\ln\left[\frac{(R(S)+1)p}{Nv}\right] \quad \textbf{(Eq.A.23)}$$

In the thermal equilibrium, the Fermi-Dirac distribution approximation at 0^0K is assumed to determine the occupancy of each state at energy E. States below dark Fermi level, E_f, are occupied and above it are empty. The charge status of each type of state is determined according to whether they are donor-like or acceptor-like. The charge neutrality in the thermal equilibrium is maintained by E_f. The net negative charge in deep defect levels equals to the net positive charge in deep defect levels. Net positive charge comes from empty donor-like states which lie above E_f and net negative charge comes from filled acceptor-like states which lie below E_f. The total charge in each type of states is integrated throughout the band gap to obtain the charge neutrality condition in the thermal equilibrium. For a given distribution of defect levels in the bandgap, the position of Fermi level and relative position of defect levels are required to be known to determine charge neutrality condition.

In the non-equilibrium steady-state condition, the net change in the positive charge density below E_f must be equal to the net change in the negative charge density above E_f.

$$n + \sum_{s=1}^{n_s}\int_{Ef}^{Ec} f(S,E)N(S,E)dE = p + \sum_{s=1}^{n_s}\int_{Ev}^{Ef}(1-f(S,E))N(S,E)dE \quad \textbf{(Eq. A.24)}$$

It can be simplified as following: It is reasonable that the density of free carriers, n and p, is much smaller than that of trapped electrons and holes in the continuous deep defect states. Therefore the terms n and p in the previous equation can be disregarded compared to the others. Then;

$$\sum_{s=1}^{n_s}\left(\int_{Ef}^{Ec} f(S,E)N(S,E)dE\right) = \sum_{s=1}^{n_s}\left(\int_{Ev}^{Ef}(1-f(S,E))N(S,E)dE\right) \quad \textbf{(Eq. A.25)}$$

This is the charge neutrality condition required only to relate p to n.

The rate of electrons, dn/dt, at which they fall in the conduction band is given by:

$$\frac{dn}{dt} = G + \sum_{s=1}^{n_s}\left[\int_{Ev}^{Ec} e_n(S,E)\, f(S,E) N(S,E) dE\right] - \sum_{s=1}^{n_s}\left[\int_{Ev}^{Ec} v\sigma_n(S,E) n(1-f(S,E)) N(S,E) dE\right] - \beta np$$

(Eq. A.26)

where G is the generation rate across the bandgap, n_s is the number of different type of states, β is a constant of proportionality. The first term in the right-hand side of the previous equation is the rate of generation of electrons from band to band, second term is the rate of electron emission from deep defects to the conduction band, third term is the rate that electrons are captured by deep defects, fourth term is the rate that electrons recombine with holes in the valance band. In the steady-state: dn/dt = 0; hence

$$G = -\sum_{s=1}^{n_s}\left[\int_{Ev}^{Ec} e_n(S,E) f(S,E) N(S,E) dE\right] + \sum_{s=1}^{n_s}\left[\int_{Ev}^{Ec} v\sigma_n(S,E) n(1-f(S,E)) N(S,E) dE\right] + \beta np$$

(Eq. A.27)

βnp is important at only extremely high light intensities (G > 10^{22} cm^{-3} s^{-1}) and it is negligible in the limit of generation rates used to study photoconductivity.

$$G = -\sum_{s=1}^{n_s}\left[\int_{Ev}^{Ec} e_n(S,E) f(S,E) N(S,E) dE\right] + \sum_{s=1}^{n_s}\left[\int_{Ev}^{Ec} v\sigma_n(S,E) n(1-f(S,E)) N(S,E) dE\right]$$

(Eq. A.28)

In the steady-state illumination condition, generation rate ,G, is equal to the recombination rate, U.

$$G = U = -\sum_{s=1}^{n_s}\left[\int_{Ev}^{Ec} e_n(S,E) f(S,E) N(S,E) dE\right] + \sum_{s=1}^{n_s}\left[\int_{Ev}^{Ec} v\sigma_n(S,E) n(1-f(S,E)) N(S,E) dE\right]$$

(Eq. A.29)

These equations are genarally used to study photoconductivity in the materials with multiple type of recombination centers.

A.1.2 Distinction Between Traps and Recombination Centers

The role of gap states in the recombination process positioned between the quasi-Fermi level E_{fn} and the conduction band and those between E_{fp} and the valence decreases exponentially with energy. Therefore, a free carrier falling into one of these gap states will, with a high degree of certainty, be re-emitted to the bands from which it came. These gap states are generally referred to as *traps.* On the other hand, all gap states positioned between the two quasi-Fermi levels are referred to as recombination centers. Carriers captured by these recombination centers will recombine with other carriers and most recombination traffic passes through these centers. This observation is contrary to what is normally expressed in semiconductor literature where the recombination efficiency is considered to be a maximum at the center of the energy gap and to decrease rapidly for higher or lower energies. The classification of gap states into traps and recombination centers has very important implications in the recombination kinetics in a-Si:H films. Recombination centers govern the lifetimes of carriers, i.e., the sensitivity of photoconductors. Trapping states, on the other hand, play only an indirect role in determining the sensitivity but are primarily responsible for the large response time observed in most amorphous semiconductors.

A direct relation of the changes in recombination mechanism due to the change of light intensity and measurement temperature can be readily observed in photoconductivity. Photoconductivity is directly determined by the density of recombination centers, occupancy and capture cross sections and can be probed by the commonly used excitation by $h\nu > E$, as well as by $h\nu$ less than E. The energy range over which recombination centers can be studied is determined by light intensity and temperature.

A.1.3 Effects of Temperature and Light Intensity on Recombination Kinetics

An increase in illumination intensity leads to an increase in the free-carrier densities n and p which requires more recombination traffic to take place. This results in the movement of quasi-Fermi levels E_{fn} *and* E_{fp} (and demarcation levels) towards their respective band edges. As the quasi-Fermi levels sweep through these gap states, they will be converted from traps to recombination centers. Decreasing the measurement temperature lowers the thermal emission probability of the trapped charges which leads to increased recombination at the original traps. This has essentially the same effect upon the demarcation levels as that of increasing the illumination intensity. Schematic diagrams showing the movement of quasi-Fermi levels with the changes in light intensity and temperature and its effects on occupancy function are illustrated in Fig. A.3(a) and Fig. A.3(b) respectively. Through the increase of light intensity and the lowering of measurement temperature, shallow traps will be converted into recombination centers. This effect can be utilized to probe the nature of gap states over a wide energy range of the gap.

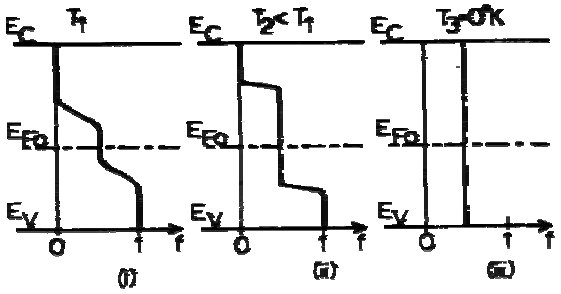

Figure A3.(a) Schematic diagrams of occupancy function as a function of different temperature.

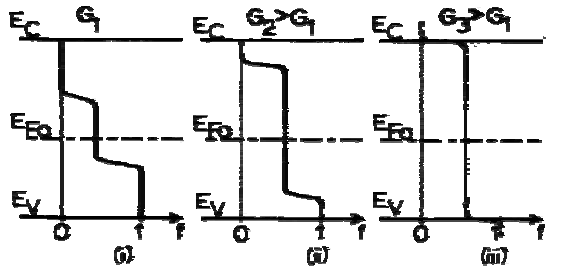

Figure A3.(b) Schematic diagrams of occupancy function as a function of different light intensity.

A.2 Photoconductivity in Hydrogenated Amorphous Silicon

A.2.1 Steady-State Photoconductivity

Photoconductivity can be divided into three mechanisms: First; absorption of photons and generation of free electron-hole pairs, Second; transport of mobile carriers and Third; recombination of excess free electrons and holes through recombination centers. Steady-state photoconductivity in a-Si:H is different from that of crystalline silicon in the following aspects: (1) a-Si:H with a wide bandgap, no,po<<n,p, is a very good photoconductor, (2) the continuous distribution of gap states in a-Si:H and their different properties yield a wide range of photoconductivity and recombination kinetics, (3) in general photoconductivity in a-Si:H is dominated by electrons because $\mu_p\tau_p<<\mu_n\tau_n$ due to wider valence band tails states where μ_n and μ_p are the free carrier mobility for electrons and holes**,** τ_n and τ_p are the lifetime for electrons and holes respectively. Photoconductivity σ_{ph} is directly related to the density of recombination centers. Using free-carrier transport model, photoconductivity can be expressed as:

$$\sigma_{ph} = q\mu_n n + q\mu_p p \cong q\mu_n n \qquad \textbf{(Eq.A.30)}$$

since n >> p and $\mu_n > \mu_p$ in undoped a - S : H

where the n and p are free carrier densities which in turn are determined by the generation rate G and the density of gap states:

$$n = G\tau_n = \frac{G}{p_r \upsilon \sigma_n} \;;\; \tau_n = \frac{1}{p_r \upsilon \sigma_n}$$

$$p = G\tau_p = \frac{G}{n_r \upsilon \sigma_p} \;;\; \tau_p = \frac{1}{n_r \upsilon \sigma_p} \qquad \textbf{(Eq.A.31)}$$

$$\sigma_{ph} = q\mu G\tau$$

$$\mu\tau = \frac{\sigma_{ph}}{qG} \qquad (\frac{\text{cm}^2}{\text{V}^{-1}}) \qquad \textbf{(Eq.A.32)}$$

where τ_n, and τ_p are lifetime for free electrons and holes, n_r, and p_r, are the density of electron-occupied and hole-occupied recombination centers, respectively. The accounting procedure for n_r, and p_r, is given below:

$$p_r = \sum_S \int_{E_v}^{E_{ft}^n} [1 - f(S,E)] N(S,E) dE \qquad \textbf{(Eq.A.33)}$$

$$n_r = \sum_S \int_{E_{ft}^p}^{E_c} f(S,E) N(S,E) dE \qquad \textbf{(Eq.A.34)}$$

When the state distribution lie outside the window between *Edn* and *Edp* does not vary faster than the Boltzmann factor, a good approximation to the recombination centers is simply the total electron occupied and hole-occupied states between *Edn* and *Edp*

$$p_r = \sum_S \int_{E_{ft}^p}^{E_{ft}^n} [1 - f(S,E)] N(S,E) dE \qquad \textbf{(Eq.A.35)}$$

$$= \sum_S \frac{p}{R(S)n + p} [E_{dn}(S) - E_{dp}(S)]$$

$$n_r = \sum_S \int_{E_{ft}^p}^{E_{ft}^n} f(S,E) N(S,E) dE$$

$$= \sum_S \frac{R(S)n}{R(S)n + p} [E_{dn}(S) - E_{dp}(S)] \qquad \textbf{(Eq.A.36)}$$

The generation rate G is determined by the external parameters and internal material parameters as:

$$G = F(1-R)\frac{1 - \exp(-\alpha d)}{d} \qquad \textbf{(Eq.A.37)}$$

where F is the flux of photons in $cm^{-2}s^{-1}$, R is the reflection coefficient at hν=E, α is the absorption coefficient of the material at energy hν=E , and d is the thickness of the film.

In general, photoconductivity can exhibit a non-integer power-law dependence on light intensity F or generation rate G over several orders of magnitude:

$$\sigma_{ph} = CG^{\gamma} \qquad \textbf{(Eq.A.38)}$$

so that

$$\mu\tau \propto G^{(\gamma-1)} \qquad \textbf{(Eq.A.39)}$$

where C is a proportionality constant, and $0.5 \le \gamma \le 1.0$. $\gamma = 0.5$ represents bimolecular recombination kinetics, where electrons in the conduction band directly recombine with the holes in the valence band. $\gamma = 1.0$ represents that electrons in the conduction band recombine with holes in the valence band through the recombination centers in the

bandgap. It is called monomolecular recombination. Detailed treatment for the intensity dependence of photoconductivity is given in the next section.

A.2.2 Intensity Dependence of Photoconductivity

The density of carriers in the respective bands and in levels in the band gap is changed from thermal equilibrium with optical excitation. These densities can be obtained from reaction-kinetic arguments. First, the carrier density in the respective bands is discussed for a number of rather simple reaction-kinetic models in order to identify the specific influence of certain defect levels.

A.2.2.1 Intrinsic Photoconductivity

The intrinsic photoconductivity involves only electrons and holes in the conduction and valance bands. They are generated at the same rate G_o, and recombine directly with each other in Figure A4 (a).

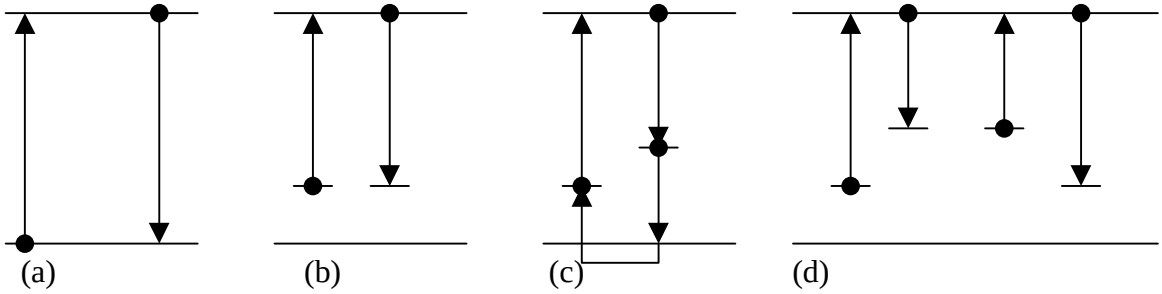

Figure A4. (a)Intrinsic photoconductivity, (b)extrinsic photoconductivity involving only one defect center, (c)involving a different recombination center, (d)involving traps.

The incremental carrier densities are equal. The change in carrier densities is given by the difference between generation ,G, and recombination ,U, rates:

$$\frac{dn}{dt} = G - U = G_0 - c_{cv} np = \frac{dp}{dt} \qquad \textbf{(Eq.A.40)}$$

where this equation is written for high generation rates when the incremental carrier densities Δn and Δp are large compared to the thermally generated densities n_0 and p_0:

$$\Delta n = n - n_0 \cong n \quad \text{and} \quad \Delta p = p - p_0 \cong p \qquad \textbf{(Eq.A.41)}$$

In steady state, with *dn/dt = dp/dt ≡ 0,* one obtains with *n = p,* from the Eq.A.40.

$$n = \sqrt{\frac{G_0}{c_{cv}}} = p \qquad \textbf{(Eq.A.42)}$$

which is usually referred to as the *bimolecular recombination* relation. Intrinsic recombination occurs at high generation rates when other recombination paths are saturated. The intrinsic photoconductivity is *ambipolar* and is given by

$$\sigma_{pc} = e(n\mu_n + p\mu_p) = en(\mu_n + \mu_p) = e(\mu_n + \mu_p)G^{0.5}C_{cv}{}^{-0.5}$$

$$\sigma_{pc} = A\,G^{0.5} \qquad \textbf{(Eq.A.43)}$$

where

$$A = e(\mu_n + \mu_p)C_{cv}{}^{-0.5}$$

In this case γ = 0.5, recombination occurs between free electrons in the CB and free holes in the VB directly.

A.2.2.2 Extrinsic Photoconductivity

Extrinsic photoconductivity involves levels in the band gap. It is either n- or p-type. A deep defect center in which carrier generation occurs is called an activator. One can distinguish three type of extrinsic photoconductivities involving such activators:

- excitation from an activator with direct recombination into the same type of level. (Figure A4 (b))
- excitation from an activator with carrier recombination through another level. (FigureA.4 (c))
- excitation into a band from which major trapping occurs before recombination. (Figure A4 (d))

When generation and direct recombination involve the same type of activator, and this activator is seperated far enough from the valance band (Figure A4(a-d)) so that thermal ionization of the optically generated hole can be neglected, the carrier density follows the same bimolecular relationship as that for intrinsic carrier generation:

$$\frac{dn}{dt} = G_0 - c_{ca} n p_a = \frac{dp_a}{dt} \qquad \textbf{(Eq.A.44)}$$

where the density of holes in activators is represented by p_a and the quasi-neutrality condition by

$$p_a = n \qquad \textbf{(Eq.A.45)}$$

$$n = \sqrt{\frac{G_0}{c_{ca}}} \qquad \textbf{(Eq.A.46)}$$

reflecting monomolecular recombination. The photoconductivity is n-type with

$$\sigma_n = en\mu_n = e\mu_n \frac{G^{0.5}}{C_{ca}^{0.5}} = BG^{0.5}, \text{ where B} = \frac{e\mu_n}{C_{ca}^{0.5}} \qquad \textbf{(Eq.A.47)}$$

At high intensities, depletion of these activators causes saturation of the photoconductivity induced by high-intensity lasers, which were pulsed in order to avoid thermal destruction of the material[55,56].

A.2.2.3 Influence of Traps on Photoconductivity

When photogenerated carries are trapped intermittently before they recombine, the carrier balance is shifted and three balance equations must be considered:

$$\frac{dn}{dt} = G_0 - c_{ct} n(N_t - n_t) + e_{tc} N_c n_t - c_{ca} n p_a \qquad \textbf{(Eq.A.48)}$$

$$\frac{dn_t}{dt} = c_{ct} n(N_t - n_t) - e_{tc} N_c n_t \qquad \textbf{(Eq.A.49)}$$

$$\frac{dp_a}{dt} = G_0 - c_{ca} n p_a \qquad \textbf{(Eq.A.50)}$$

plus the quasi-neutrality condition:

$$n + n_t = p_a \qquad \textbf{(Eq.A.51)}$$

In steady state, all time derivatives vanish. As a consequence, the two terms related to trapping drop out of Eq.A.48; hence, it becomes identical to the balance equation (Eq.A.44).

$$G_0 = c_{ca} n p_a \qquad \textbf{(Eq.A.52)}$$

The influence of the traps enters through the neutrality condition, yielding

$$G_0 = c_{ca} n (n + n_t) \qquad \textbf{(Eq.A.53)}$$

Deep traps tend to be completely filled, i.e.,

$$n_t \cong N_t \qquad \textbf{(Eq.A.54)}$$

Introducing the previous two equations into each other, one obtains for the electron density

$$n = \frac{1}{2}\left(- N_t + \sqrt{N_t^2 + 4\frac{G_0}{c_{ca}}} \right) \qquad \textbf{(Eq.A.55)}$$

for small optical generation rates, i.e., for $G_0 << N_t^2 c_{ca} / 4$

Here Eq.A.55 reduces to

$$n = \frac{G_0}{c_{ca} N_t} \qquad \textbf{(Eq.A.56)}$$

$$\sigma = en\mu = e\mu \frac{G}{C_{ca} N_t} = DG, \qquad \textbf{(Eq.A.57)}$$

where $D = \frac{e\mu}{C_{ca} N_t}$

which is referred to as a monomolecular recombination relation, and indicates that each electron finds a constant density of available recombination sites with $p_a \cong N_t$. For high optical generation rates, (Eq.A.54) converts back to (Eq.A.45) ; p_a increases and becomes $>> N_t$, and therefore $n \cong p_a$.

$\gamma = 1.0$ is valid only if defect density in the bandgap is very low. Attempts to explain the $0.5<\gamma<1$ in terms of a mixture of monomolecular and bimolecular recombination is not possible for such a large range of photoconductivity. The sub-linear dependence of photoconductivity on light intensity is a direct consequence of the continuous distribution of gap states and can be explained by the model proposed by Rose [83]. When light intensity is increased, the electron and hole quasi-Fermi levels are moved towards their respective band edges so that the higher lying states are thus converted into recombination centers. This increased density of recombination centers decreases the carrier lifetimes and yields the sub-linear dependence of photoconductivity on light intensity. In this study, the effects of the gap states in the bandgap of a-Si:H are also investigated by measuring steady-state photoconductivity at room temperature for wide range intensity of monochromatic light.

APPENDIX B

COMPUTER PROGRAM FOR LOW TEMPERATURE PHOTOCONDUCTIVITY MEASUREMENT

```
temploop:
close #1
rem ---------------------------------------------------------------
        format #1, curr["Current=", "A"], volt["Voltage=", "V"]
        input "Enter data file name:?",name$
        open #1, file= name$+".dat",desc$,overwrite
        open #1, graph= "I-V",overwrite
open #1, screen
rem ---------------------------------------------------------------

input   "Input the Set Temperature in K:?",tset;
input   "enter  range(0-11):?",range;
input   "enter initial value:?",Vin;
input   "enter final value:?",Vson;
input   "enter step value:?",Vstep;
input   "enter delay time(sec):?",t1;

        gpibwrite (24,"C3")
        gpibwrite (24,"A3")

rem ------------ PROPORTIONAL, INTEGRAL AND DERIVATIVE FOR ITC502----

        gpibwrite (24,"P50")
        gpibwrite (24,"I00")
        gpibwrite (24,"D00")

rem ------------------------------TEMPERATURE SET----------------

        tempset$="T"+str$(tset)+"0"
        gpibwrite (24,tempset$)
        print "Ramping to", tset, "K."

 ramp1:
        gpibwrite(24,"R1")
        t=val(mid$(gpibread$(24),3,5))
        t=t/10

 ? "Temperature=",t
        if  t<>tset then goto ramp1
        print "Temperature is now = ", tset, "K."
```

```
rem ------------6517A initialization-----------------

          b$=str$(range)
          gpibwrite(26,"r"+b$+"x")
          gpibwrite(26,"B0x")
          gpibwrite(26,"O1x")
          gpibwrite(26,"f1x")
          gpibwrite(26,"c0x")

rem ------------------------------------------------

loopc:

          Vin=Vin+Vstep

loopqqq:

          a$=str$(Vin)
          gpibwrite(26,"V"+a$+"x")

 gosub delay

loopf:

curr=val(mid$(gpibread$(26),5,12))
gosub delay

akim=val(mid$(gpibread$(26),5,12))

if abs(akim-curr)>1E-5 then goto loopqqq
           volt=Vin
          write #1

if Vin=Vson then goto loopc
          gpibwrite(26,"O0x")
          ? "CHANGE LIGHT LEVEL"
          goto temploop
          stop

rem ------------------------------------------------

delay:
t=time
delay1:if time-t<t1*1000 then goto delay1
       return
```